I. SYNTHESIS AND TESTING OF A SUPPORTED SHILOV OXIDATION CATALYST

&

II. INFLUENCE OF STRUCTURAL FEATURES ON ZEOLITE CHARACTERIZATION BY CONSTRAINT INDEX TESTING

Thesis by

John Reeves Carpenter III

In Partial Fulfillment of the Requirements for the

degree of

Doctor of Philosophy

CALIFORNIA INSTITUTE OF TECHNOLOGY

Pasadena, California

2010

(Defended May 28, 2009)

ACKNOWLEDGEMENTS

Behind any achievement is a group of people whose contributions either directly or indirectly provide the support necessary to reach the goal. This work is no different. I am indebted to many people for helping me along my path of learning and discovery. I will attempt to acknowledge many of those people here but am sure to miss some for which I apologize but assure your interactions were appreciated.

First I would like to thank Dr. Mark Davis for the opportunity to be a member of his research group. He has provided support and guidance that has allowed me not only to advance my knowledge scientifically and perform research but also learn on a more general level how to better attack problems and manage work processes. In his lab I have had the opportunity to mature and grow as a research engineer. Watching the various work in the lab has been exciting and I will continue to look back to see what the future holds for this lab. I also would like to thank the other members of my thesis committee: Dr. Jay Labinger, Professor Richard Flagan, and Dr. Stacey Zones. Their time, advice, and support have been invaluable to me as I have worked to complete my thesis.

Part one of this thesis received financial support from BP through the Methane Conversion Cooperative. The MC^2 program provided a unique opportunity to experience a larger effort to research between multiple academic institutions and industry. It was a program with a diverse set of views on the issues around methane activation and a interesting set of ideas. Dr. Labinger, Dr. John Bercaw, and Dr. Tom Baker from the program provided helpful guidance and suggestions to this work.

Part two of the thesis was financially supported by the Chevron Energy Technology Company with collaboration with Dr. Zones. I would like to express my gratitude to Dr.

Zones for the multitude of assistances he provided, from access to his resources to valuable insight into the issues surrounding zeolite structure and activity to his wonderful patience. Besides finical support and Dr. Zones several other members of the Cheveron Energy Technology Company were helpful in this endeavor. Dr. Shelia Yeh provided her expertise on the XPS analysis of samples and Dr. C.Y. Chen provided use of his equipment and time on the adsorption measurements. Also I thank the other colleagues of Dr. Zones—though I can not name them all—for their assistance in the procurement of several zeolite samples and facilitation of this collaboration.

During my time as a member of the Davis lab, many good people have come and gone from the family. Each has played a role in my life for which I thank them. Dr. Andrea Wight, Dr. Jonathan Galownia, and Dr. Victor Diakov were senior members when I arrived and helped my transition into the group. Heather Hunt has been a constant office mate who has shared in the attempts to maintain sanity. Dr. Yuriy Roman Leshkov, a recent addition to the lab, has proved to be a wonderful assest sharing ideas as our projects have taken similar tracks. Raymond Archer deserves lots of gratitude. He joined the lab at the same time as I and has been a solid person to lean on for technical advice, as a sounding board, or even ranting. He has done all of this with great openness and expected little back. I can continue naming all of the people but then this would never end. So to everyone in the Davis lab past and present thank you.

Finally I must thank my family without whose support this would not have been possible. I know the long distance from my parents, siblings, and extended family has been tough on them as it has been on myself, but they have remained supportive throughout, recognizing the opportunity presented to me. Also my wife Catherine: she is my constant

support providing a listening ear when needed, providing encouragement when things were not going well, providing a distraction away from work when fun was required, and tolerating my moments of stressed craziness. I only hope I can return the support.

To everyone I offer my sincere gratitude and best wishes for success.

ABSTRACT

This thesis is composed of two separate projects invoking the use of heterogeneous catalyst. However that is the point where they diverge. Part One details work on the development of a heterogeneous system for the direct oxidation of alkanes. Part Two explores the use of competitive catalytic cracking of 3-methylpentane and n-hexane as a tool for the characterization of zeolites.

Part One is about the development of a heterogeneous system for alkane oxidation. Three techniques for creating heterogeneous catalyst from homogeneous systems without adding anchoring ligands are investigated: supported molten salts, supported aqueous phases, and ion-exchanged zeolites. Each of these has been used to create Wacker oxidation catalysts, in literature and in this work, for comparison purposes. From the study of Wacker oxidation the ion-exchanged zeolites and supported aqueous phase catalyst were identified as potential methods for developing a Shilov oxidation catalyst. The supported molten salt was eliminated because of high levels of chlorinated products and low activity. Attempts were made with ion-exchanged zeolites to oxidize ethane to ethanol but no products were detected.

The supported aqueous phase system, however, provided more promising results. Initial work focused on oxidation of ethanesulfonate loaded onto the controlled pore glass support along with the catalyst. Similar turnovers were achieved on the supported aqueous system as had been seen in the homogeneous system. The reaction parameters of liquid loading, oxygen pressure, reactant concentration, copper(II) chloride concentration, and acid addition were investigated. While the supported aqueous system was successful in the

oxidation of ethanesulfonate, attempts to perform ethane oxidation in a flow system were not. The loss of chloride ions from the system is believed to lead to the deactivation.

Part Two investigates anomalous Constraint Index results for small and medium pore zeolites containing cages that are relatively larger than the pore (i.e., cages similar in size to large pore zeolites). The Constraint Index test was developed as the competitive cracking of 3-methylpentane and n-hexane for the classification of structures as having small, medium, or large pores. Small pores are defined as 8-ring pores or smaller; medium pores are 10-ring pores; and large pores have 12-rings or larger. 10-ring structures like SSZ-25 and SSZ-35 that contain cages in the structure had Constraint Index results consistent with a large pore classification and 8-ring structures with cages like SSZ-23 and SSZ-28 have Constraint Index results consistent with medium pore zeolites.

Incomplete cages on the external surface have been shown to be active in other reactions. These hemi-cages may provide a nonselective active site that would result in lower Constraint Index results. This work looks at this possibility by comparing four zeolites, ZSM-5 and BEA* as normally behaving medium- and large-pore structures, and SSZ-35 and SSZ-25 as zeolites with structures containing 10-ring pores and cages. The surface is passivated by a dealumination treatment and tested by isopropanol dehydration. Then the Constraint Index test is performed and compared on calcined samples of both the parent and treated samples. No evidence of activity on the external surface having an influence on the Constraint Index test is observed. Several techniques are used to investigate accessibility are also looked at but only indirect hypotheses can be drawn. Finally it is reported that for structures with two or more distinct features, different fouling

rates in each feature may result in observable changes in the Constraint Index value over time on stream.

TABLE OF CONTENTS

LIST OF FIGURES

Figure *Page*

LIST OF FIGURES (CONTINUED)

Figure *Page*

LIST OF FIGURES (CONTINUED)

Figure *Page*

LIST OF TABLES

CHAPTER ONE

PREFACE

This thesis is composed of two separate projects. The first is centered around the development of a supported catalyst system for Shilov oxidation of alkanes. It entails looking for methods in which a homogeneous system can be transformed into a heterogeneous system to achieve the advantages therein without losing too much activity. This work is arranged as follows:

Chapter 2 introduces alkane oxidation and some of the problems encountered. Shilov oxidation is also introduced as a possible route to products without oxidizing to carbon dioxide. Finally several techniques for methods to create heterogeneous reaction systems from homogeneous systems are described.

Chapter 3 details the experimental methods used in Part I of the thesis, both the procedures for preparing the three catalyst systems and the reactor systems used to test them.

Chapter 4 describes the work done with Wacker oxidation of alkenes to aldehydes. It is here that the supported molten salt, supported aqueous phase, and ion-exchanged zeolite catalyst are compared. The impact of water concentration in the feed stream is introduced.

Chapter 5 moves from the Wacker system to the Shilov oxidation. Trials with ion-exchanged zeolites are described, as well as with the supported Shilov catalyst. Tests are run in the plug-flow reactor for the oxidation of ethane. The oxidation of ethanesulfonate is also utilized in the batch system to explore parameters of the catalyst.

Chapter 6 presents a summary of the work on the development of a supported Shilov oxidation catalyst.

The second project, while still utilizing the reactor system, shifts from the development of catalysts for the production of desired species to the use of reactions as a characterization tool. One class of important catalysts are zeolites which have a defined uniform structure. This structure can provide useful shape-selectivity in reactions and separations. Multiple techniques exist for characterizing the structures of zeolites, especially for new materials. One such test is the Constraint Index test which classifies the pore size of structures based on the competitive cracking of n-hexane and 3-methylpentane. However structures have been recently found that are exceptions to this classification. This project looks at how the presence of large internal cages in these structures contributes to their anomalous Constraint Index test results. Part Two is structured similarly to Part One, as follows:

Chapter 7 provides an introduction to the Constraint Index test. A description of the development of structures with large internal cages is included as well. Also some of the issues surrounding hydrocarbon cracking are touched on. Chapter 8 then provides some experimental details.

Chapters 9 through 11 describe the results of the investigation. Chapter 9 explores the role of the external surface, while Chapter 10 describes methods for looking at both the accessibility provided by the structures for molecules to enter through the pores and the accessibility to bulkier transition states. Chapter 11 highlights an observation that by looking at the Constraint Index over a longer time on stream it may be possible to see evidence of multiple structure features. Chapter 12 provides an overall summary.

PART ONE

SYNTHESIS AND TESTING OF A SUPPORTED SHILOV CATALYST

CHAPTER TWO

SHILOV OXIDATION

For many decades society has consumed products derived from petrochemicals, mainly from oil. However demand has risen for these products to be produced in a more environmentally clean manner. Natural gas has become an alternative to oil as both an energy source and chemical feedstock, due to its large supply and clean burning properties. Natural gas, however, is typically composed of methane and other light alkanes for which there is no industrially practical direct process for converting them to more valuable products.[1] The activation of the C-H bond, especially for direct functionalization at mild conditions, remains a challenge.[1–4]

2.1 Methane

Methane is an example where direct functionalization could make a substantial improvement in terms of cost savings and efficiency. Currently there are over 5000 trillion cubic feet of proven natural gas reserves in the world or, in other words, enough to meet the current consumption rate for the next 200 years.[5] This abundance of natural gas reserves, along with its characteristics of being a cleaner fuel than oil, have inspired effort into developing technologies to utilize this resource as a fuel and a chemical feedstock, just like oil. Industry not only wants to harness the energy stored in natural gas as a fuel source but to develop technologies to move it into other markets much the same way oil derivatives are used today.[6]

Natural gas is mainly composed of alkanes; in fact over 80% is methane.[6] Unfortunately, there are very few direct process for converting it to a valuable product industrially.[1] The C-H bonds of a methane molecule have no empty low energy orbital

or filled high energy orbital to easily participate in chemical reactions like unsaturated hydrocarbons can.[1] However, methane has still found industrial value as the precursor to the formation of synthesis gas, a mixture of CO and H_2. Synthesis gas is then used to make products such as methanol, ammonia, and other alcohols. Methanol production is one of the primary uses of synthesis gas.

Methanol is used across a wide variety of industries. Methanol serves as a precursor of formaldehyde, which is used to make urethanes and plastics. These make many of the items we use—from seat cushions, to the plastic in cars, to engineered wood products, to synthetic fibers. Also methanol can be used in the production of acetic acid, which is used in the production of many paints and adhesives, as well as the polyethylene terephthalate (PET) plastic that makes up so many of the items we use every day. Every time one wash their windshield or their car starts on a cold morning, they are using methanol, a major component of windshield-washing fluid and antifreeze. Previously, one of methanol's biggest markets was the production of methyl tertiary butyl ether, MTBE, a fuel additive. However, due to environmental and health concerns, the use of MTBE has been phased out. Even with the reduction in MTBE usage, the transportation market still has potential as a large methanol user in the future. Much of the work on fuel cell technology involves the use of methanol as a fuel source, and dimethyl ether, DME, can be produced from methanol to be used as a power source or to make cleaner diesel fuels.

More than 30,000 metric tons of methanol were produced in 2003 worldwide.[7] BP and Methanex operate a plant in Trinidad that can produce 1.7 million tons per year.[8] A simplified process diagram of the methanol production process as described on

the Methanex website is shown in Figure 2.1. In the process, methane is fed first through zinc oxide pellets to remove sulfur before being preheated. After the sulfur removal, steam is added to the reactant stream and the mixture is heated to facilitate the reforming. In the reformer the methane/steam mixture passes over a nickel oxide catalyst at ~900°C where it is converted to synthesis gas: carbon monoxide, dihydrogen, carbon dioxide, and water. Then the water is removed from the synthesis gas and the dry gas is sent to a compressor to increase the pressure for the methanol conversion reaction. The stream is then fed to the methanol reactor, where it is passed over a copper-containing catalyst and converted to methanol and water. Finally the product stream must be separated to remove the water and unreacted gases from the methanol.

As one can see, this process is heavy in capital investment, with the multiple stages in the production as well as high energy cost to operate at high temperatures and elevated pressures. This economic motivator has spurred research into direct methods of methane-to-methanol conversion. Removing the synthesis gas production route and lowering the pressure of the methanol conversion reaction could greatly alter the economics of methanol production and thus alter the end use, making it both a more viable feedstock and fuel source.

2.2 Shilov Oxidation

Much research has gone into the area of the direct partial oxidations of alkanes, for which several reviews can be found.[1,3,9] The research ranges from organometallic catalysts to the use of enzymes. One example is the work of Periana using mercury-mediated oxidation of methane by sulfuric acid.[10] However, while this provides

production of methanol at lower temperatures, it introduces the problem of dealing with the corrosive sulfuric acid. One of the earliest reported mechanisms for direct methane conversion is that reported by Shilov and coworkers in 1972.[11] No other method has been able to achieve the conversion under the mild conditions of Shilov's approach. It is this chemistry that this study will try to utilize.

In 1972, Shilov and coworkers reported the selective oxidation of methane to methanol at 130°C using aqueous salts of $PtCl_4^{2-}/PtCl_6^{2-}$. [11] Later he proposed a three-part mechanism for this partial oxidation.[12] The first step is the activation of the C-H bond to produce an alkylplatinum(II) species. It is then followed by an oxidation to an alkylplatinum(IV) species, and finally a reductive elimination results in the product and the return to the platinum(II) catalyst. The nature of the first step has proven difficult to study[3] and is still not clearly defined as it may progess in either an associative or disassociative manner[21]. In the second step, oxidation is achieved by a two-electron transfer from the $PtCl_6^{2-}$ to the alkylplatinum(II) species. Finally the reductive elimination occurs by a nucleophilic attack of water- or chloride resulting in the oxidize or chlorinated product respectively via an S_N2 mechanism. It is also accompined by the loss of another chloride ligand resulting in the return to the platinum(II) species. [13] Since then work has gone into determining the mechanism of each step and the C-H bond activation has been shown to be the rate-determining step.[13]

However the Shilov chemistry suffers the drawback of the use of platinum(IV) as an (expensive) oxidant. It would be highly more attractive to use molecular oxygen as the overall oxidant. In 2001, Sen and coworkers reported such a modification to the Shilov chemistry.[14] In their work, they replaced the $PtCl_6^{2-}$ salt with $CuCl_2$ and

demonstrated that in the presence of molecular oxygen they were able to oxidize alkanesulfonates and ethane in water. They also provided support that the addition of a second metal does not greatly alter the proposed mechanism. The modified Shilov cycle is shown below in Figure 2.2. In this study we work with Sen's modified Shilov system using copper(II); however recent work by Weinberg [15] demonstrates several possible alternatives to copper (II) and some of the conditions another oxidant would need.

While the Shilov oxidation provides the desired selectivity not seen in many other C-H bond oxidation processes, the homogeneous system has several drawbacks. These include the low solubility of alkanes in water and the corrosive nature of the metal salts. Another drawback of running the homogenous system is the difficulty of separating the desired products from the aqueous catalyst solution. Separations with the homogenous system would require more investment in process equipment that would be exposed to the catalyst solution. Also the C-H bond activation of the alkane and desired alcohol products are similar which leads to more over-oxidation of the products and less alkane conversion as the concentration of the product increases in the solution.[16] It would be advantageous to be able to run the reaction in a continuous flow system with a heterogeneous catalyst where product is continually being removed and reactant added to maintain a high alkane/low product concentration on the catalyst.

2.3 Supported Catalysts

A heterogeneous catalyst can be developed by immobilizing the catalyst on a selected support system. The common method for accomplishing this task is to covalently bond a catalyst to the support.[17] However, in this work the desire is to use

the transition metal salts which don't lend themselves to covalent bonding without the addition of new ligands. Also utilizing covalent bonding to immobilize a catalyst may result in a loss of the effectiveness of the catalyst due to decreased mobility.[17] Other methods for immobilizing the catalyst are through hydrogen bonding or ionic, hydrophobic/hydrophilic, or fluorous interactions.[17] The supported molten salt and supported aqueous phase catalysts make use of the hydrophilic/hydrophobic interactions, whereas the ion-exchanged zeolite relies more on the ionic interactions of the materials. Each of these will be discussed further in the context of their use in this work.

In general those catalysts that are supported based on the hydrophobic/hydrophilic interactions are depicted in Figure 2.3, in which we see a porous catalyst particle provide a large surface area for increased reaction surface. Here the catalyst phase is a thin layer of a hydrophilic liquid supported on a hydrophilic surface and the reactant phase is a hydrophobic organic phase. In this setup, the actual catalyst molecules are free to move in the immobilized liquid layer and the reaction takes place at the interface of the hydrophobic and hydrophilic phases.

A similar system to the Shilov oxidation of alkanes is the Wacker oxidation of alkenes on a $PdCl_2/CuCl_2$ catalyst system. This system has been demonstrated for the supported molten salt catalyst [18], supported aqueous phase catalyst[19], and ion-exchanged zeolite[20]. These will serve as the starting point in this work that tries to use the lessons of these systems to make a heterogeneous system for Shilov oxidation. Wacker oxidation of alkenes and Shilov oxidation of alkanes share many similarities that make using the Wacker system as a starting model attractive. The both work with a transition metal from the same family as well as operate at temperatures between 100°C

and 200°C in conditions exposed to oxygen and water. They both undergo a two-electron oxidation of the metal species by 2 $CuCl_2$ and in both nucleophilic attack of water on the hydrocarbon coordinated with the metal result in the product. A couple difference do exist in that the Wacker system is Pd(II)/Pd(0) system while the Shilov system is Pt(II)/Pt(IV) also the order of the reductive elimination and oxidation are reversed between the two. As Periana points out [22] Wacker oxidation using Pd^{2+} is not a viable route for alkane oxidation since the catalyst is not a powerful enough electrophile to activate the Ch bond in alkanes. Shilov oxidation is attractive as an alkane oxidation route for many of the reasons that have made Wacker oxidation of alkenes successful. Shilov oxidation provides a direct route for methane to methanol conversion that uses oxygen as the ultimate oxidant, operates at lower temperatures (below 200°C), lower pressures than the synthesis gas route, and is water tolerable. Also the selectivity limit the over oxidation to CO2 and CO that afflict many oxidation strategies. In fact Shilov oxidation has the potential to meet many of the requirements described out in a recent report from Periana for a successful direct route catalyst for methane conversion.[22]

2.4 References

[1] J. A. Labinger, J. Bercaw, Nature 417 (2002) 507.

[2] M. Lersch, M. Tilset, Chem. Rev. 105 (2005) 2471.

[3] J.A.Labinger, J. Mol. Cat. A: Chem. 220 (2004) 27.

[4] R.A. Periana, G. Bhalla, W.J. Tenn., K.J.H. Young, X.Y. Liu, O. Mironov, C. Jones, V.R. Ziatdinov, J. Mol. Catal. A 220 (2004) 7.

[5] Gas Supply, http://www.bpgaseconomy.com/documents/Gas_Supply.pdf , accessed March 23, 2005.

[6] The Gas Economy, http://www.bpgaseconomy.com, accessed March 23, 2005.

[7] Methanol Supply & Demand, http://www.methanol.org, accessed March 25, 2005.

[8] Methanex. http://www.methanex.com, accessed March 24, 2005.

[9] A.E. Shilov, G.B. Shul'pin, Chem. Rev. 97 (1997) 2879.

[10] R. A. Periana, D. J. Taube, E. R. Evitt, D. G. Löffler, P. R.Wentrcek, G. Voss, T. Masuda, Science 259 (1993) 340.

[11] N.F. Gol'dshleger, V.V. Es'kova, A.E. Shilov, A. Shteinman, A. Zh. Fiz. Khim. (Engl. Trans.) 46 (1972) 785.

[12] L. A. Kushch, V. V. Lavrushko, Y. S. Misharin, A. P. Moravsky, A. E. Shilov, Nouv. J. Chim. 7 (1983) 7, 729.

[13] S.S. Stahl, J.A. Labinger, J.E. Bercaw, Angew. Chem. Int. Ed., 37 (1998) 2180.

[14] M. Lin, C. Shen, A. Garcia-Zayas, A. Sen, J. Am. Chem. Soc. 123 (2001) 1000.

[15] D.R. Weinberg, J.A. Labinger, J.E. Bercaw, Organometallics 26 (2007) 167.

[16] J.S. Owen, J.A. Labinger, J.E. Bercaw, J. Am. Chem. Soc. 128 (2006) 2005.

[17] J. Horn, F. Michalek, C.C. Tzschucke, W. Bannwarth, Topics in Current Chemistry 242 (2004) 43.

[18] V. Rao, R. Datta, J. Catal. 114 (1988) 377.

[19] J.P. Arhancet, M.E. Davis, B.E. Hanson, Catalysis Letters 11 (1991) 129.

[20] P.H. Espeel, M.C. Tielen, P.A. Jacobs, Chem. Comm., 10 (1991) 669.

[21] H. Zhu, T. Zeigler, J. Organometallic Chem. 691 (2006) 4486

[22] B.L. Conely, W. J. Tenn III, K.J.H. Young, S.K. Ganesh, S.K. Meier, V.R. Ziatdinov, O. Mirionov, J. Oxgaard, J. Gonzales, W.A. Goddard III, R.A. Periana, J. Mol. Chem. A: Chemical 251 (2007) 8.

Figure 2.1: Simplified process diagram of Methanex's process for the production of methanol from methane via synthesis gas

Synthesis Gas reactions

$CH_4 + H_2O \longrightarrow CO + 3H_2$

$CO + H_2O \longrightarrow CO_2 + H_2$

Methane Conversion reactions

$CO + 2H_2 \longrightarrow CH_3OH$

$CO_2 + H_2 \longrightarrow CO + H_2O$

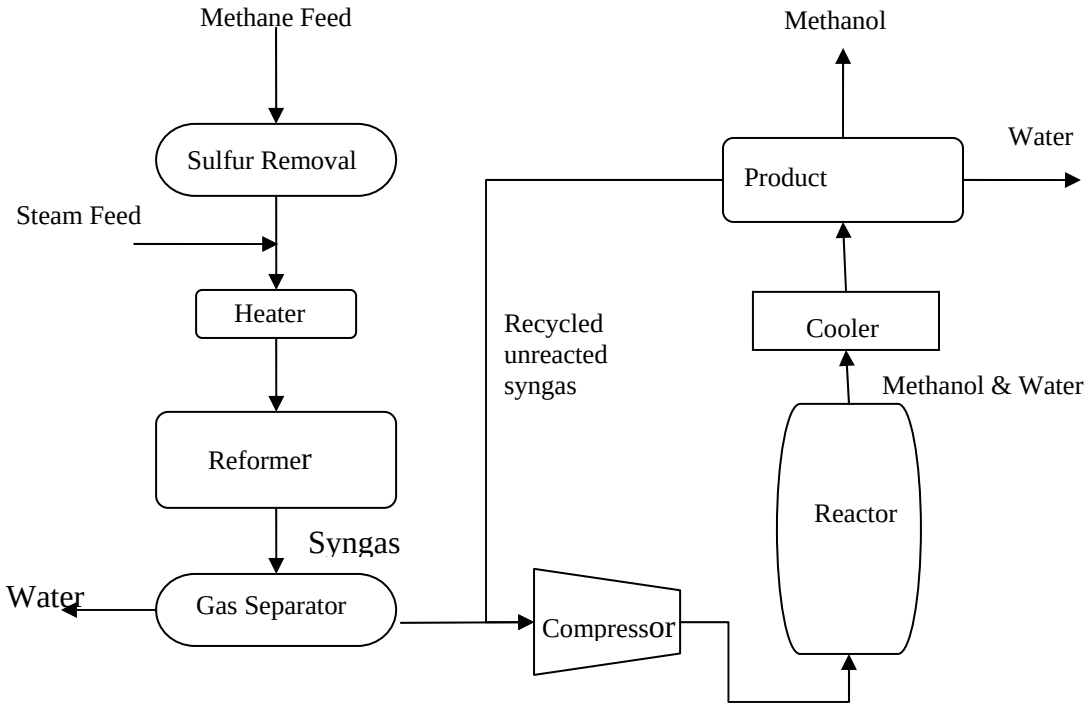

Figure 2.2: Schematic of the mechanism of modified Shilov oxidation detailing the three main steps 1) C-H bond activation 2) oxidation and 3) reductive elimination. In the oxidation step, the modification to use Copper (II) and thus molecular oxygen as the overall oxidant has been included.

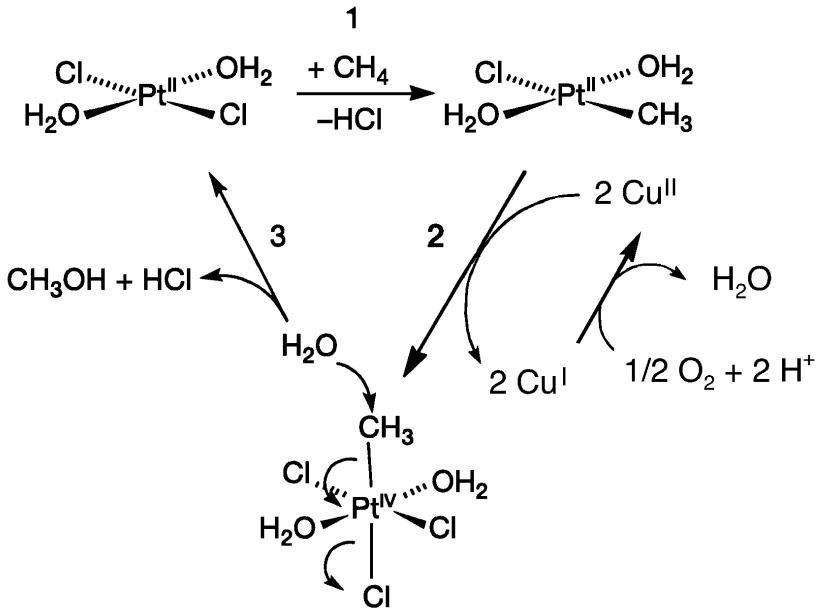

Figure 2.3: Depiction of a supported catalyst solution. In this case the solution is depicted as an aqueous solution but the water could also be a eutectic melt of molten salts.

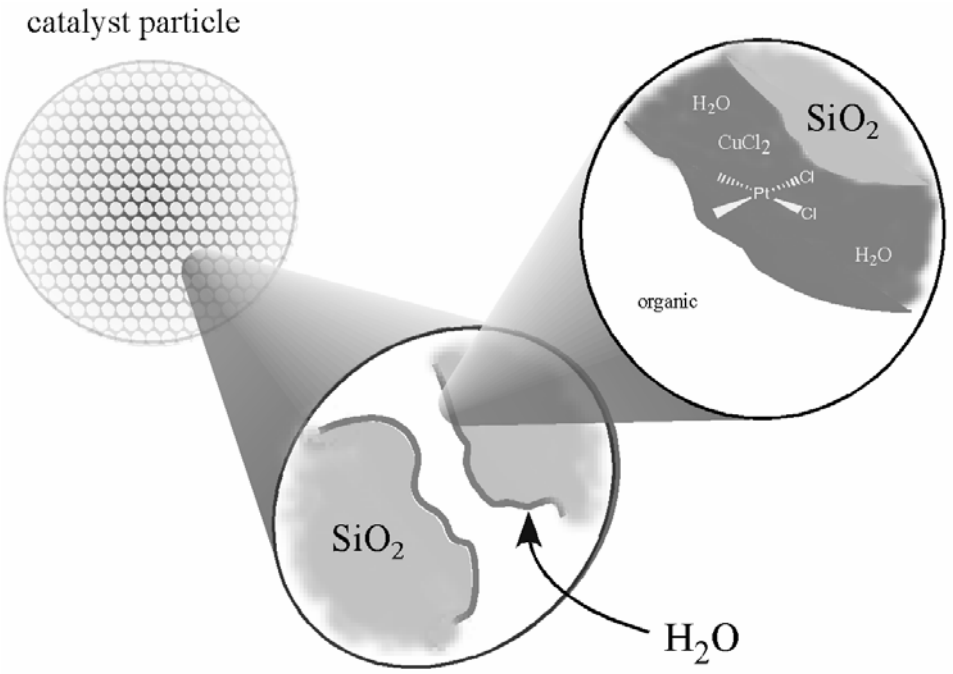

CHAPTER THREE

EXPERIMENTAL METHODS FOR SYNTHESIS AND TESTING OF SUPPORTED SHILOV OXIDATION CATALYST

3.1 Supported Molten Salt Catalyst

The supported molten salt catalyst (SMSC) was prepared following the work of Rao and Datta.[1] Palladium chloride(≥ 98%), copper(II) chloride dehydrate (≥ 99.0%), copper (I) chloride(≥ 98%), potassium chloride (≥ 99.0%), and hydrochloric acid (1.0N) were used as purchased from Sigma-Aldrich. Controlled Pore Glass from CPG, Inc., with pores of 240 nm, was used as the support. The desired amount of metal salts required to achieve the desired loading on the support were dissolved in dilute (0.1N) HCl. The desired amount of support was dried under vacuum overnight before the vacuum was broken by introduction of the catalyst solution. The sample was evacuated to a pressure of less than 150 millitorr on a Schlenk line using a DUO Seal ™ Mechanical vacuum pump and monitored with a VH-3 Hastings vacuum gauge. Unless otherwise specified this is the system used in this rest of this work. The solution was stirred under nitrogen for 24 hours. The water was removed using a rotary evaporator.

3.2 Supported Aqueous Phase Catalyst

The supported aqueous phase catalyst (SAP) was prepared in a similar manner to the SMSC, and follows the procedures of both Hanson [2] and Butt [3]. Desired amounts of the catalyst ($PdCl_2/CuCl_2$ for Wacker oxidation and K_2PtCl_4(Reagent Grade 98%)/$CuCl_2$ for Shilov oxidation), enough to typically achieve approximately 5% by weight salt loading on the CPG, were dissolved in water. In the cases of ethanesulfonate oxidation, the sodium salt of ethanesulfonate was also dissolved in the solution. CPG was measured out into a round bottom flask and evacuated for several hours using the same vacuum system as described in Section 3.1. The solution of metal salts was then

transferred to the flask containing the CPG, breaking the vacuum. The flask was then backfilled with nitrogen and the slurry was then stirred for at least 2 hours before the water was removed by using a rotary evaporator. The catalyst obtained was a free-flowing light green powder and was stored at room temperature. Thermogravimetric analysis determined the catalyst to maintain 2–3% by weight of water after the rotary evaporation.

3.3 Ion-Exchanged Zeolites

The ion-exchanged zeolites for Wacker oxidation were prepared based on the work of Jacobs.[4] BEA* and Ultrastable Zeolite Y (USY), a faujasite-type zeolite, from Tosoh were calcined as received. The parent materials were in the sodium form with BEA* having a Si/Al ratio of 13.5 and USY having a Si/Al ratio of 2.75. The USY is similar to that used for the highest conversions reported by Jacobs [4] and the BEA was the lowest ratio available from the company. They were then exchanged at room temperature for 24h in a 1M $Cu(NO_3)_2$ ($\geq$ 98%) solution with a solid to liquid ratio of 1g/L. After filtering and drying, the Cu(II)-Y and Cu(II)-BEA* were exchanged with aqueous solutions containing the desired amount, assuming all Pd is exchanged, of $Pd(NH_3)_4Cl_2$. The solution was allowed to stir at room temperature for 24 hours before filtering and washing with three times the exchange solution volume of water. The material was then dried in air at 100°C and stored in a desiccator until used. No attempts were made to determine the oxidation state of the copper after either exchange step; however the sample remained a light blue color. This is consistent with reports on Cu^{2+}-

exchanges into zeolite Y and BEA* where the copper remains in the Cu^{2+} state after exchange. [5,6]

3.4 Supported Catalyst Batch Reactions

All batch reactions were carried out in a stainless steel 25mL Parr mini reactor. The reactor is equipped with a pressure gauge, gas inlet and outlets, and a rupture disk. The desired amount of supported catalyst, usually 0.5g, was loaded into a glass liner and then hydrated by the addition of the desired amount of water. This mixture was stirred until all the water was taken up by the catalyst and the catalyst was a homogeneous powder. The glass liner was placed into the reactor and the reactor sealed. The reactor was then charged with the desired pressure of oxygen and placed in an oven. Heating to reaction temperature took approximately two hours in the oven. After the desired reaction time, the reactor was removed from the oven and allowed to cool to room temperature. Then a GC/MS analysis of the overhead was performed, and the catalyst was collected for NMR analysis in order to quantify the species remaining in the liquid phase on the CPG. This was accomplished by extracting those species in D_2O with a small addition of DMSO added as an external standard. The slurry was stirred for 1h and then sonicated for 1h before decanting the liquid. The decanted liquid was then centrifuged to remove any remaining CPG from solution before a proton NMR was taken to quantify the products of the reaction on a Varian Mercury 300 MHz spectrometer at 23°C. The signals at 1.25 ppm, 3.1 ppm, and 3.4 pmm were quantified in comparison to the DMSO signal at 2.7ppm for ethanesulfonate, 2-hydroxyethanesulfonate and 2-chloroethanesulfonate respectively in D_2O.

3.5 Supported Catalyst Flow Reactions

Reactions were carried out in a BTRS Jr. single pass vertical reactor system (Autoclave Engineers) with a ½" stainless steel reactor tube. 0.5g of catalyst was loaded into the reactor tube packed between glass wool. A thermocouple extended to the middle of the catalyst bed to measure reaction temperature. The water feed was fed as a liquid by syringe pump into a mixing assembly where it was vaporized with a sweep gas of 5% argon in helium (AirLiquide, 99.999%) in a mixing assembly at 150°C. The He/Ar , oxygen, and ethane flows were controlled by Brooks mass flow controllers. All reactions were run at concentrations above the upper flammable limit of the hydrocarbon in use. Products were analyzed by online GC/MS (Agilent GC 6890/MSD 5973N) with a Plot-Q capillary column. Products were identified from the GC/MS results by both the MS results for each peak as well as retention times from injections of individual components purchased from Sigma-Aldrich (99%+ purity). The retention times were argon, oxygen and carbon monoxide at 1.7 min and were quantified on the basis of distinct fragment counts in the MS 32 for oxygen, 40 for Ar, and 28 for carbon monoxide. The other retention times were carbon dioxide at 1.8 min, methane at 1.85min, ethene at 1.95min, ethane at 2.1min, water at 2.4min, acetaldehyde at 4.4 min, methanol at 4.8 min, ethanol at 6.8 min and acetic acid at 11.65min. The GC program had a start temperature of 150°C with a 2°C a minute ramp and a column flow of 2ml/min. The results were quantified using the argon in the He/Ar sweep gas as an internal standard. Calibration curves on the basis of mols product/mols Ar vs. MS counts product/MS counts of Ar for each of the products were generated by flowing various concentrations

of the known product mixtures with various sweep gas flow rates through the system in bypass mode

3.6 **References**

[1] V. Rao, R. Datta, J. Catal. 114 (1988) 377.

[2] J.P. Arhancet, M.E. Davis, B.E. Hanson, Catal. Letters 11 (1991) 129.

[3] I. Shaw, J.S. Dranoff, J.B. Butt, Ind. Eng. Chem. Res. 27 (1988) 935.

[4] P.H. Espeel, M.C. Tielen, P.A. Jacobs, Chem. Comm. 10 (1991) 669.

[5] A.J. Fowkes, R.M. Ibberson, M.J. Rosseinsky, Chem. Mater. 14 (2002) 590.

[6] H. Chen, M. Matsuoka, J. Zhang, M. Anpo, J. Catal. 228 (2004) 75.

CHAPTER FOUR

SUPPORTED WACKER OXIDATION CATALYST

The similarities between the Wacker chemistry and the Shilov chemistry, along with the work on supported Wacker catalyst, make it attractive as a first step screening for the development of a supported catalyst for performing the Shilov chemistry. In 1959, Smidt and coworkers discovered the oxidation of olefins to ketones or aldehydes in a palladium/copper aqueous solution.[1] The Wacker oxidation cycle can be described by the following reaction set (Figure 4.1).

One can notice right away the similarities between the two mechanisms: the use of copper(II) as the oxidant of the transition metal and the use of molecular oxygen as the overall oxidant; the fact that the added oxygen to the hydrocarbon actually comes from the water molecule even though molecular oxygen is the overall oxidant; and the two-electron oxidation. Also this system is derived from a mixture of the salts $PdCl_2$ and $CuCl_2 \bullet 2H_2O$, similar to the salts used in the Shilov cycle. The Wacker system has been adapted to several supported systems: supported molten salts, supported aqueous phase, and ion-exchanged zeolites.[3–10]

4.1 Supported-Molten Salt Catalyst

The first supported catalyst looked at was a supported molten salt Wacker catalyst. Rao and Datta reported their development of a supported molten salt catalyst (SMSC) for the Wacker process and its use for the oxidation of ethylene to acetaldehyde in 1987.[2] The main characteristic of the SMSC is the use of a eutectic melt as the reaction medium as opposed to an aqueous phase. This is important since with an aqueous phase catalyst, evaporation of the solvent will lead to catalyst deactivation. Thus the low-volatility of a eutectic melt made it an attractive choice.

Rao and Datta investigated several choices of eutectic melts and found that a melt of 65 mol% CuCl and 35 mol% KCl at 195°C had good activity and selectivity similar to an aqueous phase catalyst.[2] This eutectic melt has a melting point of 150°C; thus operating at 195°C insures the mixture is in the liquid phase. Rao and Datta supported this eutectic melt on silica pellets with catalyst concentrations in the melt of 7 mol/m^3 $PdCl_2$ and 130 mol/m^3 $CuCl_2$. Rao and Datta's work took utilized a Berty reactor at 195°C and atmospheric pressure with a flow rate of $1.2x10^{-6}$ m^3/s and a feed composition of 5 mol% ethylene and 95 mol% air and the catalyst spread as a thin layer in a crucible which sat in the catalyst basket.[2]

In this study the method Datta reported for producing a SMSC was adapted to use controlled pore glass (CPG) as opposed to the silica pellets. The SMSC-CPG was prepared as follows: (1) the CPG was washed and dried under vacuum (i.e. pressure less than 150 millitorr per section 3.1 vacuum system description and the same for the following steps) over night; (2) the catalyst and solvent salts were dissolved in aqueous hydrochloric acid; (3) the vacuum on the CPG was broken by adding the required amount of the catalyst/solvent solution to the CPG; (4) the solution and CPG were stirred for 24 hours; (5) the CPG were dried on the rotovap. The initial attempt saw the catalyst/solvent solution turn from a dark green color initially to a blue color overnight. TGA/DSC experiments were unable to observe the melting transition of the catalytic phase with the prepared SMSC-CPG or with the unsupported eutectic mixture. It is possible that the color change may have arisen from changes to the copper species, though that was not investigated, and the use of catalysts prepared from these solutions were not active.[11] Due to the inactivity of the catalyst from the solutions prepared in air, subsequent catalyst

preparations were performed under inert conditions. With this change the solution color, dark green, and the final catalyst, a light brown, are more in line with those reported by Datta[2] and Byers[11]. Also TGA/DSC experiments with the unsupported mixture show a melting point around 150°C, as seen in Figure 4.2. However, the SMSC-CPG showed much smaller effects, if any, probably due to the small amount of material actually undergoing the transition in a SMSC-CPG sample.

Most of the reactions run in this study using Wacker oxidation as a model substitute for Shilov oxidation were exploratory for developing technique and basic operating conditions as opposed to detailed studies of reaction variables and mechanism. The data for many of these runs either shows trace or no activity. For this reason only a few representative runs are detailed in Table 4.1. All reactions were run at 195°C and atmospheric pressure. The catalyst used was loaded to 20% liquid loading with the catalyst solution similar to the conditions Datta reports.[2] Besides the products acetaldehyde and carbon dioxide, dichloroethane was also produced in all runs of the SMSC likely arising from the high concentration of chloride and the use of cupric chloride at near 200°C [14]. A sample of CPG with no metal salts loaded was run and showed no products other than the feed composition.

In comparison Datta reports ~25% conversion of ethylene with a 95% selectivity to acetaldehyde.[2] As can be seen, the SMSC produced in this study perform nowhere near this level. One large difference in the two studies is the reactor type and the contact time — Datta uses a Berty reactor and this study uses a fixed-bed flow reactor. While every effort was taken to maintain identical conditions between this work and the work of Datta; i.e the same temperature, pressure, and catalyst loadings, in Datta's study the space

time is ~170s whereas the highest our current plug-flow reactor can achieve is approximately 25s. The Berty reactor Datta uses is more approximate of a continuously-stirred reactor (CSTR) than a plug-flow reactor (PFR). Typically a lower space time is required in a PFR to achieve the same conversion compared with a CSTR. The extremely large difference in the space times here however would lead to an expected lower conversion that is seen. In an ideal approximation (i.e. assuming all conditions are identical, the systems are isothermal, Datta's Berty reactor is an ideal CSTR and our PFR is an ideal PFR) for a first order reaction, which the Wacker system is under these conditions [2], a PFR with a space time of 145s would be needed to match the 25% conversion Datta achieves in the Berty reactor. Hence the large difference in the space time is likely a major cause for the lower conversions experienced in this study. Another observation that was made is that Datta claims all runs are dry except those investigating the feed of water into the system.[2] In this study, reactions with the SMSC and water in the feed had very little activity and favored the production of carbon dioxide over acetaldehyde. The physical appearance of the catalyst at different stages indicate changes in the catalyst, but these changes have not been determined as of yet. The catalyst as made and stored is a light brown color; after a reaction the removed catalyst is a more vivid brownish-orange. However if left exposed to air over time (several days), the catalyst will turn to a green color. It has also been seen that unreacted catalyst will turn to a light green if left open to air. The color change is a result of the hydration of the catalyst due to exposure to air. The CPG support is known to by hydrophilic and when exposed to air will have a 1-2 wt% of water content. The cupric chloride is hygroscopic as well. When dried the KCl and CuCl are colorless and the $CuCl_2$ will be a yellowish-

brown while the palladium chloride is a reddish brown. This is the color observed after drying. After a reaction the catalyst is dried during the cool down when dry nitrogen is flowing over the catalyst as the reactor cools before it can be unloaded. When exposed to air the green color arises from the hydration of the $CuCl_2$.$CuCl_2$ in highly concentrated aqueous solutions appears green. The green of the CuCl2 likely dominates the reddish brown of the palladium chloride as the $CuCl_2$ is present in concentrations 20 times higher than the palladium chloride. It should also be noted that it is possible that some of the CuCl is converted to cupric oxychloride as well which is also green.

4.2 Supported Aqueous Phase Catalyst

In 1989 Davis and coworkers reported on a class of supported catalysts called supported aqueous phase catalyst (SAP), [12] in which a catalyst is dissolved in water and supported on a hydrophilic material and the combination is used in an organic solvent that is immiscible in water, thus maintaining the thin layer of water on the support and the catalyst in it, with the reaction occurring at the interfacial area of the organic and aqueous phases. Low solubility of methane in water makes this an attractive catalyst. These SAP catalysts differ from previously reported supported liquid catalysts because of the loss of liquid phase when a liquid substrate is used in the reaction. Thus the supported liquid phase catalysts are mainly designed for gas phase reactions. Even though this work will be dealing with a gas phase reaction the SAP catalyst is mentioned because in 1991 Davis and coworkers reported the development of a SAP Wacker catalyst for the oxidation of 1-heptene to 2-heptanone.[3] It is their procedure that will be used for the production of a SAP catalyst in this work. However the work will be

comparable to other reported studies of supported liquid catalyst Wacker oxidation experiments.[3,9,13]

The SAP catalyst in this study was prepared according to the procedure laid out in Davis's work on Wacker SAP catalyst.[3] The catalyst was prepared as follows: (1) the CPG was washed and dried under vacuum overnight (i.e. pressure less than 150 millitorr per section 3.1 vacuum system description and the same for the following steps), (2) a desired amount of $PdCl_2$ was dissolved in ethanol, (3) the vacuum on the CPG was broken by adding the ethanol/$PdCl_2$ solution to the CPG and stirred, (4) the ethanol was removed by use of the rotovap and then placed back under vacuum, (5) a desired amount of $CuCl_2 \cdot 2H_2O$ was dissolved in water, (6) the vacuum on the $PdCl_2$/CPG was broken by addition of the $CuCl_2$/water solution and stirred, (7) the solution was dried under vacuum leaving the $PdCl_2$ and $CuCl_2$ deposited on the CPG. TGA/DSC experiments of the SAP catalyst showed that after drying the catalyst still maintained 2 – 3 wt% water. The catalyst was prepared to have 5 wt% metal salts with a Pd:Cu ratio of ~20 as is the ratio of the SMSC.

A sample of results for the SAP catalysts is also listed in Table 4.1. The reaction conditions are somewhat different than the SMSC due to trial and error to find good working conditions. One major difference is the reduction in temperature. With no requirement to reach the melt point of metal salts, the reaction can be carried out at lower temperatures, which improves the ability to maintain the water loading on the catalyst.[9] Looking at Table 4.1 comparing SAP7a and SAP7b the only difference is the amount of steam fed into the system, which when doubled increased the conversion of ethene from 34% to 56%. Increases in the water content of the feed leads to a increase in the liquid

loading on the catalyst.[9] As described previously with the SAP catalyst, as the liquid loading increases initially the mobility of the individual catalyst molecules increases leading to an increased activity till a maximum is reached. After the maximum is reached, increased water feed leads to pore flooding that can lower the interfacial surface area and increased diffusional limitations that lower the activity. Thus based on the increased conversion from 34% to 56%, it should be expected that the optimal liquid loading was not fully reached. At 125°C an increase in the steam showed little change suggesting this is near the optimal steam feed for running the Wacker oxidation. The main products seen were acetaldehyde and trace carbon dioxide, while acetic acid was also seen occasionally, but none of the chlorinated products that were seen with the SMSC were observed.

One of the dominating factors in the activity of the supported aqueous phase catalyst is the liquid loading on the catalyst.[9] Shaw shows a sixfold increase in the reaction rate by increasing the liquid loading(fraction of pore volume filled with liquid) on the catalyst from 0.05 to 0.1, and a similar reduction in activity at higher loadings going from 0.1 to 0.5.[9] Multiple factors control liquid loading on the catalyst in a flow system, such as reaction temperature, support material, support pore size, and feed water concentration. This study used controlled-pore glass pores of either 240 nm or 500 nm (the CPG has a pore distribution of ±5%) as opposed to the alumina supports with 4 – 8 nm pores Shaw used. Larger pores would be expected to need more water in the feed to achieve the same liquid loading as is seen in this work where a higher water feed rate is need to see activity than in Shaw's work.[9] Different supports will exhibit different optimal liquid loadings for maximum activity dependant on both the characteristics of the

support and the reaction.[9] Larger pores and higher reaction temperatures are expected to require more water in the feed to reach op. Figure 4.3 shows the variation in activity over both the 240 nm and 500 nm CPG over 3 different reaction temperatures. The SAP catalyst loaded for each run was adjusted between the 240nm-pore CPG supported catalyst and the 500nm-pore CPG supported catalyst to maintain equal pore surface areas and loading amounts of palladium chloride and copper chloride were in each test. The larger pore size required higher feed water content to reach similar activity as the small pore size, and higher reaction temperatures also required higher feed water contents. The required feed water content needed to reach the maximum activity was not investigated nor was pore filling, due to concerns of flooding the reactor resulting in corrosion from the chloride salts on the CPG.

It is difficult to compare these results to some of the results of published data since the work by Davis was on 1-heptene[6] and work by Shaw used a flow rate 4 times slower with different feed compositions.[9] However both report on the observed peak in a plot of reaction rate versus water feed. [3,9] Both show an increasing reaction rate with an increased water feed, which eventually peaks and then decreases as the water feed continues to increase. As the water feed increases, the liquid layer of the SAP catalyst increases, so initially the increase in water allows more mobility of the catalyst particles and greater reaction rate. However, further increasing the water feed begins to fill the pores, decreasing the surface area for reaction and increasing diffusional limitations. More work is required to find the optimal water feed for these conditions.

4.3 Ion-Exchanged Zeolite

The final catalyst type that was pursued is an ion-exchanged zeolite. There are several reports on the use of Cu/Pd exchanged zeolites to perform Wacker oxidation of alkenes to aldehydes or ketones.[4 – 8] In this catalyst the cations that act as the catalyst are held in the zeolite by the ionic interaction with the zeolite lattice. In some of the more recent work on these catalysts, Jacobs and coworkers have attempted to establish the mechanism of the Wacker oxidation and determined it to be similar to that of the homogenous reaction.[4,5] They have also demonstrated that only the faujasite type zeolite, zeolite Y, provides high activity, and that activity has a dependence on the Si:Al ratio.[4]

The procedure used in this study for producing the Cu/Pd exchanged zeolite was adapted from the work of Jacobs.[5] The procedure involved mixing a sample of NaY zeolite for 24 hours at room temperature with an excess of a .01M solution of $Cu(NO_3)_2$ and then filtering and washing the sample until there were no nitrates detectable in the wash water. The Cu-exchanged zeolite was then mixed with a solution of $Pd(NH_3)_4Cl_2$ containing a molar amount of Pd that was less than twice the estimated amount of Cu in the zeolite. The solution was then allowed to once again stir at room temperature for 1 day, after which the zeolite was filtered and washed. It was then dried overnight at 100°C. The catalyst was then tested in the same reactor as the previous catalyst. Table 4.1 also contains several results from those runs.

The conversion of ethene on these Pd/Cu-exchanged zeolites is comparable to the reports from Jacobs[5]. In the run ZEO2 high conversion of ethene is seen with high selectivity toward acetaldehyde. Over the run on ZEO2 the conversion and selectivity

remain constant. In ZEO4 and ZEO5 is set of back to back runs using the same sample of the catalyst. Runs ZEO4 and ZEO5 should results consistent with ZEO2 and the catalyst was still active at the same levels after 8 hours when the combined ZEO4 and ZEO5 runs are considered. All reaction runs were performed at atmospheric pressure and 105°C. Also each reaction was run so as to match the weight hourly space velocity and feed compositions used by Jacobs.[4] Each reaction also saw trace amounts of various other products, including acetone, acetonitrile, and acetic acid.

An initial reaction run at 195°C to match the similar temperature and pressure conditions of the SMSC only produced carbon dioxide. This is consistent with previous work on the oxidation of propylene by a Cu/Pd exchanged zeolite in which increasing the reaction temperature showed an increased selectivity to carbon dioxide and a decreased selectivity toward acetone.[6] The other reaction runs were run at a much lower temperature of 105°C, closer to the 100°C that Jacobs used.[4,5] Each of these runs shows good activity toward ethylene conversion; in fact they appear a little higher than the 50% conversion Jacobs reports [4,5]; however he does not report the product distribution for comparison of selectivity.

The low conversion and chloride products of the SMSC make it an unlikely candidate for the development of a supported Shilov oxidation catalyst, while both the supported aqueous phase catalyst and ion-exchanged zeolite may be useful techniques.

4.4 References

[1] G. Smidt, W. Hafner, R. Jire, J. Sedlmeier, R. Sieber, R. Rultinger, H. Koger, Angew Chem. 71 (1959) 176.

[2] V. Rao, R. Datta, J. of Catal. 114 (1988) 377.

[3] J.P. Arhancet, M.E. Davis, B.E. Hanson, Catalysis Letters 11 (1991) 129.

[4] P.H. Espeel, M.C. Tielen, P.A. Jacobs, Chemm. Comm. 10 (1991) 669.

[5] P.H. Espeel, G.D. Peuter, M.C. Tielen, P.A. Jacobs, J. Phys. Chem. 98 (1994) 11588.

[6] T. Kubota, F. Kumada, H. Tominaga, T. Kunugi, Int. Chem. Eng. 13 (1973) 539.

[7] B. Elleuch, C. Naccache, Y. Ben Taarit, Stud. Surf. Sci. Catal. 35 (1984) 139.

[8] K. Eguchi, T. Tokiai, H. Arai, J. Catal. 111 (1988) 111, 457.

[9] I.S. Shaw, J.S. Dranoff, J.B. Butt, Ind. Eng, Chem. Res. 27 (1988) 935.

[10] A.W. Stobbe-Kreemers, M. van der Zon, M. Makkee, J.J.F. Scholten, J. Mol. Cat.:A 107 (1996) 247.

[11] J. Byers personal communications, May 2004.

[12] J.P. Arhancet, M.E. Davis, J.S. Merola, B.E. Hanson, Nature 339 (1989) 454.

[13] H. Komiyama, H. Inoue, J. Chem. Eng. Jpn. 8 (1975) 310.

[14] P.P. Nicholas, R.T. Carroll, J.Org. Chem. 33 (1968) 2345.

Figure 4.1: Reaction scheme for the Wacker oxidation of olefins

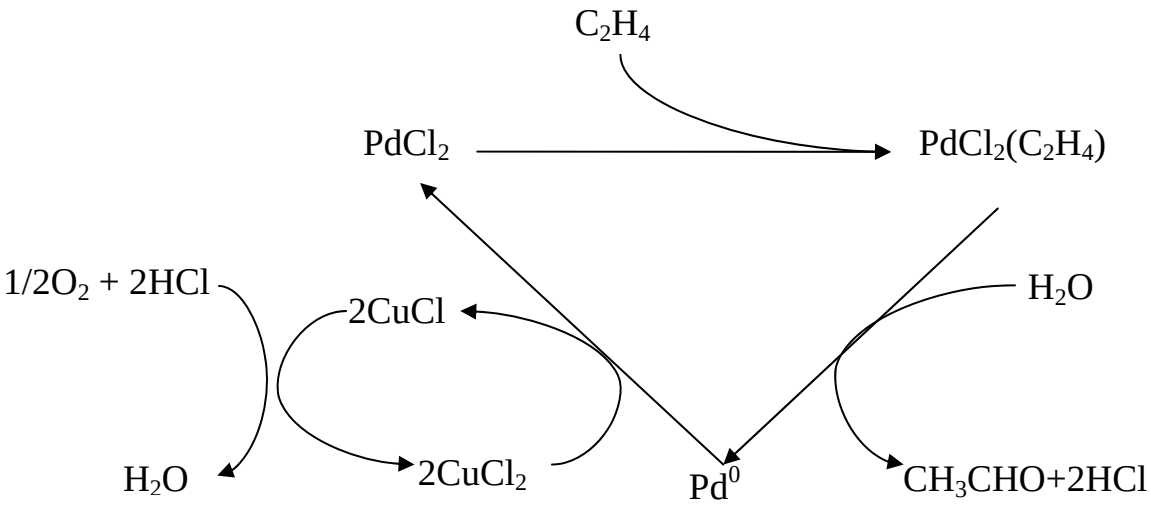

Figure 4.2: TGA/DSC analysis of the molten salt Wacker catalyst showing an endotherm beginning at approximately 150°C indicating the melting point

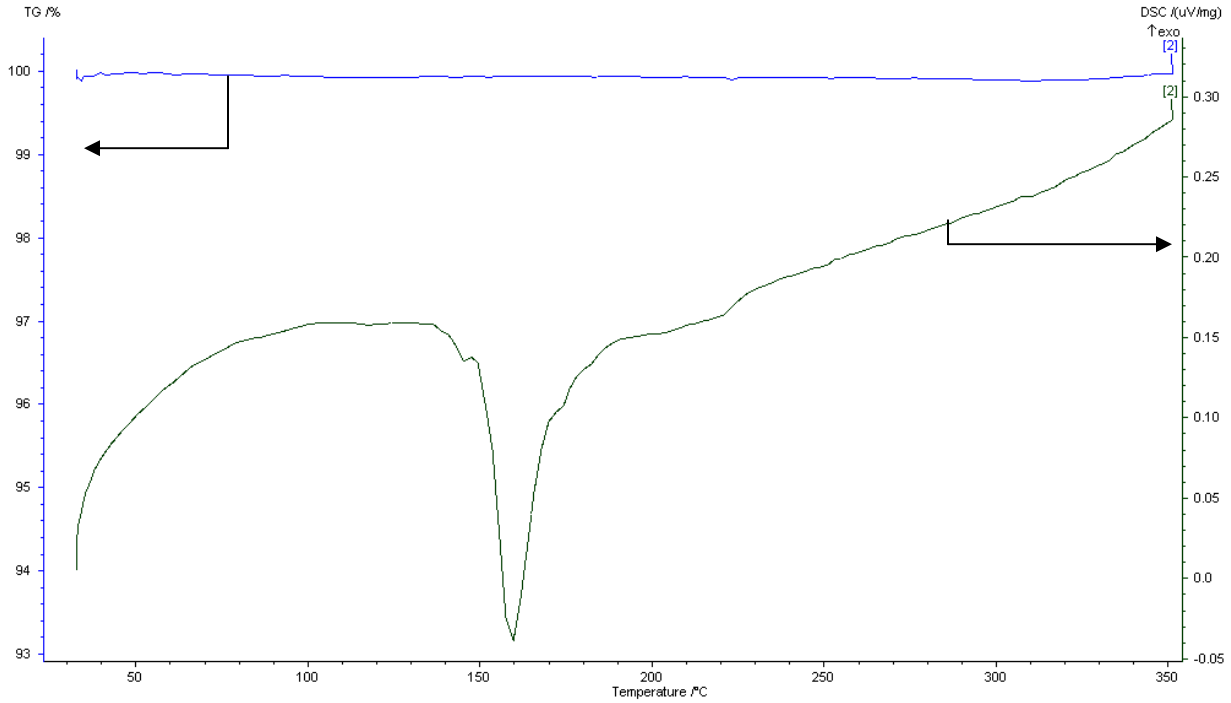

Figure 4.3: Comparison of acetaldehyde production on SAP catalyst at varying reaction temperatures and water flow rates on a) CPG with pores of 240 Å and b) CPG with pores of 500 Å

a) 240 Å CPG

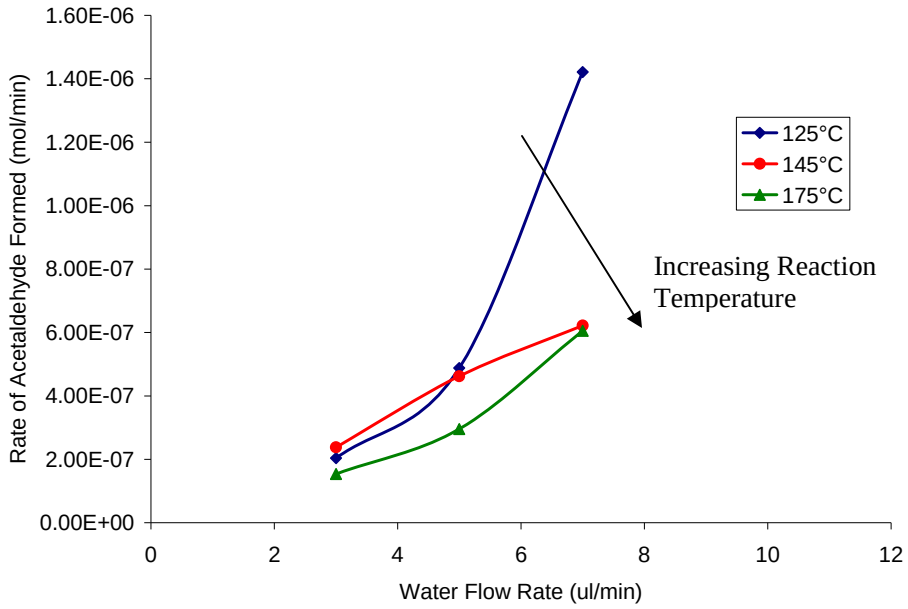

b) 500 Å CPG

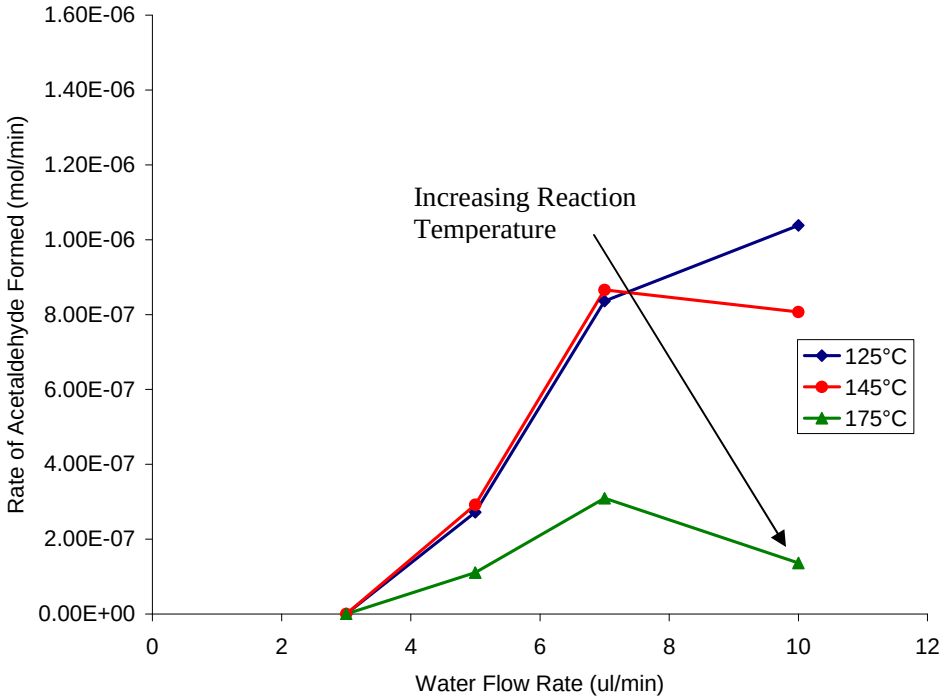

Table 4.1: Review of Wacker Catalysts used for the gas-phase flow oxidation of ethylene to acetaldehyde. SMSC=Supported Molten Salt Catalyst, SAP=Supported Aqueous Phase Catalyst

Run	Cat. Vol. (ml)	Cat. Mass (g)	Flows (ml/min) HC:O2:He/Ar: steam	Vol Cat./ Vol. Flow Rate	Conv. Ethene	Conv. O2	Selectivity Acetaldehyde
SMS Catalyst - 195°C, atm. pressure, 20 wt% loading of melt, 130 and 7 mol/m3 of CuCl2 and PdCl2 in the melt							
SMSC 8[a]	3.6	1.78	0.7: 3.0: 10.5:5.4	0.18	1.10%	0.20%	64%
SMSC 9[a]	3.75	1.82	0.7: 3.0: 10.5: 5.4	0.2	1.60%	0.50%	31%
SMSC 11[a]	3.7	1.8	0.4: 1.5: 3.1: 4.3	0.4	1.10%	0.30%	51%
SAP Catalyst - 115°C(runs 7&8), 125°C(runs 10&11), atm. pressure, 15wt% loading, Cu:Pd=3							
SAP7a[b]	3.9	1.53	0.3: 4.9: 5.4: 2.0	0.31	34.5%	1.55%	>99%
SAP7b[b]	3.9	1.53	0.3: 4.9: 5.4: 4.0	0.27	56.0%	2.52%	>99%
SAP8b[b]	3.9	1.53	0.6: 9.9: 10.9: 8.0	0.13	39.5%	1.7%	>99%
SAP10[b]	3.7	1.45	0.3: 4.9: 5.4: 4.0	0.25	47.4%	2.0%	>99%
SAP11[b]	3.7	1.45	0.3: 4.9: 5.4: 6.8	0.21	47.1%	1.8%	>99%
Zeolite Catalyst - 105°C, atm. pressure							
ZEO2[b]	2.5	1.067	0.3: 4.9: 5.4: 2.5	0.19	88%	5.80%	78%
ZEO3[b]	2.5	1.067	0.3: 4.9: 5.4: 2.5	0.19	6-20%	0.5-1.2%	42-65%
ZEO4[b]	2.4	1.012	0.3: 4.9: 5.4: 2.5	0.18	81%	5.50%	66%
ZEO5[b]	2.4	1.012	0.3: 4.9: 5.4: 2.5	0.18	81%	6.60%	75%

[a]Data is averaged over online time of hour 5 – 6 for run SMSC9 and from 4.5 – 5.5 for SMSC11 and 2 – 3 for SMSC8.

[b]Data is averaged over online time of hour 2.5 – 3.5 for all runs.

CHAPTER FIVE

SUPPORTED SHILOV OXIDATION CATALYST

From the Wacker oxidation study, the ion-exchanged zeolites and the supported aqueous phase catalyst seemed to have the most promise of providing good activity with limited undesired products such as carbon dioxide and chlorinated products.

5.1 Ion-Exchanged Zeolites for Shilov Oxidation

Using the process for the preparation of the ion-exchanged zeolites for Wacker oxidation, $Pt(NH_3)_4Cl_2$ was substituted for $Pd(NH_3)_4Cl_2$ to attempt to make a Shilov oxidation catalyst analog of the Wacker catalyst. The uptake of $Pt(NH_3)_4^{2+}$ was observed by UV-Vis. However reactions at a variety of temperatures, pressures, and feed concentrations saw no activity toward the oxidation of methane or ethane. In the Wacker system where $Pd(NH_3)_4Cl_2$ is exchanged into the zeolite in place of $PdCl_2$ used in the homogenous form, the ion-exchanged zeolite is active for the oxidation of ethene. However in the Shilov system, $Pt(NH_3)_4Cl_2$ appears to be inactive for alkane oxidation. The amine ligands appear to kill the activity of Pt(II) species in the Shilov cycle as use of $Pt(NH_3)_4Cl_2$ to oxidize ethanesulfonate supported on CPG was also inactive.

A second method of platinum addition to the copper-exchanged zeolite was the vapor deposition of platinum acetylacetonate. Reaction runs only showed an initial CO_2 product stream, not the desired products. Most of the CO_2 is attributed to the decomposition of the platinum species, as Pt^0 was observed by XRD on the spent catalyst.

A suitable method to introduce an active form of platinum into the zeolite was not found as there was concern that impregnation methods would leave the K2PtCl4 on the

external surface as opposed to internal cages in proximity to the copper species. Further studies into obtaining a Pt(II) species inside a zeolite such as other potential ligands or manipulations could provide further interesting studies. However, we chose to devote our resources to the SAP catalyst at this time.

5.2 Supported Aqueous Phase Catalyst for Shilov Oxidation

The Supported Aqueous Phase Catalyst was expected to provide a better route to a heterogenized Shilov catalyst as there was already a homogeneous aqueous system. Initial tests of the supported aqueous phase catalyst were done following the work of Sen [1] working with the terminal oxidation of ethanesulfonate. The use of ethanesulfonate provides several advantages: it provides direct comparison with the homogenous system Sen used, reduces flammability/explosion concerns as opposed to a methane/oxygen mixture, and, as a water soluble reactant already on the support, limits issues related to pore flooding. Supporting the reaction solution on the controlled pore glass gives comparable activity to that reported by Sen [1] for the homogeneous reaction. Table 5.1 details examples of both reactions. The homogenous reaction produces species of further oxidation while the SAP catalyst produces only 2-hydroxyethanesulfonic acid and 2-chloroethanesulfonic acid. The SAP system is slower than the homogenous system, at the 4h reaction times point, the SAP system has achieved 49 turnovers with respect to Pt while Sen and Byers reported turnovers of 53 and 102, respectively. The reaction system used with the SAP system seems to have a 2 hour induction period before any products are observed, attributed to the heating to reaction temperature; it is unknown from Sen's report whether a similar period is observed. Also in the homogeneous system the total

pressure is 1200psi with additional nitrogen while the SAP system was run under pure oxygen at 400psig, though the total pressures differ the oxygen pressures are similar and the pressure difference is expected to have little effect. Overall similar conversions are obtainable in the supported system as the homogeneous system.

Previous studies using a supported liquid system for catalysis have shown the importance of the thin film size on the ability of the reaction to proceed.[2,3] A minimum level of hydration is needed to maintain the mobility of the catalyst in the aqueous phase in order to achieve good activity. On the other hand, high levels of hydration lead to pore filling that reduces the interfacial area between the aqueous phase and the substrate leading to a reduction in activity.[2,3] The supported aqueous phase systems for Wacker oxidation require a liquid loading of approximately 10% of the pore volume for maximum activity on alumina support[3].

In this case, the reactant, ethanesulfonic acid, is easily dissolved in the water layer and oxygen more easily diffuses into the system than the olefins used in Wacker oxidation. With the reactant in the aqueous phase, pore flooding is not as large a concern with ethanesulfonic acid oxidation as is the need to hydrate the system to a level that provides sufficient mobility for all species, but pore filling must be considered in attempts to convert alkane feeds. Figure 5.1 shows the effect of initial catalyst hydration on the conversion of the ethanesulfonic acid and selectivity to 2-hydroxyethanesulfonic acid. The initial catalyst hydration is defined as the percent of the pore volume filled with water before the reaction begins. Some water is lost to the vapor headspace by evaporation when heating the system, meaning the actual water loading on the catalyst during reaction is lower. The controlled pore glass needs to be hydrated to between 10 –

18% of the pore volume filled before conversion of ethanesulfonic acid is observed, and selectivity improves up to between 25 – 30% pore volume filled (Figure 5.1). The onset of activity in the Shilov oxidation of ethanesulfonic acid is similar to the loading reported for ethylene oxidation on various supports at 10 vol.% [3] but lower than that required for heptene oxidation[2]. In respect to these observations further experimentation was carried out with a system hydrated to at least 25% of the pore volume filled with water.

Oxygen concentration had little effect on the system. Table 5.2 shows results for increasing the oxygen pressure from 60psig to 500psig. A small increase in conversion is noted between 60psig and 140 psig of oxygen with no additional increase to 250 psig of oxygen. This is similar to Sen's observation in the homogenous system where an increase of the oxygen pressure from 300psig to 1300psig resulted in only a doubling of the reaction rate.[1] Looking at the analogous Wacker oxidation of ethylene on supported liquid phase catalyst, Shaw determined the reaction to be zero order with respect to oxygen.[3] This suggest that in both systems the oxygen reoxidizing the copper species is rapid compared to the other steps of the reaction.

While not affected by the oxygen concentration, the turnover frequency has a strong dependence on the concentration of the organic substrate. Increasing the organic substrate/Pt ratio from 84 to 152 increased the turnovers from 72 to 120, with both reactions reaching around 80% conversion with similar selectivities of approximately 94% to 2-hydroxyethanesulfonic acid after 9 hours. This suggests that little deactivation is occurring in the batch system and in these tests the limit to turnovers is the amount of organic substrate loaded into the system.

Another important aspect of the Shilov oxidation with the Pt/Cu system is the influence of the chloride ion. Similarly to the Wacker oxidation [5], this system requires an excess of chloride ions to reoxidize the platinum species and prevent platinum metal formation, but excess chloride concentration inhibits the organic substrate oxidation. It is presumed that the excess chloride inhibits C-H Bond activation by reducing accessibility of the metal substrate to the substrate. [1] In a similar manner, recent DFT studies by Zeigler have suggested how presence of different platinum species and the amounts of each in the solution can effect the rate of the methane uptake/activation rates. The chloride concentration may cause shifts to larger population of less active species. [6] Figure 5.2 shows the product evolution over time for the batch reaction of the SAP catalysts with Cu/Pt ratios of 10, 26, and 37. Increasing the Cu/Pt ratio in the SAP catalysts slows the reaction — increasing the time before products are observed and increasing the time to reach a similar level of conversion as that observed with the catalyst with Cu/Pt ~10. Another unique feature is the presence of chlorinated products. Sen does not report the formation of chlorinated products in the homogeneous system.[1] However using the SAP catalyst as shown in Figure 5.2, chlorinated products appear to be formed and then are consumed as the reaction proceeds. At a Cu/Pt ratio of 10, chlorinated products are seen from the beginning but only decline over time. At Cu/Pt of 26, there is a quick build-up of chlorinated products that disappears over the rest of the run and at Cu/Pt of 37 the build-up is slowed down as well as the disappearance.

The appearance and disappearance over time of the chlorinated species was not reported in the work on the homogenous system by Sen.[1] The chlorinated species likely arise during the final step of the Shilov mechanism, as shown in Figure 2.2 step 3,

when instead of H_2O, Cl^- acts as the nucleophile in the reductive elimination. As seen in Figure 5.2, increases in the Cu/Pt ratio, and thus increases of the Cl^- concentration in the system, lead to a higher level of chlorinated species observed. The disappearance of the chlorinated species is likely due to hydrolysis. Table 5.3 details chloroethanesulfonate conversion to the desired 2-hydroxyethanesulfonic acid, indicating that 2-hydroxyethanesulfonic acid can be derived via the chlorinated species. The amount of 2-hydroxyethanesulfonic acid arising from oxidation via the Shilov mechanism as opposed to hydrolysis of the formed chloroethanesulfonate was not determined.

The ability of the supported aqueous phase system for Shilov oxidation of ethanesulfonic acid to reach similar conversion levels as the homogeneous system, and Sen's observation for the homogeneous system of ethane being as reactive as the ethanesulfonic acid in solution [1], makes the supported system a good candidate for the direct oxidation of light alkanes to alcohols in a flow reactor. However, using a variety of reaction conditions resulted in no measurable product by GC/MS or offline NMR of captured effluent. The reaction pressure was maintained at 500 psig over all tests with varying oxygen, ethane, and helium concentrations in the range above the upper flammability limit for ethane. A wide range of water feed rates were also used to vary the liquid loading on the catalyst. The catalyst was the 5 wt% metal salt loading with a Cu/Pt ratio of 25. In all instances the catalyst changed color from a light green to grey color, probably indicating the formation of platinum metal. Another sign of the deactivation is the detection of chloride in the trapped effluent by precipitation with silver nitrate addition. It appears that the supported catalyst is losing a large amount of its chloride concentration quickly in the flow setup and the reaction is unable to proceed. In

the Shilov reaction while the conditions are at a mild reaction temperature of 150°C, this temperature is still above the boiling point for any aqueous HCl solution. While the steam fed to the system maintains a vapor pressure of water above the supported film, the feed contains no chloride and thus by equilibrium some of the HCl in the film is being lost to vapor that is then swept from the system in the effluent. In the Shilov system, chloride is released in both the C-H bond activation and the reductive elimination step. These ions are then reused in the oxidation of the cuprous chloride to cupric chloride. However any HCl loss to the vapor phase before the oxidation occurs is swept away with the effluent. The loss of chloride ions leads to the loss of cupric chloride as an oxidant and eventually the Pt(II) species can also be consumed as an oxidant resulting in the formation of platinum metal and shutting down the system. It is plausible that the system actually undergoes a few turnovers which we do not observe and in those processes the chloride is lost

The initial inactivity of the flow system does not preclude this from being a useful catalyst or technique. While probably not advantageous for light alkane oxidation, a system where the chlorine concentration can be replenished by added HCl may prove active for various terminal oxidations. Similarly systems with other ligands that are not swept away like the chloride ions in the Shilov system, either by quicker uptake with the metal centers or less volatility, could work well as a supported system for chemical transformations.

5.3 References

[1] M. Lin, C. Shen, A. Garcia-Zayas, A. Sen, A. J. Am. Chem. Soc. 123 (2001) 1000.

[2] J.P Arhancet, M.E. Davis, B.E. Hanson, Catalysis Letters 11 (1991) 129.

[3] I.S. Shaw, J.S. Dranoff, J.B. Butt, Ind. Eng, Chem. Res. 27 (1988) 935.

[4] J. Byers personal communications, May 2004. Unpublished data.

[5] S.S. Stahl, J.A. Labinger, J.E. Bercaw, Angew. Chem. Int. Ed., 37 (1998) 2180.

[6] H. Zhu, T. Zeigler, J. Organometallic Chem. 691 (2006) 4486

Figure 5.1: Oxidation of ethanesulfonate over various levels of liquid loading on the catalyst

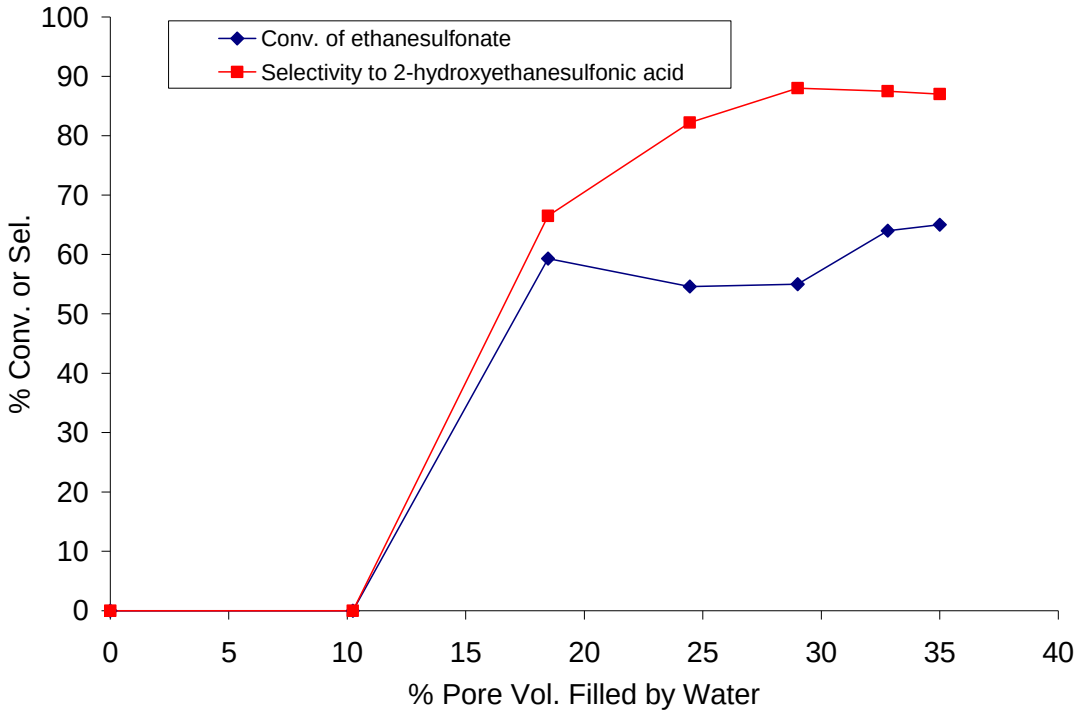

Reactions conditions: Cu/Pt ~10, $C_2H_5SO_3^-$/Pt ~80, 500psig O_2 @ RT, 160°C, 6h

Figure 5.2 Profile of reaction species on a per mol Pt basis over time for varying Cu/Pt ratios

A) Cu/Pt ~10

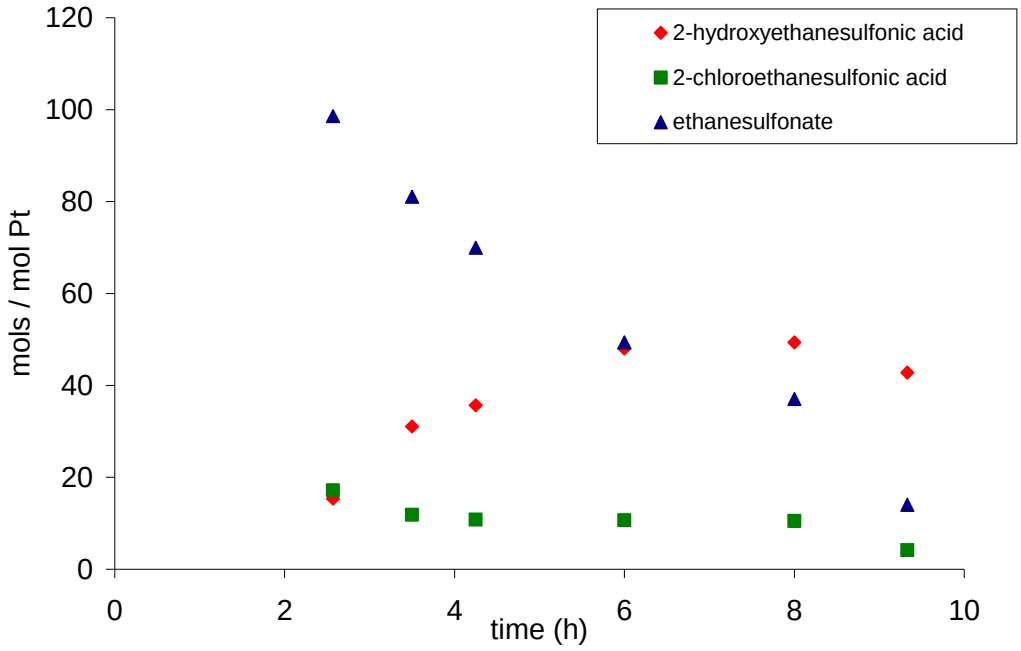

B) Cu/Pt ~26

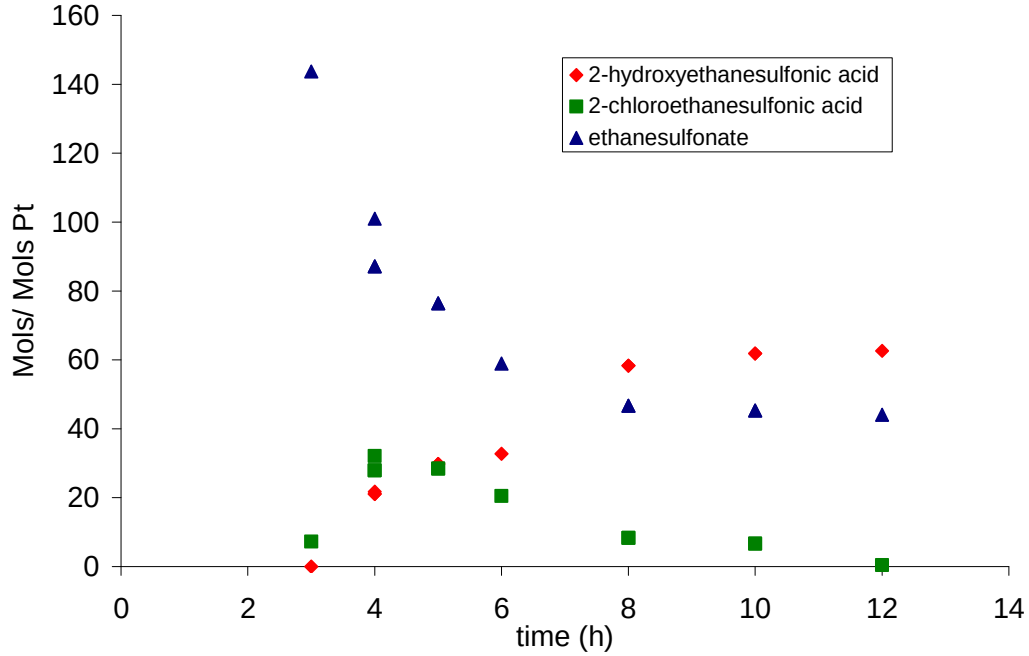

C) Cu/Pt ~37

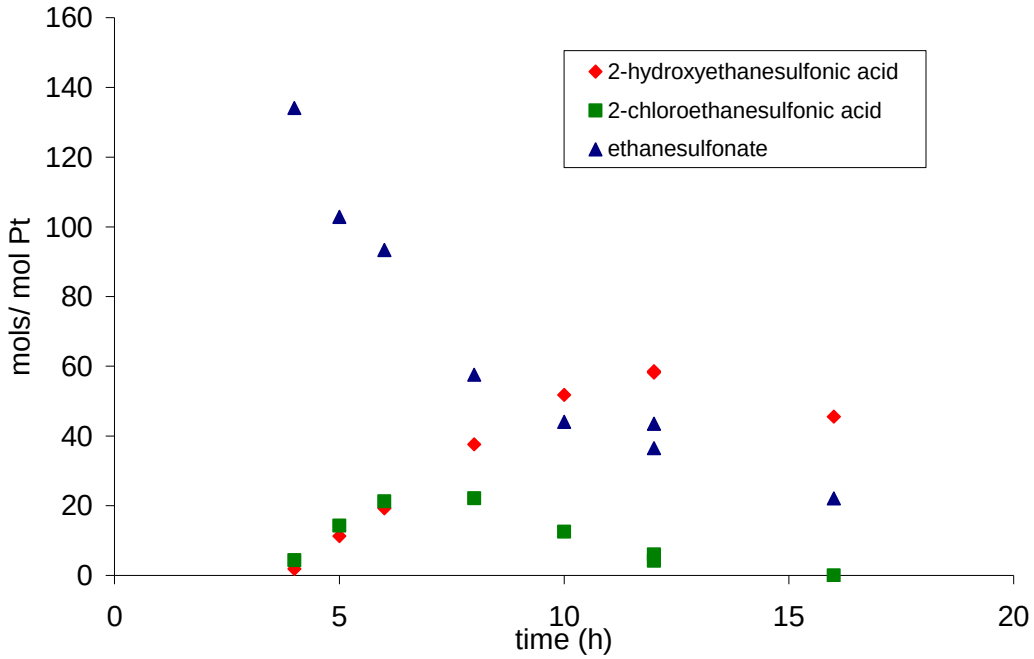
160
140
120
100
80
60
40
20
0
mols/ mol Pt
0
5
10
15
20
time (h)
2-hydroxyethanesulfonic acid
2-chloroethanesulfonic acid
ethanesulfonate

Table 5.1: Comparison of supported aqueous phase Shilov catalyst with the homogenous system

		Reagent Ratios (mol/mol)			Products (% based on total liq. products)							
Catalyst	Type	Substrate/ Pt	Cu/Pt	O_2/Cu	1	2	3	4	5	6	Conv.(%)	TO/Pt
Sen[1]	Homogenous	167	6	203	78	0	19	2	2	0	32	53
Byers[2]	Homogenous	194	7	212	88	tr	0	0	11	tr	61	102
Byers[3]	CPG	82	9	1517	47	45	0	0	0	6	29	24
Carpenter[4]	CPG	152	10	850	76	23	0	0	0	0	33	49

1. 2.0mmol substrate; 2.0ml water; 0.1ml H_2SO_4; 300psi O2; 1200psi N_2; 160°C; 4h. [1]
2. 2.0mmol substrate; 2.0ml water; 160°C; 4h. [4]
3. 0.0109mmol (Pt)/g(CPG); 0.103(Cu)/g(CPG); 0.891(substrate)/g(CPG); 160°C; 4h. [4]
4. 0.011mmol (Pt)/g(CPG); 0.29(Cu)/g(CPG); 1.7(substrate)/g(CPG); 150°C; 4h. – mass loss to vapor phase

Products:

1=$HOCH_2CH_2SO_3^-$ 2=$ClCH_2CH2SO_3^-$ 3 = $(HO)_2CHCH_2SO_3^-$

4=$HOCH_2COOH$ 5=CH_3COOH 6= $CH_3CH(OH)SO_3^-$

Table 5.2: Variation in oxygen pressure in the oxidation of ethanesulfonate on a supported aqueous phase Shilov catalyst

		Reagent Ratios (mol/mol)			Products (% based on liquid products)					
Run	mass used (g)	Substrate /Pt	Cu/ Pt	O_2/ Cu	$HOC_2H_4SO_3^-$	$ClC_2H_4SO_3^-$	other	Conv. (%)	TO/ Pt	% vol Added H_2O
60 psig	.61	77	10	42	87	13	tr	55	42	30
140 psig	.51	77	10	117	87	13	tr	64	50	33
250 psig	.60	77	10	178	86	14	tr	65	50	35
500 psig	.59	77	10	363	78	22	0	62	48	24.5

Table 5.3: Conversion of chlorinated products to desired products over time

Reaction Time (h)	Initial Reagent Ratios					Mass Balance	**Final mols $HOEtSO_3$/ mols Pt**	**Final mols $ClEtSO_3$/ mols Pt**
	Pt mmol/ g cat	Cu mmol/g cat	$ClEtSO_3$ mmol/g cat	Cu mol/ Pt mol	$ClEtSO_3$ mol/ Pt mol			
0	0.0170	0.2130	2.25	12.55	132.39	100	**0.0**	**132.4**
5	0.0170	0.2130	2.25	12.55	132.39	86	**55.2**	**59.2**
10	0.0170	0.2130	2.25	12.55	132.39	86	**105.7**	**8.6**

CHAPTER SIX

CONCLUSIONS ON SUPPORTED SHILOV OXIDATION CATALYST

In Part One three different techniques for creating a heterogeneous catalyst system were investigated. Methods for preparing Wacker oxidation catalysts in the forms of a supported molten salt catalyst [1], as a supported aqueous phase catalyst [2,3], and as an ion-exchanged zeolite[4] were explored. Comparisons of these catalysts under similar reaction conditions for the oxidation of ethene to acetaldehyde were made in a plug-flow reactor system. Due to the need to reach the melting point of the eutectic mixture of KCl and CuCl, the supported molten salt catalyst system required a higher temperature, 195°C, than the supported aqueous phase system or ion-exchanged zeolites, 100°C – 125°C. Also the supported molten salt system showed lower conversion of ethene than those systems (1 – 2% versus 55+ %) and a higher selectivity to chlorinated products (50% versus less than 25% on the zeolites or virtually none in the supported aqueous phase catalyst). The supported aqueous phase system demonstrated the previously reported [2, 3] importance of the concentration of water in the feed stream. Increasing the steam fraction of the feed from .15 to .4 increased the conversion of the ethene from 35% to 87%. The supported aqueous phase catalyst and ion-exchanged zeolites met the criteria of mild operating temperature with good activity and high selectivity toward the desired products.

Attempts were made to use an analogous ion-exchanged zeolite in the Shilov oxidation by changing the $Pd(NH_3)_4Cl_2$ to $Pt(NH_3)_4Cl_2$. Unfortunately over various reaction conditions — increased pressure, various feed concentrations, multiple temperatures, and heeding the lesson of Wacker oxidation, different water concentrations by varying the steam feed — no oxidation products of ethane were detected. The lack of

activity is not from a lack of Pt; following the UV-Vis spectra shows almost complete uptake of the platinum species during the exchange process, much like that reported by Jacobs for the palladium species. [4] Unlike with the Wacker oxidation of ethylene, the use of a Pt(II) species with amine ligands and/or supporting the catalyst in the cages of a zeolite resulted in no products from Shilov oxidation of alkanes or ethanesulfonate. Other attempts to introduce different platinum species were also unsuccessful, as vapor phase deposition of platinum acetylacetonate only resulted in the formation of Pt^0 upon testing.

In the supported aqueous phase system, the homogenous reaction solution that has been shown to work by Sen[5] is dispersed as a thin layer on a hydrophilic support. This allows the system to maintain many of the characteristics of a homogeneous solution by not having to add extra ligands to an organometallic catalyst with which to anchor it, but at the same time massively increasing the surface area for interaction between aqueous and gaseous species. Also it provides the potential to contain potentially corrosive species on the support as opposed to being in close contact with a reactor wall.

Initial work was successful in following Sen [5] in oxidizing the terminal methyl group of ethanesulfonate with dioxygen as the ultimate oxidant, except doing it on the controlled pore glass support. Similar turnovers of the platinum were seen in both systems. Sen achieved 53 turnovers to products of platinum [5] while similar conditions on the supported aqueous phase system saw 62 turnovers on platinum. Higher turnovers of platinum, 102, were achieved in the homogenous system with some changes in reaction conditions. [6] Various reaction parameters were investigated with the ethanesulfonate oxidation to provide guidance for alkane oxidation. As with the Wacker

system, a minimum amount of liquid loading was required to achieve activity, in this case the required loading seems to be between 15 % and 20 % of the pore volume. Similar to Sen [5] little dependence on the oxygen concentration was observed. The platinum species was required to see oxidation. Unlike in Sen's work [5], the SAP catalyst did not require a spike of sulfuric acid in the system to observe oxidation, and the presence of sulfuric acid did not enhance the activity. The increase in chloride concentration by increasing the copper(II) chloride slowed down the reaction and increased initial formation of chlorinated products. However the chlorinated products disappeared with increased reaction time. Some were converted to increasing carbon dioxide concentration in the head space but some were converted to the desired isethionic acid product. This was observed by loading the catalyst with only the chlorinated species and following the conversion to isethionic acid over ten hours. This raises questions as to the true mechanism occurring in the supported system, as there may be a second pathway to the product than directly through the Shilov mechanism.

With a successful oxidation of ethanesulfonate on the supported aqueous phase system, trials were run for the oxidation of ethane in a plug-flow reactor system. Using the lessons learned from both the Wacker oxidation and the ethanesulfonate work, reaction conditions were varied within safety limits and no oxidation was observed. The catalyst changed color from a light green to a grey color, leading to suspicion about the formation of Pt^0. At the same time chloride ions were detected in the trapped effluent. It seems the catalyst, when used in the flow system, lost chloride ions rapidly leading to deactivation before any products were detected. In the batch system with

ethanesulfonate, it is likely that this was not as noticeable, as chloride loss was minimized by using a static system.

While the oxidation of a small alkane on heterogeneous system in a flow mode was not achieved, a supported system catalyst that performed similar to the homogeneous system was demonstrated for ethanesulfonate oxidation. This system remains a highly viable route for creating a heterogeneous system provided a catalyst species can be identified that overcomes the problem of ligand loss. Similarly a future direction could be in the application of this catalyst to more specialty chemical applications such as a liquid/liquid phase oxidation in batch systems where the mobility of the chloride ion and its corrosiveness can be better contained.

References

[1] V. Rao, R. Datta, J. of Catal. 114 (1988) 377.

[2] J.P. Arhancet, M.E. Davis, B.E. Hanson, Catalysis Letters 11 (1991) 129.

[3] I.S. Shaw, J.S. Dranoff, J.B. Butt, Ind. Eng, Chem. Res. 27 (1988) 935.

[4] M. Lin, C. Shen, A. Garcia-Zayas, A. Sen, A. J. Am. Chem. Soc. 123 (2001) 1000.

PART TWO

INFLUENCE OF STRUCTURAL FEATURES ON ZEOLITE CHARACTERIZATION BY CONSTRAINT INDEX TESTING

CHAPTER SEVEN

CONSTRAINT INDEX TESTING OF ZEOLITES

7.1 Constraint Index Test

Zeolites are microporous, aluminosilicate materials with a defined three-dimensional framework and uniformly sized pores. These materials have been used in a wide array of fields such as laundry detergents, oil and petrochemical industry, adsorbents, catalysis, separations, and agriculture.[1] The amount of research into zeolites can be demonstrated by a simple search for the term zeolite in SciFinder Scholar — this will return over 4,000 publications for each year in the current decade. These structures are both naturally occurring and synthetically produced. There are currently 191 registered structures for zeolites, of which 15 have been added in the last two years [2].

As the library of zeolite and zeolitic materials has expanded over the years, many techniques to determine both structure and shape-selectivity of these materials have been developed. One of the first described was the Constraint Index (CI) test.[3] The CI test is based on the competitive cracking of 3-methylpentane and n-hexane. The CI is calculated by Equation 1.(*X* denotes the fractional conversion of each reactant.)

$$\mathrm{CI} = \frac{\log\left(1 - X_{\text{n-hexane}}\right)}{\log\left(1 - X_{\text{3-methylpentane}}\right)} \qquad \textbf{(1)}$$

Thus, it is proportional to the observed cracking rate constants of n-hexane to 3-methylpentane.

In describing the CI test, Frillette and colleagues were looking for an easy test to probe the shape selectivity of new materials and to gain insights into the pore structure of those materials. From Equation 1, it can be seen that the more selective a material is for

cracking n-hexane the higher the CI for that material. On the basis of CI, Frillette classified materials with a CI greater than 12 as small pore, that is, having ≤ 8 - ring pores; CI less than 1 are defined as large pore, with ≥12 - ring pores; and materials with CI between 1 and 12 as intermediate pores, having 10 - ring pores.[3] Table 7.1 lists various zeolites and their CI values, depicting the different classifications.

Since the introduction of the CI test multiple other catalytic tests have been used to probe the shape selectivity and structure of zeolites from Modified Constraint Index[4], the Spaciousness Index [5], the Shape Selectivity Index with m-xylene isomerisation [6], the alkylation of meta-diisopropylbenzene [7], and the conversion of methanol to larger hydrocarbons [8] as examples. However even with all of these tests, the CI test is the one used as a key characterization in many patents for new materials and for choosing materials in patents for new processes. Similarly it is used to help determine the unknown structures of novel materials, such as in the case of IM-5 and SSZ-57.[9] With the use of the CI test it is important that it be correct and understood why materials may deviate from the trends so that researchers are not lead to incorrect conclusions on the basis of the test. Catalytic tests are only one technique and provide a piece of information to the puzzle for understanding structures, but they can sometimes be ambiguous.

For example, the decane test reaction suggested the structure of MCM-22 had both 10 -ring and 12 -ring pores that later were determined to both be 10-ring pores.[10] There have been several structures whose CI results deviate from the classifications defined. In the earlier study by Zones and Harris it had been shown that some zeolites with known portal sizes have CI results inconsistent with the structures [11] and had

shown catalytic selectivities of larger pore materials. As has been mentioned before, SSZ-35 seemed to show this anomalous behavior with Constraint Index selectivities favoring the reaction of the larger 3-methylpentane, even though the portal for the structure is closer to 5.6Å [12], not much larger than ZSM-5. Similarly SSZ-28 also falls outside the expected range based on the 8-ring pores in the structure (Figure 7.1).

7.2 Structures Containing Internal Cages

In a number of the materials in the Zones/Harris study, where there were deviations from expectations, it appeared that the structures, once known, had portals that opened into larger cages. This is not so surprising, in retrospect, as a number of new high silica zeolites have been discovered with the use of rigid polycyclic quaternary ammonium guest molecules. A recent review surveys some of this chemistry and shows the molecular modeling to illustrate the favorable energetics in locating a close host wall structure around the organo-cation guest [13]. Indeed, in terms of the details of the favorable energetics of fit, Burton et al. have recently shown interesting cage-structure selectivity for the formation of zeolite SSZ-73 [14] over another zeolite cage-structure with the use of one of two isomeric configurations for the guest molecule [15].

In this study we focus on some of these types of materials and while there is a central cage feature for locating the guest organo-cation, the consequences (if we can look at the nucleation and crystal chemistry this way for a moment) are that some pores are created as part of the unit cell. In SSZ-35 there are 10-ring portals that connect the large, shallow, 18-ring cages. Likewise SSZ-25, once calcined, has 12-ring cages that are accessed by 10-ring portals. Figure 7.2 depicts these structures with their 10-ring pores

opening into larger cages. SSZ-23 with a very unusual structure of 9 and 7-rings is still a zeolite with a cage large enough to accommodate the N,N,N-1-trimethyl adamantammonium cation [16]. SSZ-28, with the DDR structure, has 8-ring portals but they traverse through larger cages formed in surrounding the bicyclic Structure Directing Agent (SDA) used in the synthesis[13]. Figure 7.3 shows the 4 different SDA used in synthesizing the cage-based zeolites in this study.

If one is crystallizing zeolites with the SDA at the center of a cage, it is natural to ask whether the external surface, at the point of terminating the crystallization, is actually not covered by "completed" cages but possibly fragments of cages. Part of the goal on the present study is to determine if such open cages exist after thermal removal of the SDA guest. And do these cages lead to non-selective surface-cracking reactions that belay the shape-selectivity that might have otherwise been observed from the pore system alone? This question had to be asked, in light of the unusual behavior of SSZ-25, whose catalytic selectivities were difficult to understand, before a structure solution came forth for the **MWW** topology [17]. In this material there appeared to be large pore zeolite selectivity that switched to intermediate pore behavior over time. We describe that, once again, in our Constraint Index studies here. Later it came to be appreciated that the material had, in essence, at least 3 types of sites for catalysis [18]. There is a hindered 10-ring which runs through the layers of the material. Cross-linking the layers leads to the creation of large cages bounded by 10-rings (larger than those within the layers). But either an incomplete cross-linking or the purposeful attempt to expose the "half-cavities" at the surface of the layers leads to a third site. While one might expect there to be less, or no shape-selectivity for these "cups" on the surface, the work of Corma on studying

the selectivity for benzene alkylation — once the layered had been moved apart (ITQ-2 material) — showed shape-selectivity was nonetheless maintained [19]. So a component of our study here was to remove such exposed surface sites in all materials and answer the question as to how shape-selective behavior is affected.

7.3 Zeolite Catalyzed Hydrocabon Cracking

The Constraint Index test is based on an observed relationship of the apparent cracking rate of 3-methylpentane and n-hexane in a competitive reaction. While this study focuses on the CI test, and as such the apparent cracking rates observed on the various zeolites, one should be mindful of the multiple aspects that go into the observed cracking of hydrocarbons over acid sites on zeolite structures. Understanding the aspects of cracking from reactant adsorption to reaction mechanism to product desorption has been the focus of much work.[20 – 28] In hydrocarbon cracking, the branched isomer has a higher intrinsic reactivity than the linear isomer.[3] Any CI greater than 1 would represent a selective influence of the zeolite on the reaction.

One method by which a zeolite can impose shape selectivity on a reaction is through reactant selectivity excluding large reactants while smaller reactants can enter the structure [27] or through significant differences in diffusion into and through the structure. Work on ZSM-5 has shown the cracking rate of n-hexane and 3-methylpentane was insensitive to crystal size [3, 28] and the diffusivities of the two reactants were similar [28]. Since the cracking rates of both reactants were not affected by crystal size on ZSM-5, medium and large pore zeolites do not impose significant transport limitations or large differences in reactant diffusivities in the CI test; however, for smaller pore

zeolites the influence of reactant selectivity and reactant diffusivities must be considered.

Another form of shape selectivity a structure can provide is a transition-state selectivity in which the structure has an effect on the transition states of the reaction mechanism by either sterically hindering the transition state [27] or by effects on entropy and enthalpy factors [26]. Catalytic cracking of alkanes has been shown to proceed through two mechanisms, either monomolecular cracking or bimolecular cracking [20 – 26]. In the monomolecular mechanism, a single reactant molecule undergoes a C-C bond cleavage on an acid site and desorbs to create an olefin and paraffin and regenerate the acid site. [23] In the bimolecular pathway, a carbenium ion left on the site reacts with another reactant molecule to form cracking products and leave a carbenium ion on the surface. [23] It has also been suggested that the intermediate is a covalent alkoxide species. [21] In either case, a transition-state is required for these mechanisms. The biomolecular mechanism would be more susceptible to steric restrictions as more space is needed for a reactant molecule to interact with a surface species. The biomolecular mechanism is favored at lower temperatures and higher surface concentrations of alkanes.[20] The increasing contribution of the monomolecular mechanism with increasing temperature has been credited with the decrease in CI value with increasing temperature observed on ZSM-5. [3] Several studies have shown how structural effects on hydrocarbon conversions over zeolites extends beyond steric restrictions.[25,29 – 32] Bokhoven showed the difference in observed activity for n-hexane monomolecular cracking over several structures arises in large part from the difference in the heat of adsorption which increases with decreasing pore size.[29] Earlier work by Lercher detailed that this relationship between increasing pore size and decreasing heat of

adsorption, as well as the unhindered adsorption of singly branched alkanes, is limited to pore sizes of 0.5nm and greater.[30] In another example, Bokhoven demonstrates how the ability of geometrical and electronic environment around the active site influences the stability of alkoxide species in the dehydrogenation of propane and as such has a strong influence on the observed activity, as the rate-limiting step is the desorption of that species.[31] In a similar observation of structural effects on transition states, Iglesia expounds upon the cracking of propane and n-butane in the 8-member ring side pockets of H-MOR and explains the entropy gains from the partial transition confinement in the side pockets that lead to a decrease in the transition state free energy.[26] Zeolites containing cages can demonstrate transition-state selectivity that differs from other structures with similar sized pore windows by having less steric hindrance in the cage or almost no steric hindrance in external surface features.

Work by Corma [24] and van Santen [22] have shown the determination of cracking mechanism for hexane cracking is very difficult if at all possible and open to different interpretations based on reaction results alone, since the complex set of possible secondary and side reactions can lead to similar results for multiple schemes. Based on the work of Corma [22] and van Santen [24], this study has not attempted to quantify the contributions of each reaction mechanism on the CI test. Instead the conditions for the CI test on the medium and large pore zeolites are performed at conditions (i.e., low temperature, 330°C, and high hydrocarbon partial pressure, 35 kPa) that strongly favor bimolecular cracking. These conditions are similar, including contact time, to those shown by Lunsford [20] and are predominately bimolecular cracking for BEA* and ZSM-5 (and — due to the similar pore window size and large internal cages — should

also be bimolecular for SSZ-25 and SSZ-35). The temperature in the CI test on the smaller pore zeolites had to be raised to achieve reasonable conversions and thus may have increased influence from the monomolecular mechanism on the results.

7.4 **References**

[1] T. Maesen, B. Marcus, in H.V. Bekkum, E.M. Flaningen, P.A. Jacobs (eds) Studies in surface Science and Catalysis 137, Elsevier Science, 2001, p.1

[2] IZA Structure Commission, *Framework Type Codes*, accessed 4/15/2009 at www.iza-structure.org

[3] V.J. Frillette, W.O. Haag, R.M. Lago, J. Catal. 67 (1981) 218.

[4] J.A. Martens, M. Tielen, P.A. Jacobs, J. Weitkamp, Zeolites 4 (1984) 98.

[5] J. Weitkamp, S. Ernst, R. Kumar, Appl. Catal. 27 (1986) 207.

[6] F. Joensen, N. Blom, N.J. Tapp, E.G. Derouane, C. Fernandez, Stud. Surf. Sci. Catal., 49(A) (1989) 1131.

[7] M.H. Kim, C.Y. Chen, M.E. Davis, ACS Symp. Ser. 1993, 517, 222.

[8] L-T Yuen, S.I. Zones, T.V. Harris, E.J. Gallegos, A. Auroux, Microporous Mater. 2 (1994) 105.

[9] S.I. Zones, C.Y. Chen, A. Corma, M.T. Cheng, C.L. Kibby, I.Y. Chan, A.W. Burton, J. Catal. 250 (2007) 41.

[10] W. Souverijns, W. Verreist, G. Vanbutsele, J.A. Martens, P.A. Jacobs, J. Chem. Soc., Chem. Commun., 14 (1994) 1671.

[11] S.I. Zones, T.V. Harris, Micro. Meso. Mater. 31 (2000) 35.

[12] P. Wagner, Y. Nakagawa, G.S. Lee, M.E. Davis, S. Elomari, R.C. Medrud, S.I. Zones, J. Am. Chem. Soc. 122 (2000) 263.

[13] A.W. Burton, G.S. Lee, S.I. Zones, Micro. Meso. Mat. 90 (2006) 129.

[14] D.S. Wragg, R.E. Morris, A.W. Burton, S.I. Zones, K.K. Ong, G.S. Lee, Chem. Mat. 19 (2007) 3924.

[15] C. Kim, S-J. Hwang, A.W. Burton, S.I. Zones, Micro. Meso. Mat. 116 (2008) 227.

[16] M.A. Camblor, M.J. Diaz-Cabanas, J. Perez-Pariente, S.J. Teat, W.W. Clegg, I.J. Shannon, P. Lightfoot, P.A. Wright, R.E. Morris, Angew. Chem. Intl. Ed. 37 (1998) 2122.

[17] M.E. Leonowicz, J.A. Lawton, S.L. Lawton, M.K. Rubin, Science, 264, (1994) 1910.

[18] P. Matias, J.M. Lopes, S. Laforge, P. Magnoux, M. Guisnet, F.R. Ribeiro, Appl. Catal. A: Gen. 351 (2008) 174.

[19] A. Corma, V. Fornes, S.B. Pergher, Th.L.M. Maesen, J.G. Buglass, Nature 396 (1998) 353.

[20] S. Kotrel, M.P. Rosynek, J.H. Lunsford, J. Phys. Chem. B 103 (1999) 818.

[21] A.M. Rigby, G.J. Kramer, R.A. Van Santen, J. Catal. 170 (1997) 1.

[22] M.V. Frash, R.A. Van Santen, Topics Catal. 9 (1999) 191.

[23] A. Corma, A.V. Orchilles, Micro. Meso. Mat. 35-36 (2000) 21.

[24] A. Corma, P.J. Miguel, A.V. Orchilles, J. Catal. 172 (1997) 355.

[25] A. Bhan, R. Gounder, J. Macht, E. Iglesia, J. Catal. 253 (2008) 221.

[26] R. Gounder, E. Iglesia, J. Amer. Chem. Soc. 131 (2009) 1958.

[27] S. Csiscery, Zeolites 4 (1984) 202.

[28] W.O. Haag, R.M. Lago, P.B. Weisz, Faraday Discuss. Chem. Soc. 72 (1981) 317.

[29] J.A. van Bokhoven, B.A. Williams, W.Ji, D.C. Koningsberger, H.H. Kung, J.T. Miller, J. Catal. 224 (2004) 50.

[30] F. Eder, J.A. Lercher, J. Phys. Chem. B 101 (1997) 1273.

[31] B. Xu, C. Sievers, S.B. Hong, R. Prins, J.A. van Bokhoven, J. Catal. 244 (2006) 163.

[32] Q.L. Wang, M. Torealba, G. Giannetto, M. Guisnet, G. Perot, M. Cahoreau, J. Caisso, Zeolites 10 (1990) 703.

Figure 7.1: Examples of two structures whose CI values fall outside expected ranges for their pore size

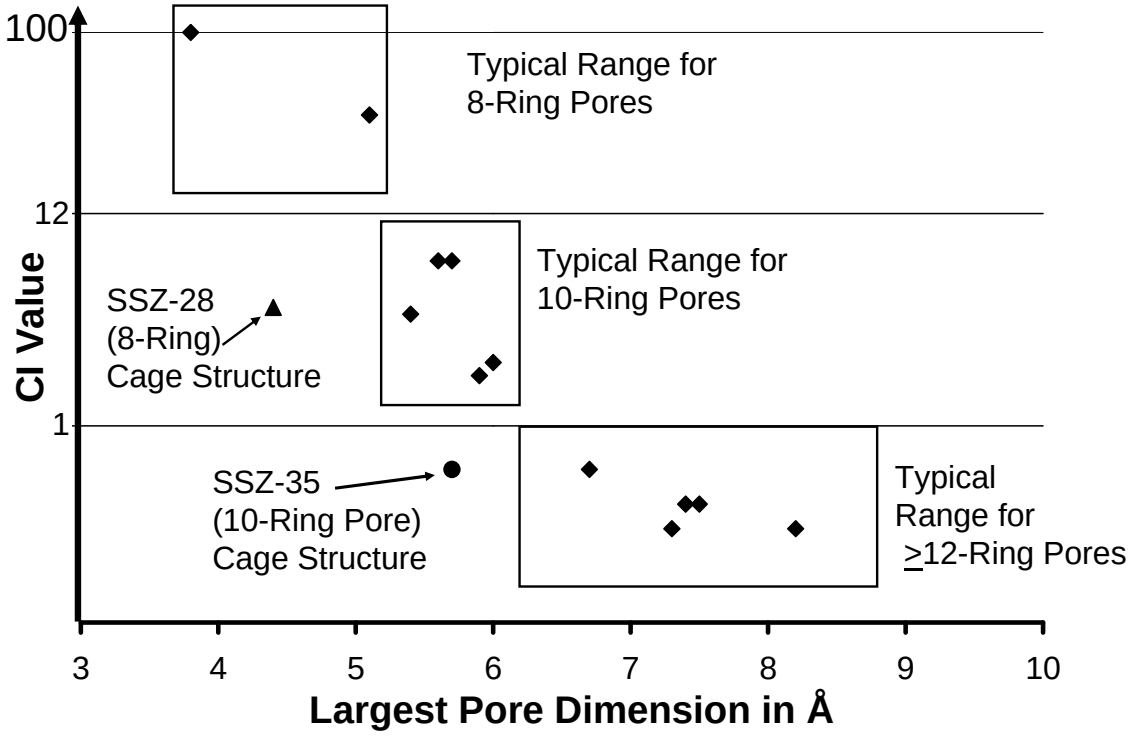

Figure 7.2: Examples of structures (a) STF, (b) STT, (c) MWW and (d) DDR with pores opening into larger cages along with (e) MFI and (f) BEA as comparisons of structures without cages

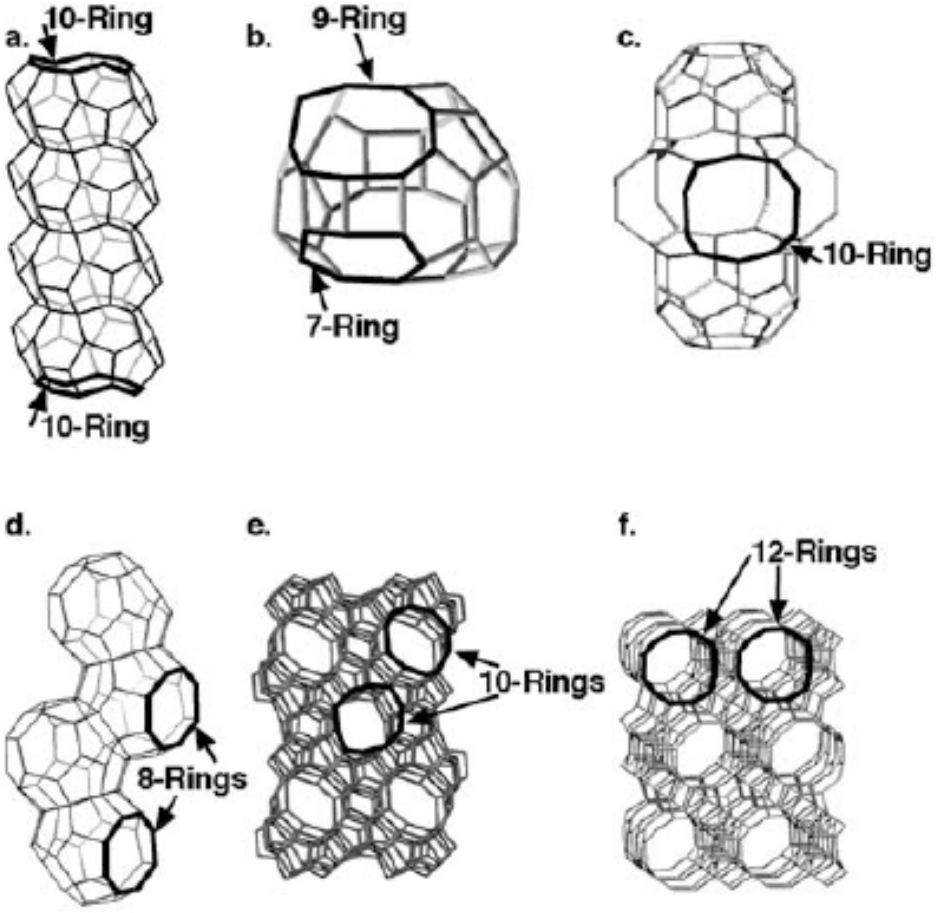

Figure 7.3: Structure Directing Agents used to make the 4 structures with cages in Figure 7.2. SSZ-35 (STF), SSZ-23 (STT), SSZ-25 (MWW) and SSZ-28 (DDR)

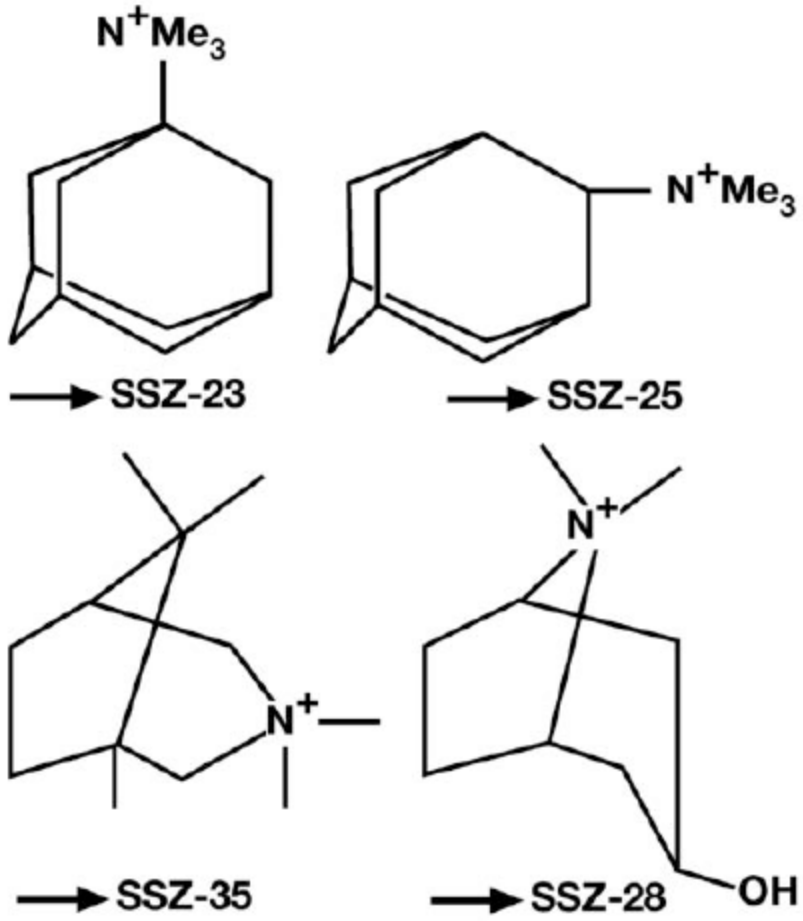

Table 7.1: Examples Constraint Index Values

Zeolite	Pore Apertures	CI
SSZ-13	8-ring	>100
Erionite	8-ring	38
ZSM-23	10-ring	10.6
SSZ-20	10-ring	6.9
ZSM-5	10-&10-ring	6.9
EU-1	10-ring	3.7
ZSM-12	12-ring	2.1
SSZ-31	12-ring	0.9
LZY-82	12-rings	0.4
CIT-5	14-ring	0.4
SSZ-24	12-ring	0.3
UTD-1	14-ring	0.3

CHAPTER EIGHT

EXPERIMENTAL METHODS FOR INVESTIGATION OF CONSTRAINT INDEX TESTING

8.1. Zeolite Synthesis

The zeolites used in the study were synthesized at Chevron by the following procedures in all cases except for the Beta zeolite. This material was obtained from the TOSOH Corporation as product number HSZ930NHA still containing the structure-directing agent. Unless specified, the BEA* sample was calcined upon receipt and 2 ion-exchanges with Ammonium nitrate (95 °C, 2 hours) were performed before use.

ZSM-5

In a 23 ml Teflon Cup for a Parr 4845 reactor the following set of reagents were combined. 0.11 grams of Reheis F-2000 alumina hydroxide gel (25% Al) was dissolved into a basic solution of 1.9 grams of 40% tetrapropylammonium hydroxide, 3.35 grams of 1 N NaOH, and 1 ml water. Once the solution was clear, 4.5 grams of Ludox AS-30 was stirred in. The reactor was closed, loaded onto a spit in a convection heated oven and tumbled while being heated at 170 ºC for 5 days. The product was collected upon cooling and verified to be ZSM-5 by XRD analysis. The product was then given a calcination to 595 ºC by a program of heating at 1ºC/min to 120 ºC (hold for 2h), at 1 ºC/min to 540 ºC (hold for 5h), and at 1 ºC/min to 595 ºC (hold for 5h) to remove the SDA. After which, 2 ion-exchanges with ammonium nitrate solution (95 ºC, 2 hours each) were performed before use in catalytic studies.

SSZ-25

The sample of SSZ-25 used in this study came from a 5 gallon preparation of the material using a mixed SDA systems of N,N,N, 2-trimethyladamantammonium

hydroxide (see Fig. 7.3) and piperidine as a pore filler.[1] A similar post–crystalllization was provided except the SSZ-25 is given 4 ion-exchange treatments after the calcination.

SSZ-23

A reaction was set up as in ZSM-5 above with the following reagents and quantities. For Reheis F-2000 we dissolved 0.03 grams into a solution of 3.75 mMoles of N,N,N 1trimethyl adamantammonium hydroxide (Fig. 7.3) in 7 ml of water. An additional 4.5 ml of water with 10-4 Molar concentration of methylene blue was added in [2]. 1.2 grams of 1N KOH solution were added. Once clear, 0.90 grams of Cabosil M-5, fumed silica (~ 15 mMoles) were stirred in and the reactor was given 3% seeds of SSZ-23 [19] and heated at 160 ºC and 43 RPM for 7 days. The product work-up was similar to that for ZSM-5.

SSZ-28

In a manner similar to the ZSM-5 synthesis, the following reagents were mixed. 3.25 mMoles of N-methyl tropinium hydroxide (Fig. 7.3) in 10ml of water is given 1.5 mMoles of NaOH . Y zeolite is added as an AL source for the reaction (LZY-52 which has about 16 wt % Al2O3). 0.76 grams of Cabosil M5 was stirred in and the reaction was run at 160 ºC and 43 RPM tumbling for 6 days. The work-up of this material differs from the others. The washed crystalline solid was analyzed and found to be all SSZ-28. But as a precaution, since Y zeolite is employed in the synthesis, we degraded any remaining trace Y by heating the solids in 10ml N HCl/gm zeolite material at 95 ºC in a closed reactor for 2 days. The product was then washed and calcined and ion-exchanged as above. This process may remove any surface sites in the SSZ-28 as well, prior to our surface studies.

SSZ-35

The sample of SSZ-35 was taken from a batch made in a 1 gallon reactor run at 160 ºC, 75 RPM for a course of 16 days. The ratio of reagents was as follows: The organo-cation to SiO2 ratio was 0.10 with the reagents being the SDA from pentamethyl (1,6,6,8,8,) bicyclo[3.2.1]-6-ammonium-octane (Fig. 7.3) and Ludox AS-30 (30 % SIO2). SiO2/Al2O3 = 35 with Reheis F2000 as Al source. KOH/SiO2 = 0.20 and H2O/SiO2 = 35.

8.2. External Surface Modification

In several cases the samples' external surfaces were dealuminated following the procedure described by Breck and Skeels[3] using an aqueous ammonium hexafluorosilicate treatment. Samples were taken before calcinations to maintain the SDA inside the structure. 2g of zeolite were stirred in 50ml of an aqueous ammonium acetate solution (2M, 75 °C). Separately, 1.5g ammonium hexafluorosilicate was dissolved in 50ml of water. The ammonium hexafluorosilicate solution was added drop wise over 3 hours to the zeolite mixture once the mixture had reached 75° C. After addition of the ammonium hexafluorosilicate solution was complete the mixture was heated to 95 °C and stirred with condenser for 12 hours. The zeolite was then filtered from the mixture and washed with a minimum of 500ml hot water before air drying.

8.3 Reactivity Tests

Reactivity was tested in by both hydrocarbon cracking and isopropanol dehydration. Samples for reaction tests were prepared by pelletizing and then crushing

that pellet of either the acid or NH4+-form of the zeolites. The crushed samples were sieved to collect the 20 – 40 mesh fraction. Typically 0.50g (~1ml) of sample was loaded into the reactor tube packed between glass wool. The sample was then heated to 350 °C under an argon flow of 25cm^3/min for at least 4 hours before reactions commenced.

All reactions were performed in a BTRS Jr. Reactor (Autoclave Engineers, see Figure 8.1 for reactor schematics) equipped with a ½-inch stainless steel reactor tube. The system also has a reactor bypass loop allowing equilibration of the feed stream in the system before introducing the feed to the catalyst. The hydrocarbon feeds for both tests were fed as a liquid by syringe pump into a mixing assembly where it was vaporized with a sweep gas of 5% argon in helium (AirLiquide, 99.999%) in a mixing assembly at 150 °C. The n-hexane, 3-methylpentane, and isopropanol feeds were all used as purchased form Sigma-Aldrich with purities greater than or equal to 99.9%. The helium/argon feed was controlled by a Brooks Instrument mass flow controller and the hydrocarbons by the Harvard Apparatus syringe pump. The reactor effluent was fed directly to a multi-port valve for gas sampling. The product lines from the reactor and the sample valve were heated to approximately 150^{o}C to prevent liquid condensation. The product analysis was done by GC/MS (Agilent GC 6890N/MSD 5973N) utilizing a capillary column (HP Plot Q). Samples were run at a temperature program of 150^{o}C for two minutes (to allow gas sampling) and then heating to 175^{o}C at 2.33^o/min Products were identified from the GC/MS results by both the MS results for each peak as well as retention times from injections of individual components purchased from Sigma-Aldrich (99%+ purity). The retention times were argon at 1.3 min, methane at 1.35min, ethene at 1.44 min, ethane at 1.54min, propene at 1.8min, propane at 1.87min, isobutane at 2.63,

isobutene at 2.73min, n-butane at 2.93min, n-butene at 3.02, n-pentane at 5.64min, 2mehtylbutane at5.1 min, n-hexane at 9.49min and 3-methylpentane at10.3min. The results were quantified using the argon in the He/Ar sweep gas as an internal standard. Calibration curves on the basis of mols product/mols Ar vs. MS counts product/MS counts of Ar for each of the products were generated by flowing various concentrations of the known product mixtures with various sweep gas flow rates through the system in bypass mode.

Typical Constraint Index test and single reactant cracking conditions were a reaction temperature of 330 °C and atmospheric pressure with 0.5g of zeolite. The reactant liquid feed was at a LHSV of 1.67h-1. Isopropanol dehydration used a lower temperature of 150°C. For the Constraint Index test a mixture of 50mol% n-hexane and 50mol% 3-methylpentane was used. These conditions were adjusted to try and reach conversions between 10 – 60% when possible for the Constraint Index test.

8.4. Zeolite Characterization

Zeolite structures were determined and monitored powder X-ray diffraction on a Scintag XDS 2000 diffractometer. Micropore volumes of the zeolites were measured by nitrogen adsorption on a Micromeritics ASAP 2000 instrument. SEM on a LEO 1550 VP field emission scanning electron microscope was used to measure crystal size. Elemental analysis data for calculating the silicon to aluminum ratio (SAR) of the bulk material were obtained from Galbraith Analytical in Knoville, TN, utilizing inductively coupled plasma–optical emission spectroscopy (ICP-OES). A Netzsch STA 449C Jupiter system was used to record simultaneous thermogravimetric analyses (TGA) and differential

scanning calorimetry (DSC). Samples were loaded into Al_2O_3 crucibles and heated to 900^oC at 5 K/min under 50mL/min inert gas. The TGA/DSC measurements were utilized for measuring at what temperature SDA degradation began and the mass of carbon-species built up during cracking reactions. The measurements of surface compositions were made using a commercial XPS, an Ulvac Phi Quantera Scanning Microprobe. The particles making up the samples were like small grains of sand of dimension approximately 0.5 – 1.5 mm, and closely packed for analysis. The X-ray spot defined the analysis area, a rectangle 1.4mm x 0.1 mm, and so many analyses sampled more than one particle. The scans were made with a nominal spectral resolution of 1.05 eV. For all samples multiple analysis areas were scanned, and the tabulated data represent the determined average and standard deviation. The XPS raw signal intensities were normalized using empirical sensitivity factors by standard XPS data handling software, and compositions are given in atom-%.

8.5. n-Hexane and 3-Methylpentane Adsorption

Adsorption of n-hexane and 3-methylpentane was carried out using a Cahn C-2000 balance couple with a computer interface previously described in the literature [4]. Approximately 20mg of sample was dehydrated in vacuum at 450 °C for 1 h prior to the adsorption. The relative partial pressure P/Po of both n-hexane and 3-methylpentane was kept at ~0.3 during the adsorption of each individually. The measurements were made at room temperature.

8.6 References

[1] S.I. Zones, S.J. Hwang, M.E. Davis, Chemistry — A European Journal 7 (2001) 1990.

[2] S.I. Zones, Y. Nakagawa in: L. Bonnevoit, S. Kaliaguine (Eds.) Zeolites: A refined Tool, Elsevier, Amsterdam (1995) 45.

[3] D. Breck, G. Skeels, US patent 4 503 023 (1985) to Union Carbide Corporation.

[4] C.Y. Chen, S.I. Zones, Micro. Meso. Mat. 104 (2007) 39–45.

Figure 8.1: Flow diagram of BTRS Jr. reactor system for ispropanol dehydration and hydrocarbon cracking

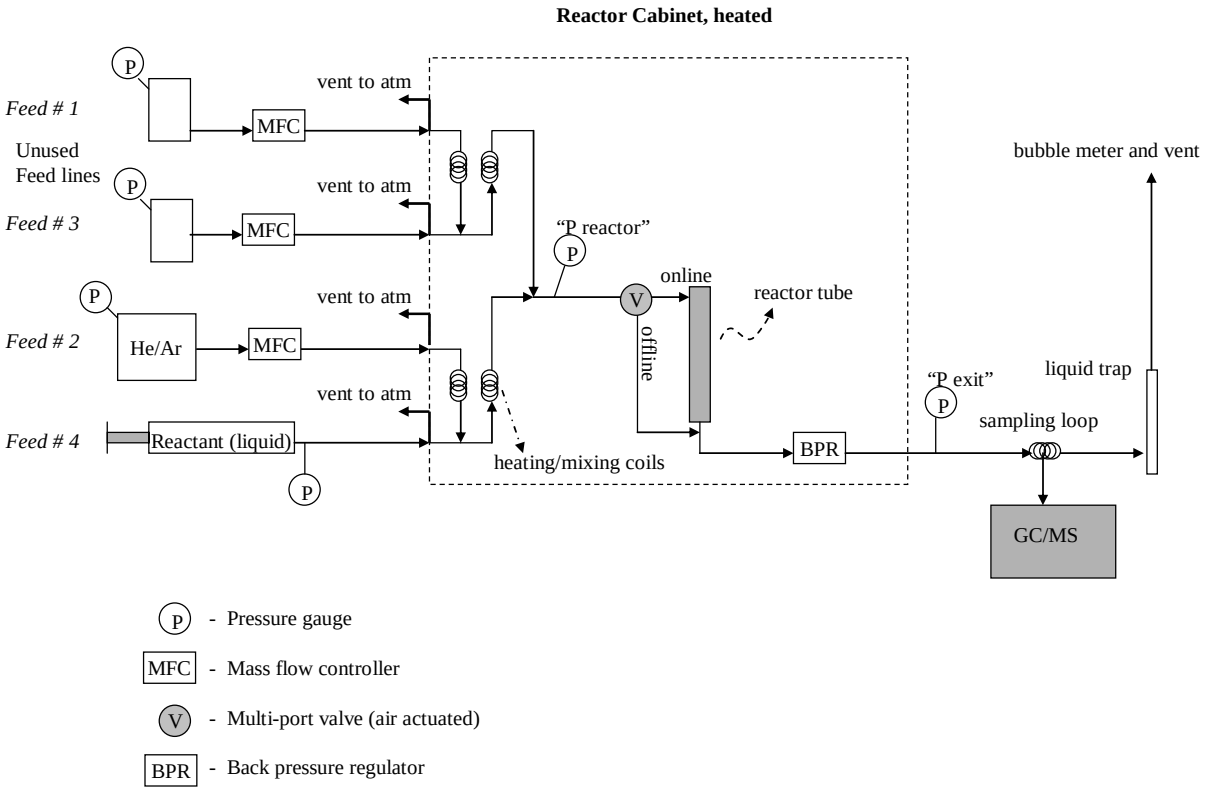

CHAPTER NINE

EFFECT OF EXTERNAL SURFACE ACTIVITY ON CONSTRAINT INDEX TESTING

When faced with reduced selectivity in a shape-selective reaction, one must consider situations that would reduce the selective influences, whether from reactant selectivity imposed by a pore size blocking large reactants, or steric constraints at the active site limiting the viable transition-states. In zeolites these shape selective limits arise from the majority of active sites being internal to the pore structure. However, sites located on the external surface would not be restricted by the structure and have less shape selective limits. In fact for small crystal zeolites, the external surface can have an important contribution to activity especially for reactions that are either very rapid or highly diffusion limited.[1] For the **MWW** structure (the structure of SSZ-25), incomplete cages have been shown to form cup-like hemicages on the external surface.[2] These cups on the surface have been shown to be active in the cracking of 1,3-diisopropylbenzene and vacuum gasoil on ITQ-2 [3] and in methylcyclohexane transformations on MCM-22 [4].

The influence of the external surface on Constraint Index characterization of structures containing large cages waas investigated in this work by passivating the external surface. Reduction in external surface activity was accomplished by removal of external active sites by dealumination. The dealumination of zeolites can be accomplished through multiple techniques, many detailed in review on the subject by Beyer.[5] Hydrothermal treatment and acid leaching result in increased defects and mesopores.[5] Isomorphous subsititiution by $SiCl_4$ must be performed at elevated temperatures around 500°C which would degrade and lead to loss of the SDA[5]. Aqueous isomorphous substitution with ammonium hexafluorosilicate, on the other hand,

proceeds at temperatures near 100°C[6]. This temperature allows the SDA to remain in the pores, limiting the dealumination to the external surface if performed before calcinations. As such, ammonium hexafluorosilicate treatment was utilized to passivate the external surface. This process is shown in Figure 9.1

9.1 Characterization

Samples of ZSM-5, BEA*, SSZ-25, and SSZ-35 were dealuminated following the process of Breck and Skeels[6] except the SDA was left in the structure during the modification to block the interior pores and limit the dealumination to the external surface. Table 9.1 details the characterization of each sample in both the parent zeolite and the dealuminated samples. XPS analysis of the external surface demonstrates a larger increase in the Si/Al ratio for the external surface than the change in the bulk Si/Al. It should be noted the XPS technique samples a near surface depth (2-20nm, or the equivalent of a few unit cells [12]) into the sample thus the actual Si/Al ratio for the external surface may be higher than the XPS measurement. (See section 8.4 for XPS details.) Also the decrease in the micropore volume by the ammonium hexafluorosilicate dealumination process is expected from previous work.[7] XRD (Figure 9.2) and SEM (Figure 9.3) analysis show little change in the crystallinity and crystal size of each sample by the treatment. All samples in the study were crystals 1μm or less in size, which led to difficulty in getting good morphologies from the SEM.

9.2 Isopropanol Dehydration

Isopropanol dehydration was also used to characterize the effect of the dealumination process on the BEA*, ZSM-5, and SSZ-35 samples. The low temperatures, 170 – 180°C, needed to transform isopropanol to propene and diisopropylether[8] over acid zeolites makes this an attractive test reaction because the SDA can be maintained in the pores of the zeolite limiting the measurement to the external surface activity only. These zeolites can be activated by thermal treatment at 350 °C in a flowing stream of inert gas and still maintain their SDA inside their structure. 350 °C was found to be the lowest treatment temperature that could be used for zeolite activation to achieve the same activity of calcined materials. Figure 9.4 shows the SDA of ZSM-5, BEA*, and SSZ-35 maintained at temperatures below 350 °C. The SDA of SSZ-25 undergoes decomposition at temperatures below 350 °C (Figure 9.5) and thus was not characterized this way. Figure 9.6 shows the rate of isopropanol consumed at 15 minutes on stream and 180 °C. The dealumination process does not completely eliminate the activity of the samples to the same level of pure silicon sample of BEA*. This is probably due to the ability of the smaller isopropanol molecule to reach sites located in the pore entrances that the hexafluorosilicate could not access but is not also blocked by the SDA. However, for all samples we see a greater than 50% reduction in the rate of isopropanol consumed. The parent sample of SSZ-35 has a lower external surface activity than the BEA* sample and a lower activity than the calcined sample of SSZ-35 suggesting a small impact, if any, on the external surface of SSZ-35. While the external surface activity toward isopropanol dehydration is not completely quenched by the ammonium hexafluorosilicate treatment the large reduction would still produce an observable change in the Constraint Index test

if the external surface activity is important.

9.3 Constraint Index Testing

Figure 9.7 shows the comparison of the CI Test for the calcined parent and calcined dealuminated samples. The observed behavior of BEA* and ZSM-5 is consistent with literature reports for these structures and the dealumination process appears to only slightly reduce the activity. Similarly SSZ-35 shows only a small reduction in activity and similar CI values over time on stream. For all three samples, the dealumination process had no major effect on the CI Test. This suggests the external surface has little impact on the CI Test, and is not the reason for the CI value of SSZ-35 resembling a large pore structure, even though it is a medium pore structure. The reductions in activity likely arise from the loss of some internal sites due to pore blocking, as evident from the decrease in micropore volume detailed in Table 9.1. More evidence of the lack of surface activity for the cracking of n-hexane and 3-methylpentane can be seen on SSZ-35 where the SDA is left in the structure as a pore blocking agent and limits the activity to the external surface. The SDA of SSZ-35 blocks the pores of the structure throughout the reaction as seen by the TGA/DSC analysis as well as N2 adsorption before and after testing. When the CI Test is run on SSZ-35 still containing the SDA no cracking was observed, even at the initial time point. The external surface either deactivates by the rapid build-up of deactivating carbon species or is inactive toward cracking and with either case has no influence on the CI test, whose values are typically reported at the 10 to 20 minute time point.

SSZ-25 in Figure 9.7 does show a significant deviation in the behavior of the

parent and dealuminated sample in the CI Test. The initial 45 minutes are similar. However, after that the dealuminated sample deactivates quicker and the CI value of the dealuminated sample increases at a slower rate. This change in the CI value is opposite the change expected if the external surface is having a significant effect. The external surface would be expected to have no shape selectivity and thus lower the CI value. Reducing the external surface effect by dealumination would be expected to give a higher initial CI value and quicker increase than the parent sample. As such, the external surface does not appear to be responsible for the low CI value of SSZ-25, or the increasing behavior of the CI value.

This behavior is consistent with the recent study by Guisnet for the transformation of n-heptane over MCM-22. Guisnet showed that the large initial drop in activity is from the deactivation of the large cages by coke formation with a quasi-plateau in activity remaining from the sinusoidal channels and in the cracking reaction the external cups were not active [9]. The activity pattern in Figure 9.7d for SSZ-25 follows the same deactivation behavior for the CI test as Guisnet's n-heptane cracking. The increasing CI value over time on stream could then be thought of as coming from the shift from most of the activity occurring in the large cages initially with a low CI, to most of the activity occurring at later times in the sinusoidal channels with a high CI value.

A similar indication that the behavior of SSZ-25 is not related to the surface but instead the internal structure is the shift in the i-C_4/*n*-C_4 product ratio over time. Zones and Harris [10] detailed the link between i-C_4/*n*-C_4 product ratio and the CI value where materials with higher CI values have lower i-C_4/*n*-C_4 ratios presumably due to less conversion of 3-methylpentane. It should be noted that they saw no change in the ratio on

ZSM-5 when changing temperatures and thus change the total feed conversion.[10] On both the parent sample and the surface deactivated sample of SSZ-25, the i-C_4/*n*-C_4 ratio is around 5 at 15 minutes on stream and decays to 2.2 by 6 hour on stream, indicating a significant reduction in the branched products over time. For zeolites ZSM-5, BEA*, and SSZ-35 the ratios are 1.1, 4.5, and 4, respectively, and remain relatively constant over 6h on stream. With an inactive surface, this change in SSZ-25's i-C_4/*n*-C_4 in comparison to the constant values of the other structures would result from a shift in the reaction from the cages in the structure to the more restricted sinusoidal channels. Since the pore sizes into the cages and the channels are similar and smaller than ZSM-5 [11], SSZ-25 suggest the larger internal space is responsible for the CI value rather than external surface activity or pore size.

9.4 References

[1] M. Farcasiu, T. F. Degnan, Ind. Eng. Chem. Res. (1988) 27, 45.

[2] S.L. Lawton, M.E. Leonowicz, R.D. Partridge, P. Chen, M.K. Rubin, Micro. Meso. Mater. 23 (1998) 109.

[3] A. Corma, V. Fornes, S.B. Pergher, Th.L.M. Maesen, J.G. Buglass, Nature 396 (1998) 353.

[4] P. Matias, J.M. Lopes, S. Laforge, P. Magnoux, P.A. Russo, M.M.L. Ribeiro Carrott, M. Guisnet , F. Ramoa Ribeiro, J. Catal. 259 (2008) 190.

[5] H.K. Beyer in H.G. Karge, J. Weitkamp (eds.), Molecular Sieves Science and Technology, Springer, 2002, 203.

[6] D Breck, G. Skeels, US patent 4 503 023 (1985) to Union Carbide Corporation.

[7] Q.L. Wang, M. Torealba, G. Giannetto, M. Guisnet, G. Perot, M. Cahoreau, J. Caisso, Zeolites 10 (1990) 703.

[8] S.J. Gentry, R. Rudham, J. Chem. Soc. Faraday I 70 (1974) 1685.

[9] P. Matias, J.M. Lopes, S. Laforge, P. Magnoux, M. Guisnet, F.R. Ribeiro, Appl. Catal. A: Gen. 351 (2008) 174.

[10] S.I. Zones, T.V. Harris, Micro. Meso. Mater. 31 (2000) 35.

[11] M.E. Leonowicz, J.A. Lawton, S.L. Lawton, M.K. Rubin, Science, 264, (1994) 1910.

[12] K. Klier in " Spectroscopic studies of zeolites and mesoporous materials" in J. Cejka, H. van Bekkum (eds.) Studies in Surf. Sci. 157 (2005) Elsevier B.V., Netherlands, 205.

Figure 9.1: Ammonium hexafluorosilicate dealumination scheme

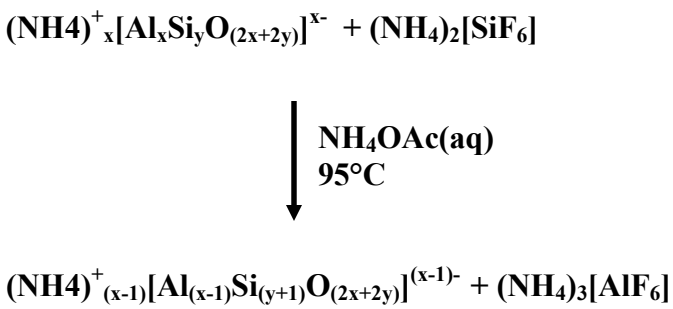

Figure 9.2: XRD patterns of ZSM-5, BEA*, SSZ-35 and SSZ-25 before and after dealumination treatment. Bottom pattern is calcined material while top pattern is from the calcined dealuminated sample

A) ZSM-5 (Offset from difference in alignment of Instrument between measurements.)

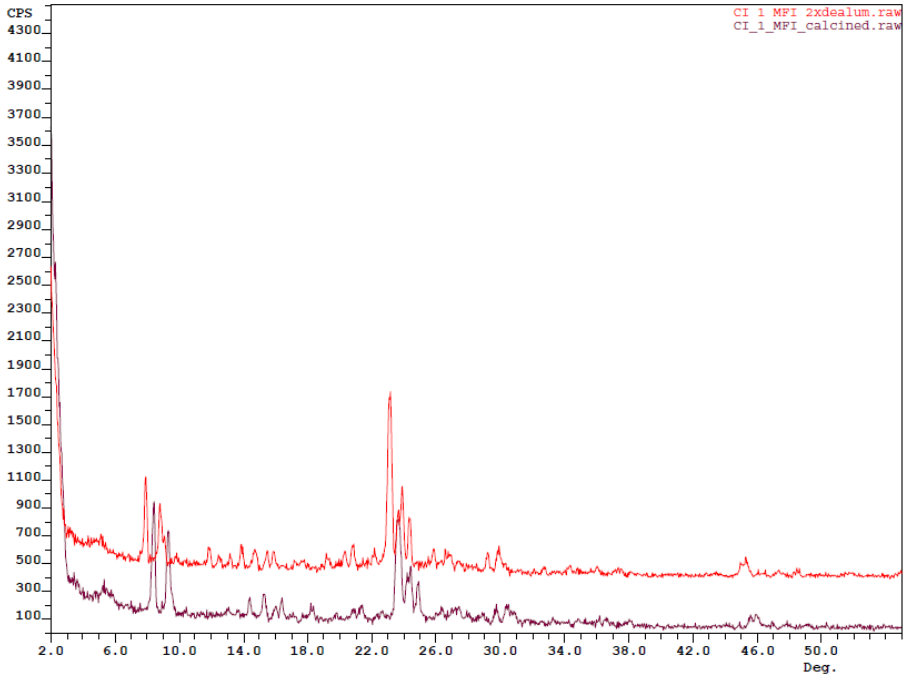

B) BEA*

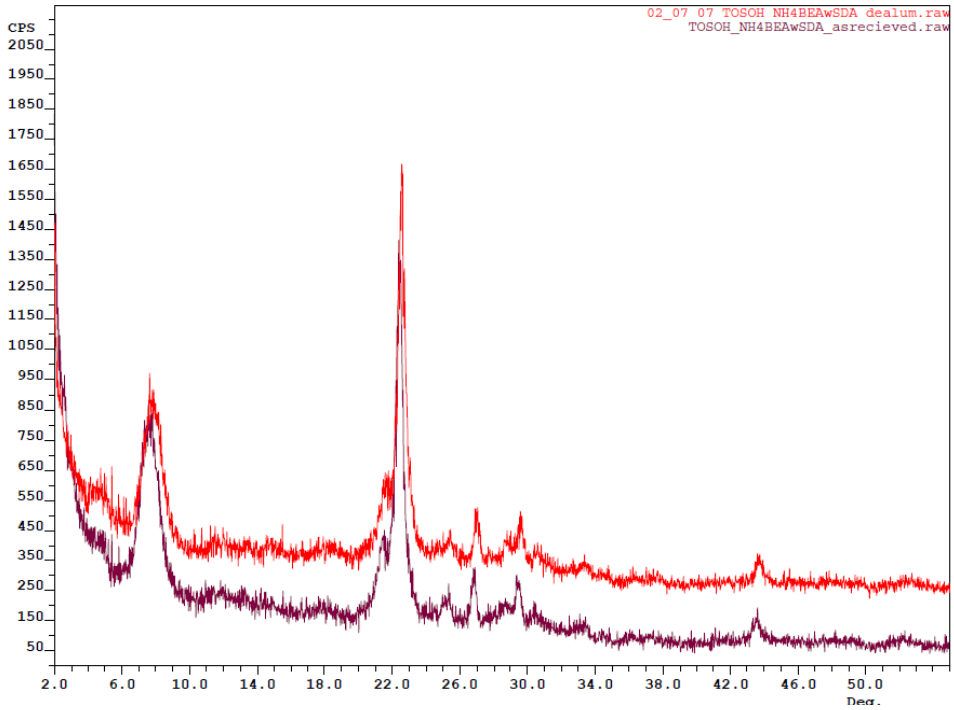

C) SSZ-35

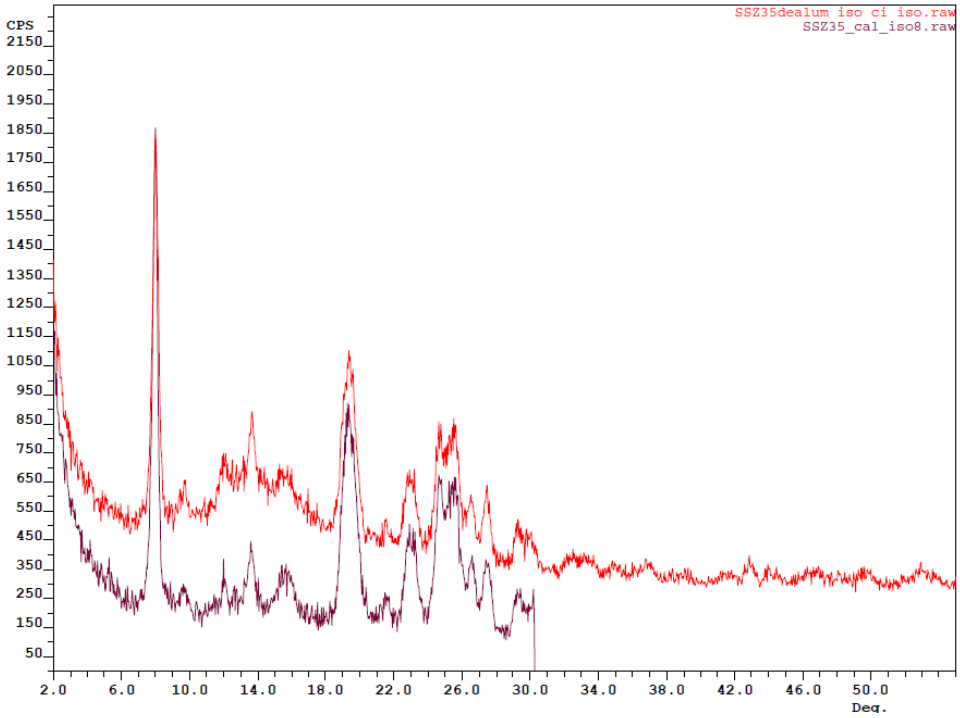

D) SSZ-25

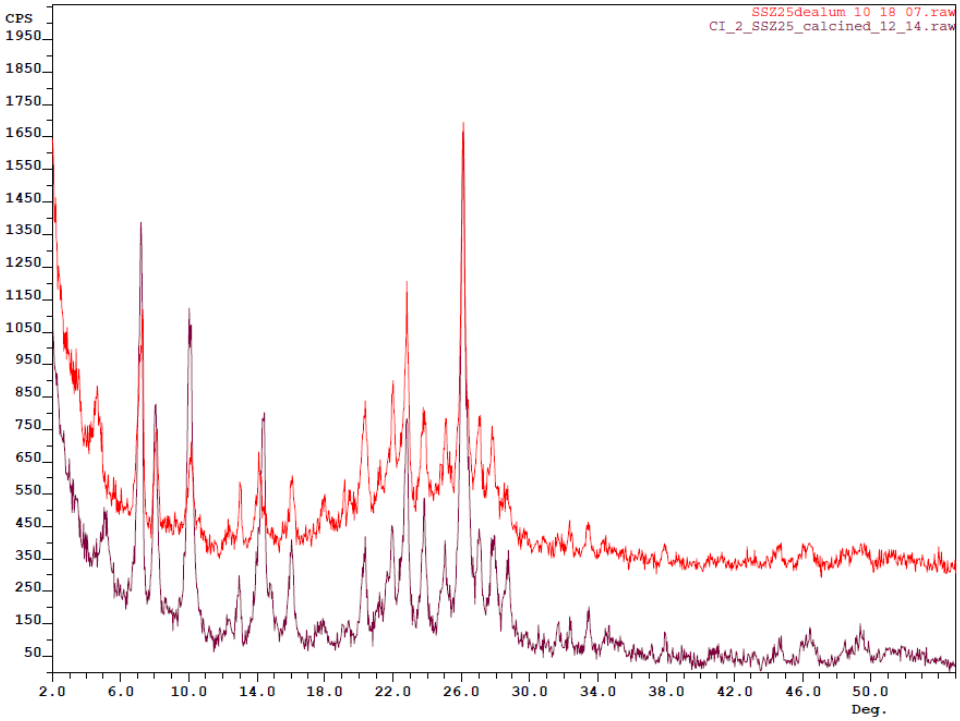

Figure 9.3: SEM images of ZSM-5, BEA*, SSZ-35, and SSZ-25 before and after dealumination procedure

A) ZSM-5 As Made

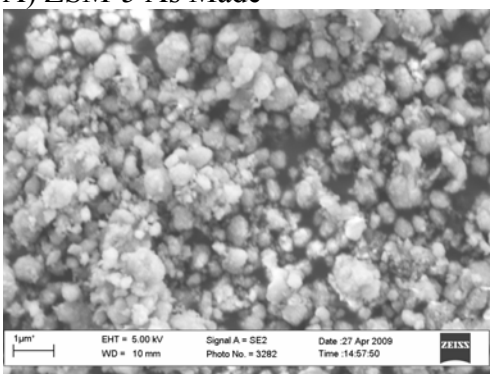

ZSM-5 Dealuminated

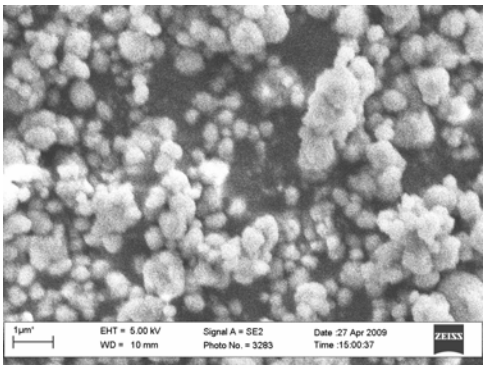

B) BEA* As Made

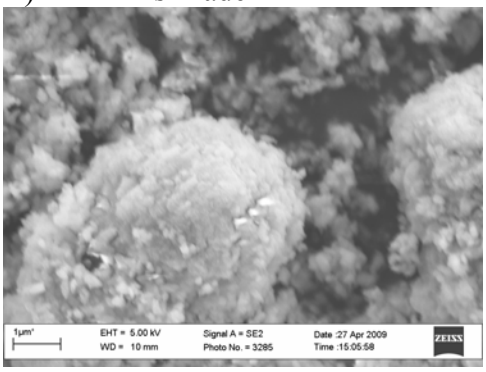

BEA* Dealuminated

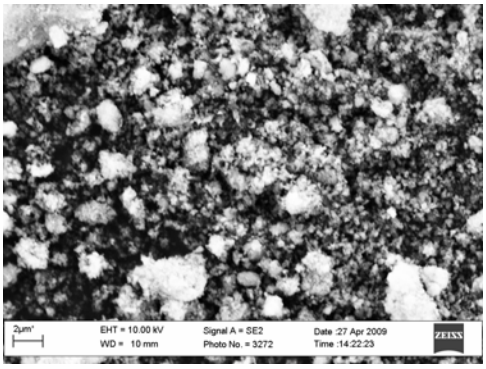

C) SSZ-35 As Made

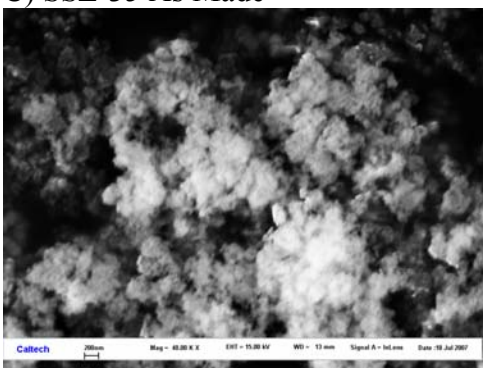

SSZ-35 Dealuminated

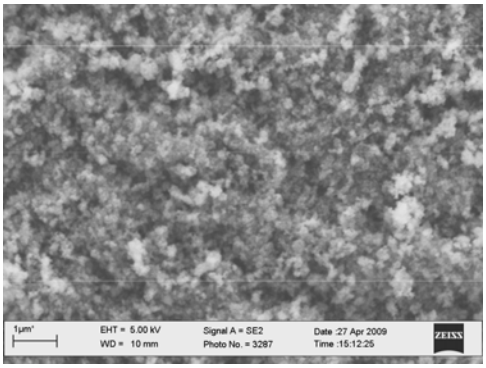

D) SSZ-25 As Made

SSZ-25 Dealuminated

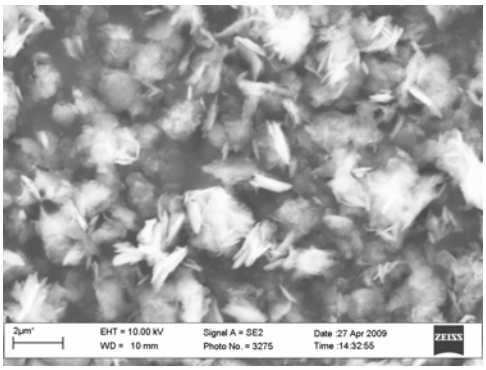

Figure 9.4: TGA/DSC of ZSM-5, BEA*, and SSZ-35 demonstrating SDA degradation above 350°C

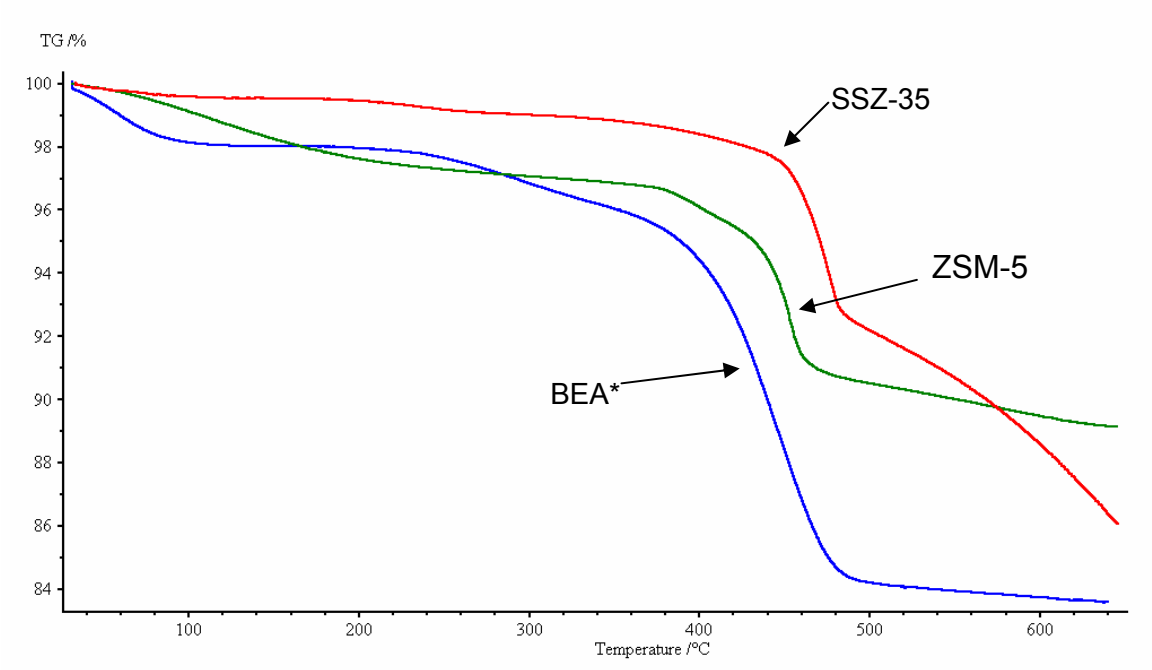

Figure 9.5: TGA/DSC of SSZ-25 demonstrating SDA degradation below 350°C.

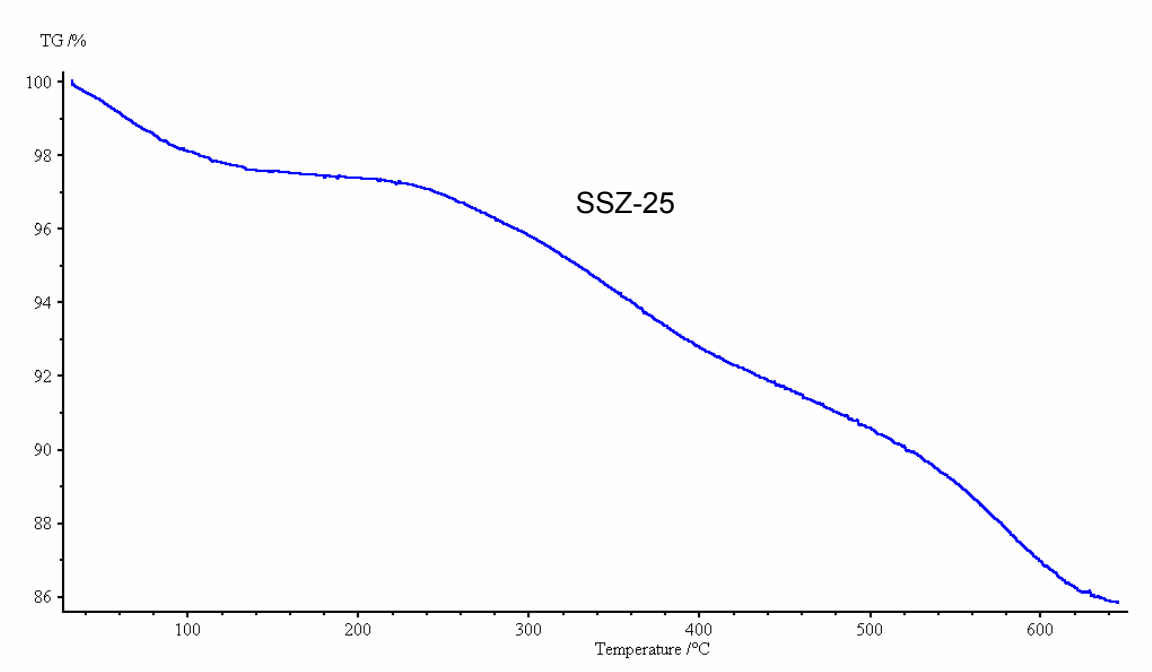

Figure 9.6: Isopropanol dehydration activity on the external surface of ZSM-5, BEA*, and SSZ-35 before and after dealumination treatment as well as calcined SSZ-35

Reactions were run using 0.5g zeolite, pelletized and crushed using a 20/40 mesh sieve. The Feed was 5 ml/min (room temp. measurement) of He/Ar and a liquid isopropanol feed rate of 10µl/min at atmospheric pressure and 150 °C."

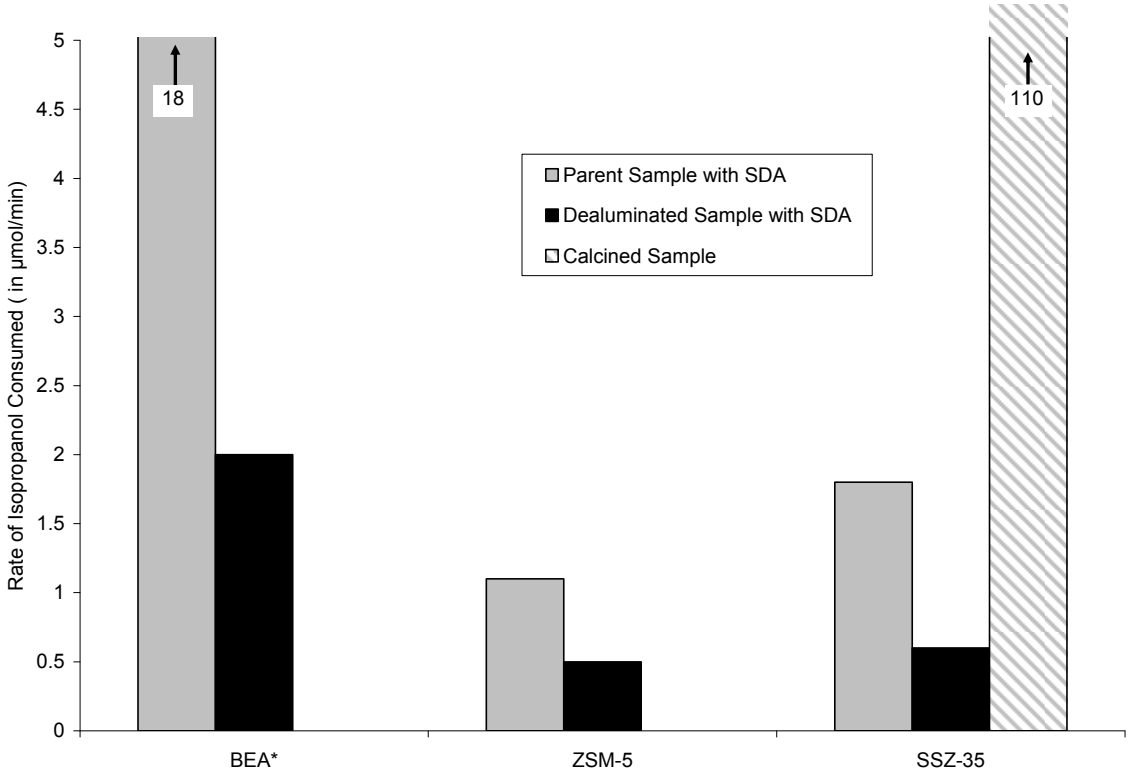

Figure 9.7: Constraint Index testing on zeolites before and after dealumination treatment

Reactions were run using 0.5g zeolite, pelletized and crushed using a 20/40 mesh sieve. The Feed was 5 ml/min (room temp. measurement) of He/Ar and a liquid 50 mol% n-hexane/50 mol% 3-methylpentane feed rate of 10µl/min at atmospheric pressure and 330 °C."

A)ZSM-5

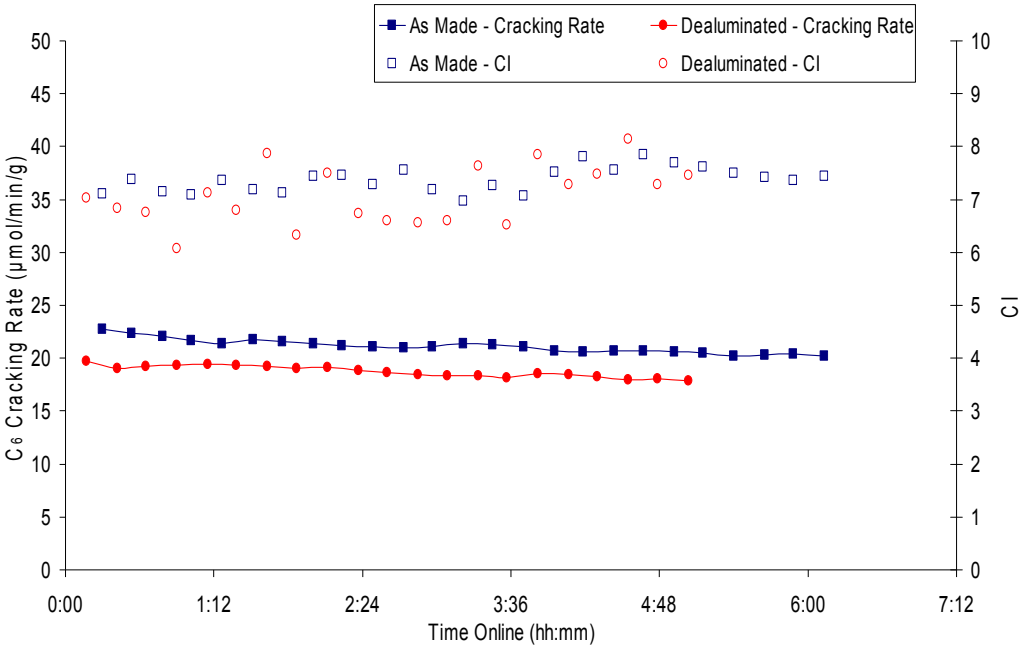

B) BEA*

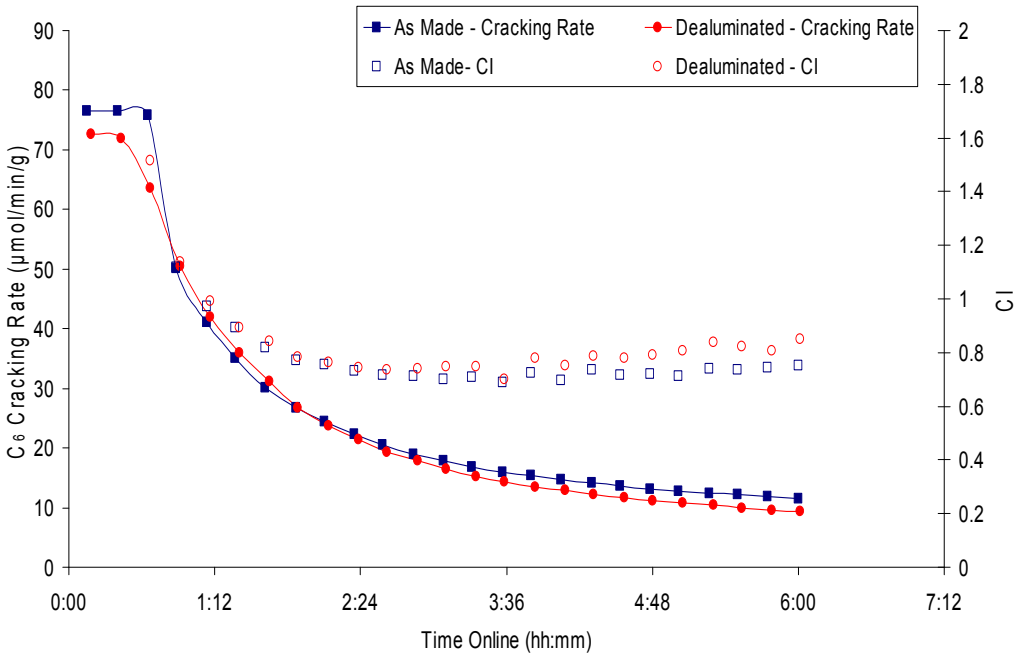

C) SSZ-35

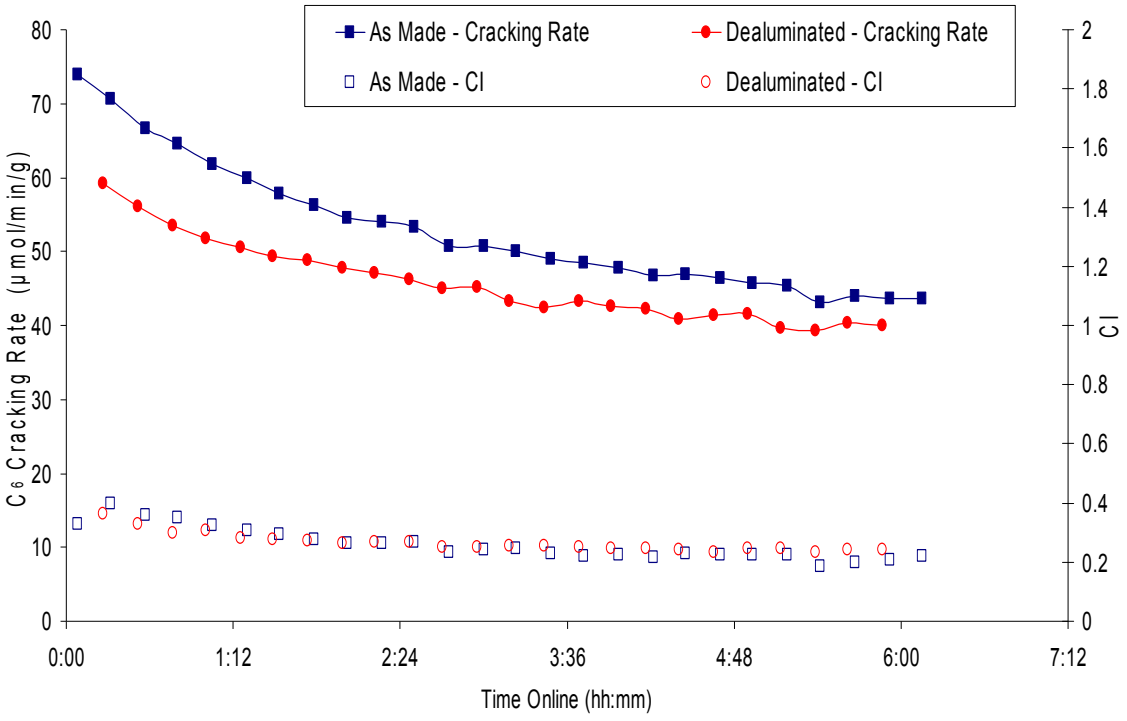

D) SSZ-25

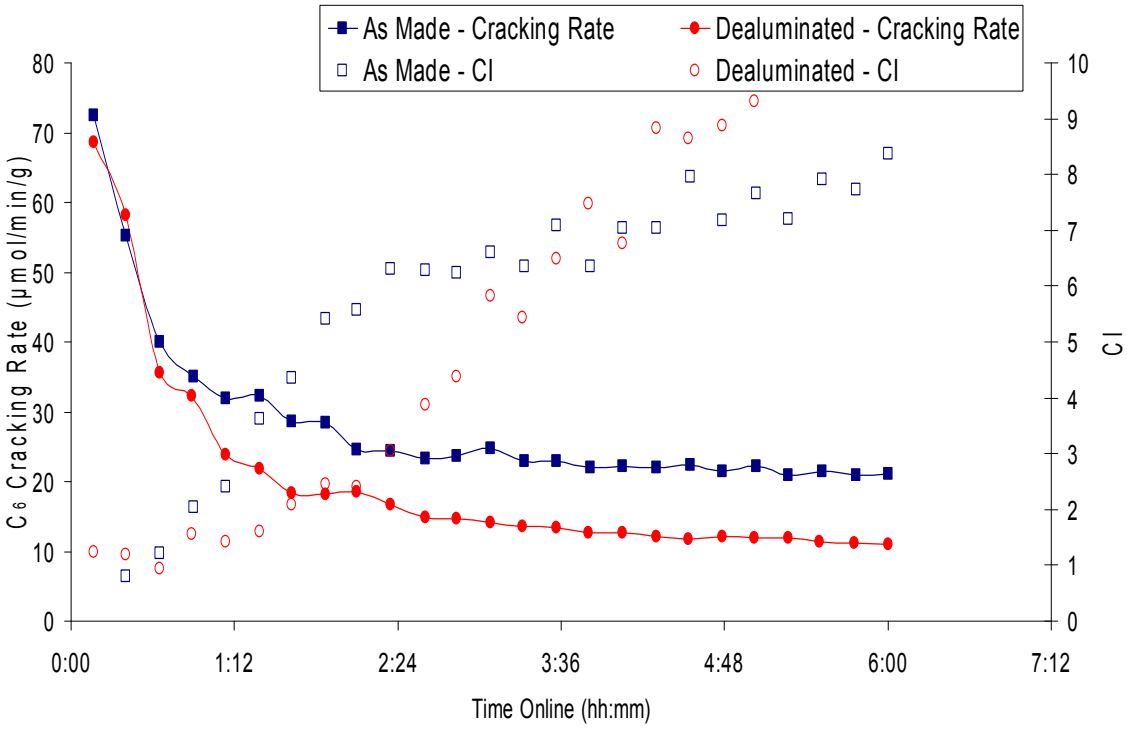

Table 9.1: Characterization data of zeolite samples before and after dealumination treatment (D-Denotes Dealuminated Samples)

.

Zeolite	Surface Si/Al[a]	Bulk Si/Al[b]	Micropore Volume (cc/g)[c]	Crystal Size µm
BEA	16.6	13.5	0.22	<0.25
D-BEA[d]	21.4	19.7	0.18	<0.25
ZSM-5	21.5	19.4	0.13	<0.5
D-ZSM-5[d]	30.1	19.8	0.11	<0.5
SSZ-25	18.2	16.0	0.13	0.5, thin plates
D-SSZ-25[d]	40.9	23.6	0.11	0.5, thin plates
SSZ-35	17.9	16.3	0.15	<0.1
D-SSZ-35[d]	26.4	20.2	0.11	<0.1

[a] Surface Si/Al determined by XPS. [b] Bulk Si/Al determined by ICP.
[c] Determined by t-plot method. [d] D- denotes dealuminated samples.

CHAPTER TEN

EVIDENCE OF INCREASED ACCESSIBILTY IN THE INTERIOR OF STRUCTURES WITH LARGE CAGES

With the external surface producing no discernable effect on the CI test for all of these structures, the effect of the cage on the accessibility of the internal structure to the reactant molecules and reaction transition-states must be considered. Zones and Harris raised this possibility in their observations of unusual results in the CI testing of zeolites[1]. Similarly the ability of reactant molecules to access the internal structure of a zeolite, as well as the limits on transition-states due to space around the active site, have been attributed to many observations of various forms of shape-selectivity[2]. Evidence of accessibility of n-hexane and 3-methylpentane can be viewed through adsorption experiments while transition state accessibility can lead to differences in deactivation and product selectivity.

10.1 Adsorption of n-Hexane and 3-Methylpentane

The uptake of hydrocarbons has been shown to be a useful tool in characterizing zeolites; such as the comparison of the rate of uptake of 2,2,-dimethylbutane on SSZ-57 and IM-5 with other known structures to gain insight into those structures.[3] In a similar manner the uptake of n-hexane and 3-methylpentane on the structures in this study may provide insight into their behavior and accessibility. Figure 10.1 depicts the adsorption of n-hexane and 3-methlypentane on the three 10-ring structures in this study; ZSM-5, SSZ-25, and SSZ-35. Across all three structures little discrimination is seen between the two adsorbates in the initial uptakes. Each of the initial uptakes is on a similar time scale and reaches >70% uptake in the first minute. ZSM-5 shows the largest difference in total uptake between adsorbates while both SSZ-25 and SSZ-35 have little difference in

adsorption of the two molecules. For SSZ-35 it could be argued that this is due to the large pore of 5.7Å x 5.4Å [4], as opposed to 5.6Å x 5.3Å and 5.1Å x 4.1Å[4] for ZSM-5. However SSZ-25 (with pore sizes 5.5Å x 4.0Å and 5.1Å x 4.1Å[4]) shows the least discrimination between adsorbates even with the smallest pore size. For SSZ-25, it should be noted that the structure of SSZ-25 may have pore openings larger than the crystallographic portal size since the structure is believed to be formed by cross-linking layers during calcination which could result in incomplete cross-linking or misalignments that may not be seen by XRD and would increase the size of the pore openings. Looking at the adsorption on the smaller pore structures SSZ-23 and SSZ-28 in Figure 10.2, a larger resistance to uptake is observed. SSZ-23 with 9-ring pores with size 5.3Å x 3.7Å has a large distinction in the uptake between n-hexane and 3-methylpentane. However the CI value for SSZ-23 is lower than that of ZSM-5. This difference between adsorption selectivity and reaction selectivity highlights the cage effect on the CI test. It would be expected on the smaller pores of SSZ-23 that the 3-methylpentane reactant would be more hindered than on ZSM-5 and increase the observed CI value; however this is not the case. SSZ-28 also in Figure 10.2 shows decreasing adsorption with decreasing pore size, 8-rings of 4.4Å x 3.6Å[4], which would accountant for the lower activity than the 10-ring structures, but the CI value is still lower than that of ZSM-5. Adsorption profiles of these smaller pore structures do not correlate with the observed CI results for them.

10.2 Deactivation Characteristics of Caged Structures

As mentioned previously, another type of shape-selectivity observed in zeolites is transition-state selectivity [2]. This has been used to explain the results of the CI test on

some structures [5], as well as the reason for ZSM-5's limited deactivation in hydrocarbon cracking[2]. Similarly the deactivation of n-heptane transformation has been shown to happen by coking limited to the large cages and not the sinusoidal channels [6]. It is not a hard stretch to visualize how the presence of cages in a structure would create large space around the active sites and fewer limitations on transition states. This increased transition state space is easily observed in looking at the deactivation of these structures over time in the CI test. Looking back at Figure 9.7, ZSM-5's activity remains fairly constant over 6h online while the other 10-ring structures and BEA* show larger deactivation. Similarly deactivation is seen in the small pore structures as well in Figure 10.3. Table 10.1 shows a closer look at the deactivation on the basis of mass accumulation in the structure over time on stream at 1h and 6h time points. ZSM-5, while experiencing an accumulation of mass, does so to a lesser degree than either of the other 10-ring structures when looked at on a per-site basis and less deposition per amount of reactant cracked (Figure 10.4). All of the caged structures continue to have mass accumulation at a larger rate than ZSM-5. Extrapolating the data from Table 10.1 to 8.2 mmol C6 cracked/mmol Al for all samples, the g deposited/mmol Al ranks the structures as ZSM5<SSZ-25<SSZ-28<SSZ-35<SSZ-23 at 39.6, 42.1,42.6,46.6, and 53.8 g/mmol Al, respectively. They show a larger tendency than ZSM-5 toward carbon deposition which can be attributed to the larger transition-state space afforded by the larger cages in the structures. The accumulation can be attributed to the internal void spaces by looking at the reduction in micropore volume for each sample. SSZ-25 and SSZ-35 both show micropore volume reductions greater than 80% of the volume of the parent material while ZSM-5 remains relatively open with only a 15% reduction in micropore volume.

XPS and elemental analysis of the deactivated samples show consistent trends as those observed by thermal gravimetric analysis. Table 10.1 also shows the ratio of C/(Si +Al) for the samples. ZSM-5 shows the smallest increase in carbon from 1h to 6h with an increase of 50% while SSZ-35 has a 60% increase and the other samples increase at least 80%. By XPS analysis, the surface increases are smaller for all samples and actually decrease for SSZ-35 and SSZ-28. The XPS analysis and elemental analysis showed the most similar change on ZSM-5 than for the other samples.

Looking at the increase in carbon content from both XPS and elemental analysis provides insight into the location of the deposition. XPS analysis only looks at the carbon deposition near the surface of the zeolite and can be attributed mainly to accumulation on the external surface. Elemental analysis on the other hand provides information on the entire sample. Identical increases would be observed for deposition only on the external surface while interior build up would result in a higher value from elemental analysis. For ZSM-5 this the mol% carbon of the sample shows a 50% increase by elemental analysis and a 30% increase for XPS analysis, suggesting interior deposition is suppressed as expected. For SSZ-35, a 60% carbon increase is observed for the bulk and the surface actually has a 30% decrease, for SSZ-25 the increases are 80% for the bulk and 30% for the surface, for SSZ-23 the increases are 90% for the bulk and 2% for the surface and for SSZ-28 the bulk has a 90% increase in the carbon while like SSZ-35 a 30% decrease is observed by XPS. As can be seen the XPS data includes two decreases in the surface carbon content. A closer inspection of the data reveals that for all samples the data was spread out over a large range, the problems in reproducibly have partially been attributed some to difficulty in focusing the x-ray spot onto only the coked

crystals. In fact the data from data for each sample from the 1h time point overlap with the 6h time point suggesting that the surface content between the two is similar and the increases in the carbon content are closer to 0% and thus still evidence that the carbon accumulation in the samples is internal to the structure. All of these values suggest larger internal deposition than seen in ZSM-5 indicating there is significant accumulation of carbon species internally in the structures and that the micropore volume reductions are from lost internal space rather than just external pore blockage. The ratios for SSZ-25 would most likely show a larger difference if an earlier time point had been used because, as can be seen in Figure 9.7d, a large portion of the deactivation attributed to the large cage has already occurred by the 1 hour time point. These increases would also indicate the larger space of the cages provide fewer limitations to the formation of the deactivating carbon species than in ZSM-5. This would be indicative of less transition-state selectivity in the CI test for these zeolites than in ZSM-5, which would result in lower CI values for these zeolites than ZSM-5 even with smaller or similar pore openings.

10.3 Hydrocarbon Cracking in Caged Structures

Another aspect in which we can see the cage effect comes from looking at the cracking of n-hexane and 3-methylpentane individually on the structures of SSZ-23, SSZ-25, and SSZ-28 in Figure 10.3. For the small pore structures of SSZ-23 and SSZ-28 the reaction rate is much lower than the larger 10-ring structures shown, however the similarity in reactivity between n-hexane and 3-methylpentane suggest that 3-methylpentane is reacting on internal sites as opposed to external sites. Also while isomerization of the 3-

methylpentane to n-hexane is possible, the i-C_4/*n*-C_4 ratios indicate a different product distribution for 3-methylpentane cracking than n-hexane cracking on SSZ-23 or SSZ-28. If the 3-methylpentane were reacting by undergoing isomerization to n-hexane then cracking similar product distributions to n-hexane cracking would be expected. On SSZ-23, the i-C_4/*n*-C_4 ratio is 0.7 for n-hexane cracking and around 2.0 for 3-methylpentane cracking. SSZ-28 had ratios of 0.5 and 1.7, respectively. In the CI test this ratio was 1.4 for SSZ-23 and 1.1 for SSZ-28 which are more similar to the 10-ring structures like ZSM-5 than the reported value of 0.14 for the 8-ring structure SSZ-13[1]. It was also observed in this study that the external surface of a completely pore blocked structure of SSZ-35 showed no reactivity on the external surface after only 15 minutes online. SSZ-23's higher initial n-hexane activity can be attributed to the large disparity in uptake seen between n-hexane and 3-methlypentane in the adsorption results in Figure 10.2. As with SSZ-23, SSZ-28 shows a larger deactivation with n-hexane cracking than 3-methylpentane cracking. There may be a limit on the formation of deactivation species from 3-methylpentane, much like the limit seen in ZSM-5 but for the smaller n-hexane the limit is reduced leading to more deactivation for n-hexane cracking. SSZ-25 provides a unique opportunity to look at the contribution of the cage due to the presence of two separate pore systems in the structure, a series of cages connected by 10-rings and a separate set of 10-ring sinusoidal channels. As seen in Figure 10.2, initially SSZ-25 shows a very high activity with little difference in the activity for 3-methylpentane or n-hexane cracking. However, as the system deactivates, a higher level of activity remains for n-hexane than 3-methylpentane. Since the pore size of SSZ-25 is smaller than that of ZSM5, it is reasonable to consider the sinusoidal channel system would have limited

deactivation and favor n-hexane cracking like ZSM-5, and the large cages is where the majority of deactivation and carbon species accumulation occurs. As is seen in Figure 10.2, this is what happens as the cage system deactivates the reaction profile shifts from looking like a large pore structure to a medium pore structure like ZSM-5. The effect of internal cages in lowering selectivity in the CI test by increasing accessibility to reactants and transition-states is evident through these results.

10.4 References

[1] S.I. Zones, T.V. Harris, Micro. Meso. Mater. 31 (2000) 35.

[2] A.M. Rigby, G.J. Kramer, R.A. Van Santen, J. Catal. 170 (1997) 1.

[3] S.I. Zones, C.Y. Chen, A. Corma, M.T. Cheng, C.L. Kibby, I.Y. Chan, A.W. Burton, J. Catal. 250 (2007) 41.

[4] M.V. Frash, R.A. Van Santen, Topics Catal. 9 (1999) 191.

[5] A. Corma, A.V. Orchilles, Micro. Meso. Mat. 35 – 36 (2000) 21.

[6] P. Matias, J.M. Lopes, S. Laforge, P. Magnoux, M. Guisnet, F.R. Ribeiro, Appl. Catal. A: Gen. 351 (2008) 174.

Figure 10.1: Adsorption of n-hexane and 3-methylpentane on 10-ring pore structures

Adsorption measurements made at P/P_o of 0.3 on a Cahn C-2000 balance in the manner detailed by Chen in previous work[7].

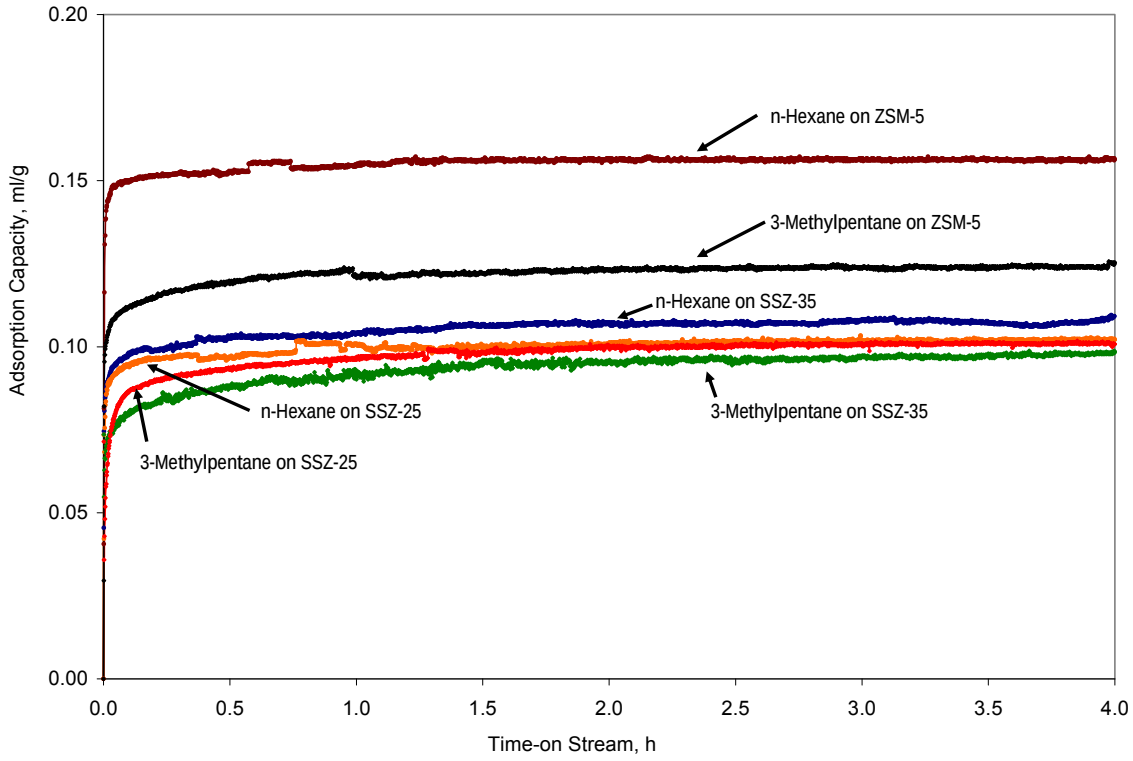

Figure 10.2: Adsorption of n-hexane and 3-methylpentane on small pore structures Adsorption measurements made at P/P_o of 0.3 on a Cahn C-2000 balance in the manner detailed by Chen in previous work[7].

A) SSZ-23

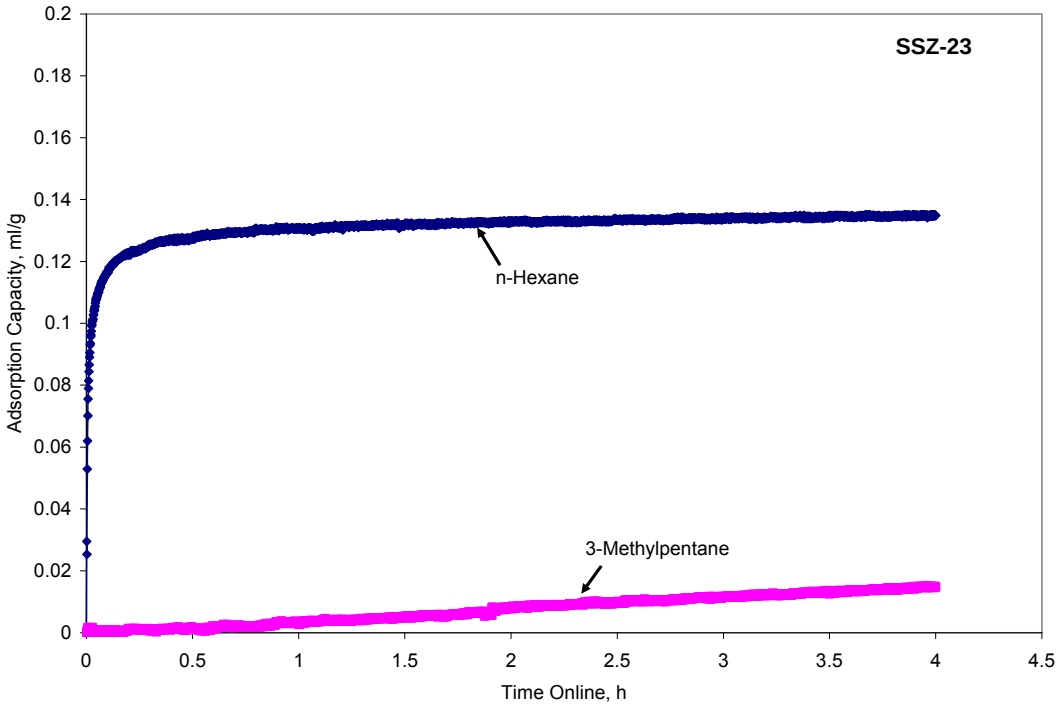

B) SSZ-28

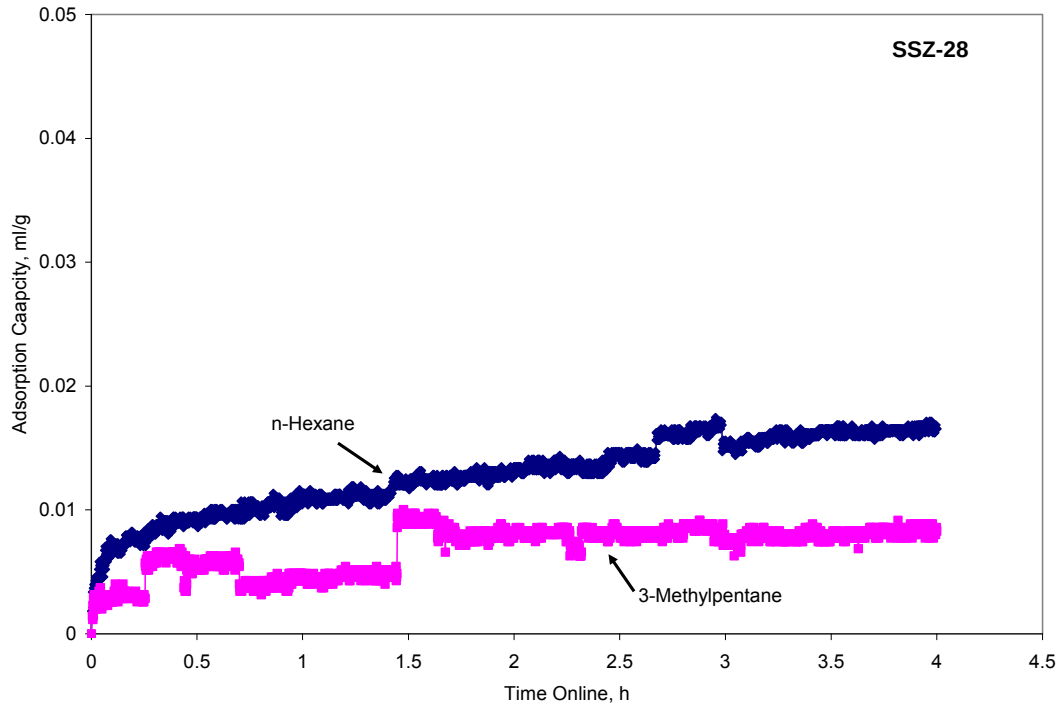

Figure 10.3: Constraint Index and cracking rate of individual pure reactants over time on stream for the small pore structures SSZ-23 and SSZ-28 as well as SSZ-25

Reactions were run using 0.5g zeolite, pelletized and crushed using a 20/40 mesh sieve. The Feed was 5 ml/min (room temp. measurement) of He/Ar and a liquid 50 mol% n-hexane/50 mol% 3-methylpentane feed rate of 10µl/min at atmospheric pressure. SSZ-25 was run at 330 °C while SSZ-23 and SSZ-28 were run at 375 °C."

A) SSZ-23 (375°C)

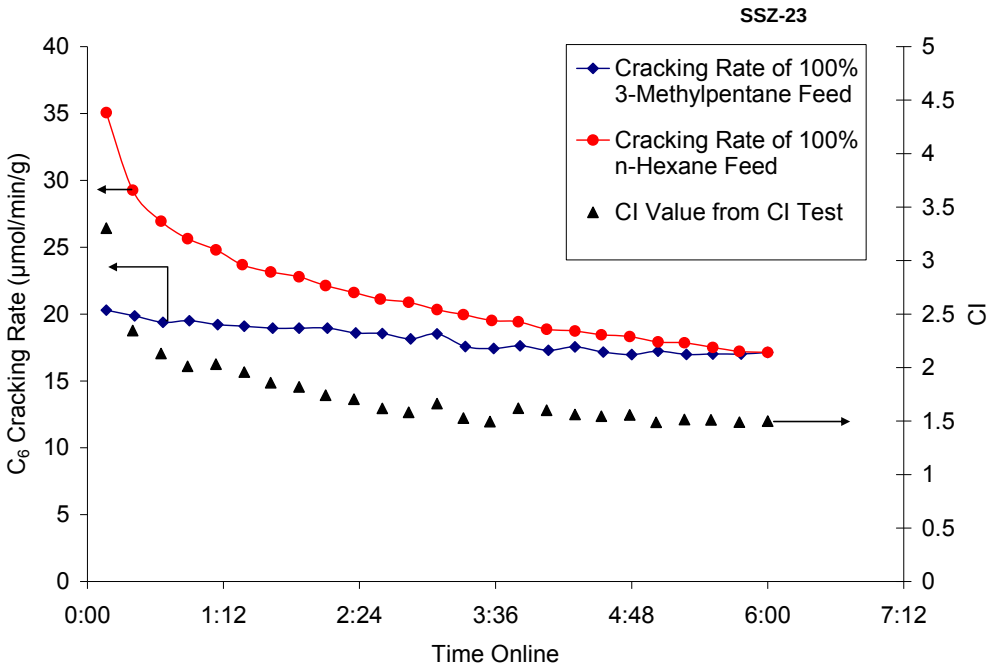

B) SSZ-28 (375°C)

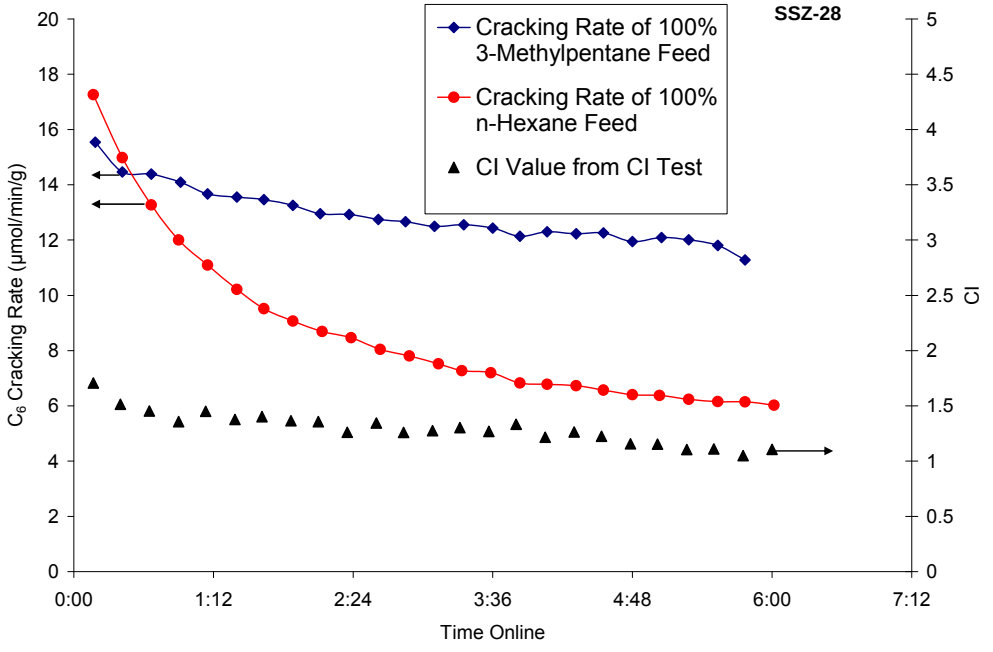

C) SSZ-25 (330°C)

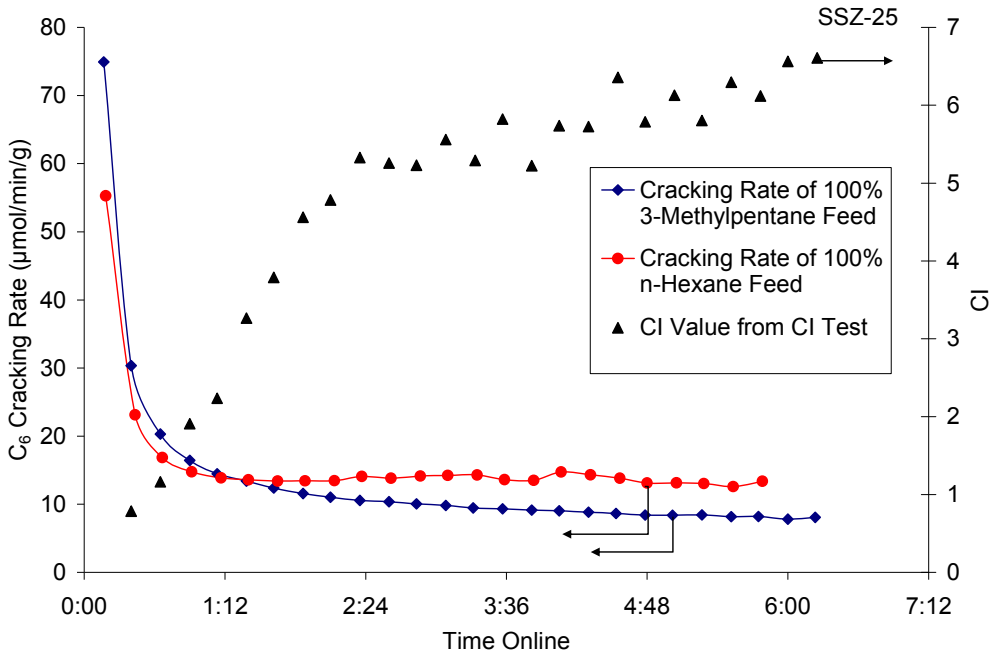
SSZ-25
C_6 Cracking Rate (µmol/min/g)
CI
Time Online
0:00
1:12
2:24
3:36
4:48
6:00
7:12
0
10
20
30
40
50
60
70
80
0
1
2
3
4
5
6
7
Cracking Rate of 100% 3-Methylpentane Feed
Cracking Rate of 100% n-Hexane Feed
CI Value from CI Test

Figure 10.4 Comparison of mass accumulation on structures with the amount of C_6 cracked on those structures during Constraint Index testing

Reactions were run using 0.5g zeolite, pelletized and crushed using a 20/40 mesh sieve. The Feed was 5 ml/min (room temp. measurement) of He/Ar and a liquid 50 mol% n-hexane/50 mol% 3-methylpentane feed rate of 10µl/min at atmospheric pressure. ZSM-5, SSZ-35 and SSZ-25 were run at 330 °C while SSZ-23 and SSZ-28 were run at 375 °C."

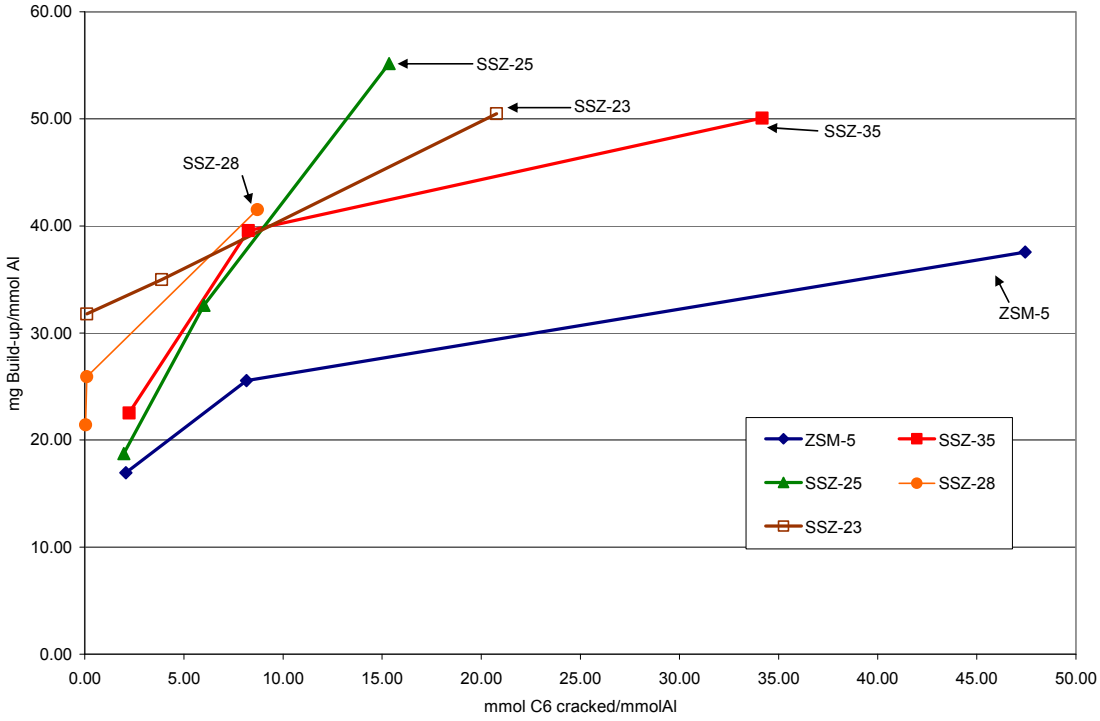

Table 10.1: Characterization of mass deposition from samples at the 1h and 6h time point in the Constraint Index test

Zeolite	Time on Stream	mmols C_6 Cracked[f]		Mass Deposited mg of mass		Micropore Vol. ml/g zeolite[b]	% Carbon Increase from 1h to 6h on Stream	
		/g zeolite	/mmol Al[a]	/g zeolite	/mmol Al[a]	(% reduced)[c]	Bulk[d]	Surface[e,g]
ZSM-5	1h	5.5	8.2	26.7	39.6			
	6h	32	47	31.3	46.4	0.11 (15%)	50%	30%
SSZ-35	1h	7.0	8.3	39.6	46.7			
	6h	29	34	56.9	67.0	0.03 (80%)	60%	-30%
SSZ-25	1h	5.1	6.0	33.8	37.1			
	6h	14	15	52.7	57.8	0.02 (85%)	80%	30%
SSZ-23	1h	1.4	3.9	16.6	46.0			
	6h	7.5	21	27.8	77.0	0.11 (31%)	90%	20%
SSZ-28	1h	0.045	0.10	15.8	34.4			
	6h	4.0	8.7	19.8	43.1	0.10 (33%)	90%	-30%

[a] mmols Al determined from elemental analysis, assumes all Al is in the framework
[b] Determined by N_2 adsorption
[c] % reduced as compared with calcined parent sample
[d] Determined from elemental analysis
[e] Determined from XPS measuring the near surface region
[f] ZSM-5, SSZ-35 and SSZ-25 were tested at a reaction temperature of 330°C while SSZ-23 and SSZ-28 were at 375°C.
[g] The XPS data for 1h and 6h carbon content fell within a standard deviation of each other and the data range was fairly wide. The points are likely much closer to 0%

CHAPTER ELEVEN

EVIDENCE OF MULITPLE STRUCTURE FEATURES IN CONSTRAINT INDEX TESTING

Besides the lower than expected Constraint Index values seen on the structures with large cages, another unique feature of the Constraint Index test observed was the change in the value for the SSZ-25 structure. Zones and Harris [1] interpret this behavior as the expression of the difference in fouling rates for the two pore systems in the structure. This again is consistent with the work of Guisnet on n-heptane transformation over MCM-22 (the same **MWW** structure as SSZ-25).[2] A similar behavior in the Constraint Index test over time on stream has been observed for offretite.[3] Again this result is interpreted to be due to the fouling of the larger 12-ring channels while slower deactivation in the gmelinite cages is observed. This is observed by poisoning the feed with pyridine and observing an increased initial CI value for the same sample.[3]

Typically the Constraint Index value is reported at one time point between 20 and 40 minutes online. However based on these two observations, the Constraint Index test may also provide evidence indicating the presence of different features in structures, i.e., different pore systems, different pore sizes, additional cages, etc. Figure 11.1 shows the Constraint Index behavior over time on stream for various structures. The structures of MOR and FER each have multiple features show similar changing Constraint Index over time; while MOR increases much like offretite and SSZ-25, FER shows a large decrease. Fouling of the catalyst alone does not result in the changing behavior of the Constraint Index. USY and BEA* both have large-pore 3-dimensional structures that quickly foul but maintain a similar Constraint Index value over 6 hours online. Similarly the 1-dimensional structure of ZSM-12 has large pores that show quick fouling but also maintains a fairly constant Constraint Index value over 6 hours online. The Constraint

Index of ZSM-12 is slightly higher than expected for 12-ring structures; this is attributed to the smaller pore sizes of ZSM-12 compared to other 12-ring structures and having no internal intersections. The behavior of MOR (Si/Al ~6.5) can be explained similar to that of SSZ-25 and offretite where the large 12-ring channel fouls and the influence of the smaller side cages contributes to an increasing Constraint Index value. FER on the other hand shows a decrease which may be attributed to the distribution of sites in the smaller 8-ring cages and the 10-ring channels which can vary based on synthesis method.[4,5,6] Figure 11.2 shows the fractions of n-hexane and 3-methylpentane remaining in the Constraint Index test over MOR(Si/Al ~6.5), FER, and SSZ-25. In the case of the MOR and SSZ-25 there is initial fouling and decrease in the activity of both n-hexane and 3-methylpentane. Then the cracking rate of n-hexane levels off to a quasi-steady level while the cracking rate of 3-methylpentane drops further. In FER however the cracking rate of 3-methylpentane is constant over the run, while a decrease in n-hexane occurs resulting in the dropping Constraint Index value.

Several studies have shown through adsorption experiments n-hexane does not enter the small cages of ferrierite [7,8] or the side pocket of MOR[5]. This would suggest that the CI time dependence for these materials does not arise from the different features in the structure as the small cages and side pockets might not be accessed by the reactants. However these adsorption experiments occur at temperatures lower than the reaction conditions of the CI test. Distinguishing the ability of n-hexane and 3-methylpentane to enter the small cages and side pockets under reaction conditions would provide better insight. This can be accomplished by limiting the reaction to one feature of each structure.

Various work has shown that Na^+ cations preferentially exchange into the 8-ring side pockets in MOR.[5,9,10] Similarly, Na^+ cations preferentially exchange into the small channels of ferrierite.[11] Using the same ion-exchange conditions as the Igelsia work partial Na+ exchanges were performed on the MOR(Si/Al ~6.5) and FER and then tested in the Constraint Index test. Figure 11.3 demonstrates the results of those tests. In the MOR sample the Constraint Index value remains low at a level not unexpected for a large pore zeolite over the entire length of the run and the cracking rate is less than half the cracking rate of the as-made sample. In the FER sample, partial Na^+ exchange depressed the initial Constraint Index values to a level expected for that of a 10-ring zeolite and that level is maintained over the entire run. The conflicting results of these Constraint Index results with the adsorption studies demonstrating n-hexane can not enter the small cages and side pockets of ferrierite and mordenite, respectively, may be explained by the difference in experimental temperature of the Constraint Index test and the adsorption experiments. Looking further at the ferrierite sample reducing the temperature to 375°C reduces the Constraint Index value as shown in Figure 11.4. In these two tests the cracking rate of 3-methylpentane is similar but the cracking rate of n-hexane decreases with decreasing temperature. If a shift from monomolecular to bimolecular cracking were occurring, the Constraint Index would be expected to increase, much like that observed by Haag on ZSM-5 over temperature.[12] Ferrierite shows the opposite, suggesting a reduction in the ability of n-hexane to reach some sites.

While these are examples of evidence of multiple features by Constraint Index testing that may not always be the case. A sample of MOR also from Zeolyst but with a Si/Al ~ 10 showed no increase in the Constraint Index behavior over 6 hours on stream at

the same conditions. Room exists for future exploration into the differences between these mordenite samples. Similarly methods to eliminate the sites in the large channels would provide more evidence of the influence of sites in the smaller channels and cages of ferrierite and mordenite. The Constraint Index test has the ability to provide insight into multiple features of a structure by observing changes in the Constraint Index over time, but the absence of change does not rule out multiple features.

11.1 References

[1] S.I. Zones, T.V. Harris, Micro. Meso. Mater. 31 (2000) 35.

[2] P. Matias, J.M. Lopes, S. Laforge, P. Magnoux, M. Guisnet, F.R. Ribeiro, Appl. Catal. A: Gen. 351 (2008) 174.

[3] F.R. Ribeiro, F. Lemos, G. Perot, M. Guisnet, in R.Setton (ed.) Chemical Reactions in Organic and Inorganic Systems, Reidel Pub. Co., (1986) 141.

[4] V.L. Zholobenko, D.B. Lukyanov, J. Dwyer, W.J. Smith, J. Phy. Chem. B. 102 (1998) 2715.

[5] A. Bhan, A.D. Allian, G.J. Sunley, D.J. Law, E. Iglesia, J. Am. Chem. Soc. 129 (2007) 4919.

[6] A.B. Pinar, C. Marquez-Alvarez, M. Grande-Casas, J. Perez-Pariente, J. Catal 263 (2009) 258.

[7] W.J.M. van Well, X. Cottin, J.W. de Haan, B. Smit, G. Nivarthy, J.A. Lercher, J.H.C. van Hooff, R.A. van Santen, J. Phys. Chem. B 102 (1998) 3945.

[8] W.J.M. van Well, X. Cottin, B. Smit, J.H.C. van Hooff, R.A. van Santen, J. Phys. Chem. B 102 (1998) 3952.

[9] M.A. Makarova, A.E. Wilson, B.J. van Liemt, C. Mesters, A.W. de Winter, C.J. Williams, J. Catal. 172 (1997) 170.

[10] V.A. Veefkind, M.L. Smidt, J.A. Lercher, Appl. Catal., A 194 (2000) 319.

[11] B. Wichterlova, N. Zilkova, E. Uvarova, J. Cejka, P. Sarv, C. Paganini, J.A. Lercher, App. Cat., A 182 (1999) 297.

[12] V.J. Frillette, W.O. Haag, R.M. Lago, J. Catal. 67 (1981) 218.

Figure 11.1 Constraint Index test over time on stream for various zeolite structures
Reactions were run using 0.5g zeolite, pelletized and crushed using a 20/40 mesh sieve. The Feed was 5 ml/min (room temp. measurement) of He/Ar and a liquid 50 mol% n-hexane/50 mol% 3-methylpentane feed rate of 10µl/min at atmospheric pressure. ZSM-5, SSZ-35, BEA*, SSZ-25 and USY were run at 330 °C. MOR, FER, SSZ-23, SSZ-28 and ZSM-12 were run at 375 °C.

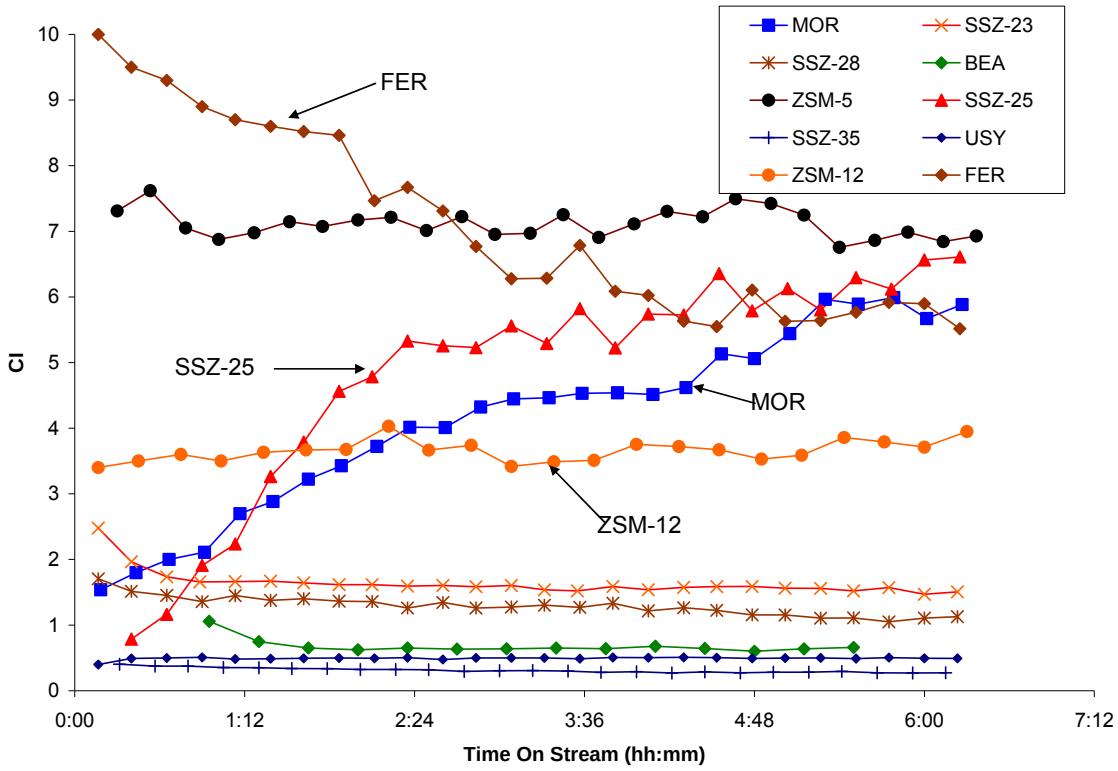

Figure 11.2: Fraction of n-hexane and 3-methylpentane remaining during the Constraint Index test on MOR, FER, and SSZ-25

Reactions were run using 0.5g zeolite, pelletized and crushed using a 20/40 mesh sieve. The Feed was 5 ml/min (room temp. measurement) of He/Ar and a liquid 50 mol% n-hexane/50 mol% 3-methylpentane feed rate of 10µl/min at atmospheric pressure. SSZ-25 was run at 330 °C while SSZ-23 and SSZ-28 were run at 375 °C."

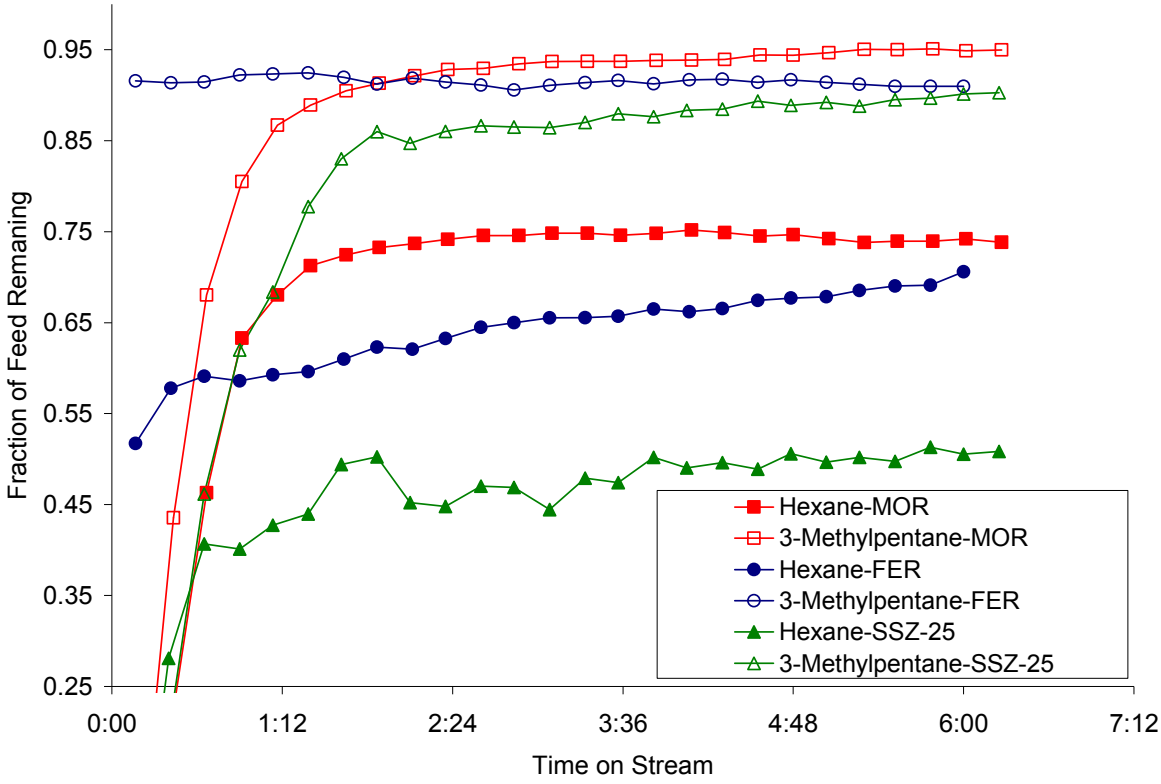

Figure 11.3: Constraint Index testing on partial Na-exchanged MOR and FER. (As made samples are depicted by blue and partial Na+-exchanged samples by red, solid points = rate of C6 cracking and hollow points = CI.)
Reactions were run using 0.5g zeolite, pelletized and crushed using a 20/40 mesh sieve. The Feed was 5 ml/min (room temp. measurement) of He/Ar and a liquid 50 mol% n-hexane/50 mol% 3-methylpentane feed rate of 10µl/min at 425 °C and atmospheric pressure.

A) MOR

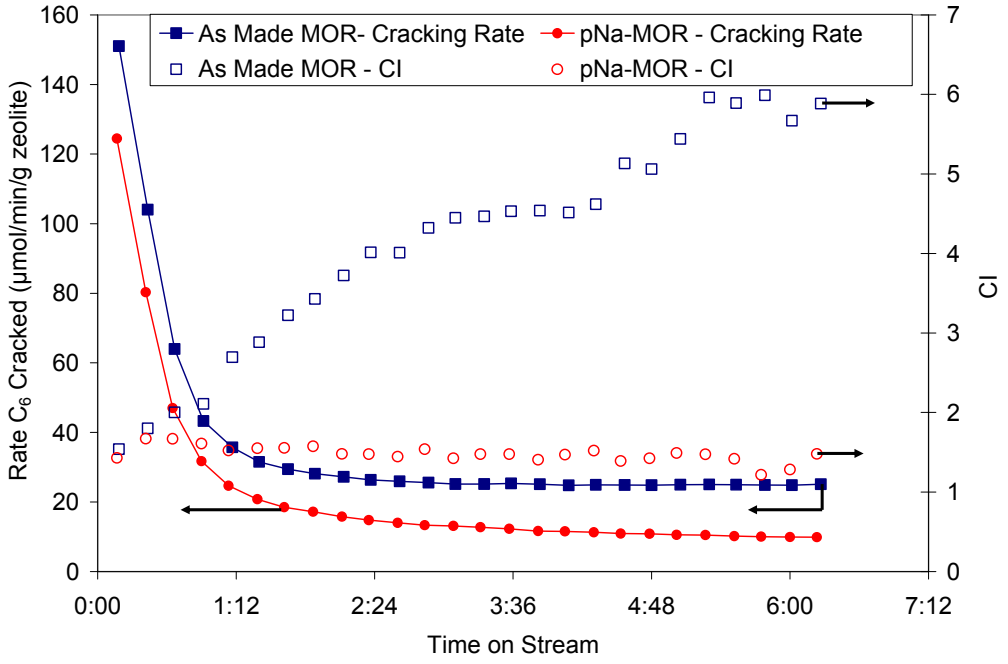

B) FER

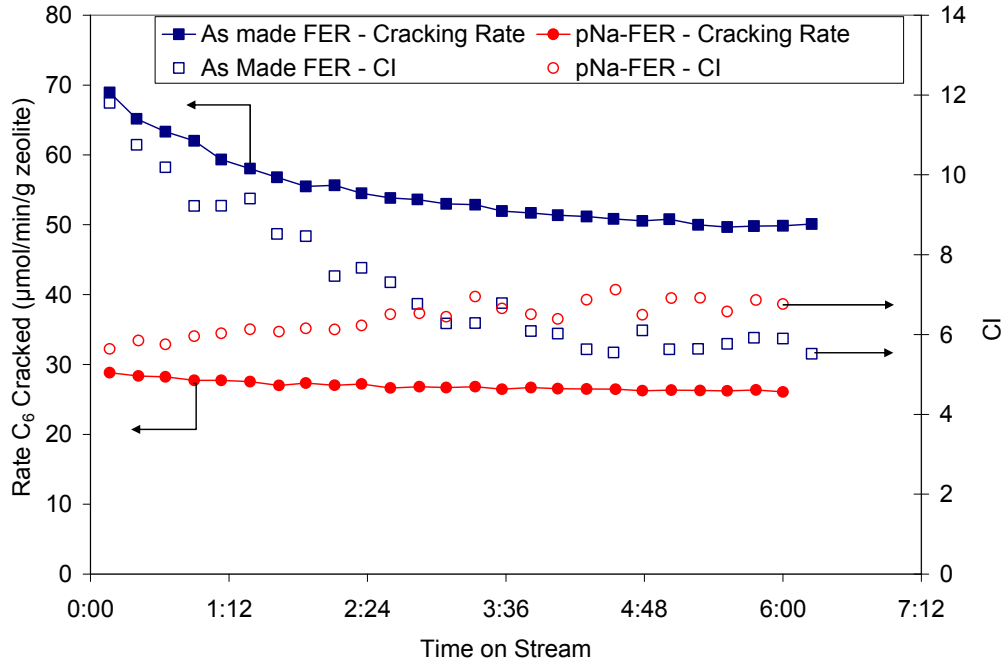

Figure 11.4: Constraint Index test on at 425 °C and 375 °C on ferrierite
Reactions were run using 0.5g zeolite, pelletized and crushed using a 20/40 mesh sieve. The Feed was 5 ml/min (room temp. measurement) of He/Ar and a liquid 50 mol% n-hexane/50 mol% 3-methylpentane feed rate of 10µl/min at atmospheric pressure.

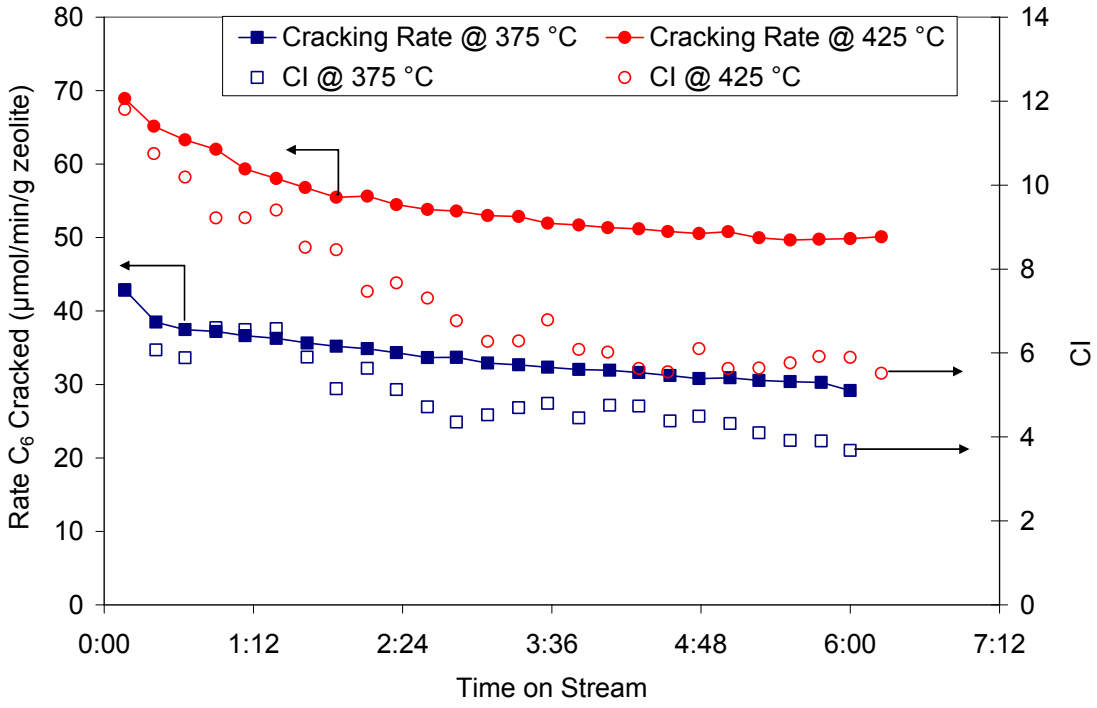

CHAPTER TWELVE

CONCLUSIONS ON STRUCTURE EFFECTS IN CONSTRAINT INDEX TESTING FOR ZEOLITE CHARACTERIZATION

Part Two describes an exploration into the Constraint Index results and possible reasons why the behavior of zeolite structures that contain large cages result in Constraint index values that are typically lower than that expected for the actual pore size of the structure.

The first explanation investigated was that the activity of sites on the external surface may provide a non-selective influence on the cracking reaction and lower the Constraint Index results. The goal was to compare the compare the results on Constraint Index testing on samples of a structure and on the samples of the same structure in which any external surface activity has been removed. ZSM-5 and BEA* were used as a comparison standard of medium and large pore zeolites comparatively and SSZ-35 and SSZ-25 were used as examples of structures with cages. This was accomplished by dealumination by ammonium hexafluorosilicate treatment with the pores of the structure still blocked by the structure directing agent. Little change was noted in the powder X-ray diffraction pattern and scanning electron microscope images of the materials before and after treatment. A small amount of pore blocking was noted by nitrogen adsorption. The Si/Al ratio was seen to predominately be changed at the surface when comparing the surface measurement by x-ray photoelectron spectroscopy analysis or the bulk value measured by inductively coupled plasma optical emission spectroscopy. Samples of ZSM-5, BEA*, and SSZ-35 were then tested for external surface activity by isopropanol dehydration on the samples with and without surface dealumination but before calcinations to keep the pores blocked. External surface activity on all three samples was reduced by over 50 %. After dealumination samples were calcined and tested in the

Constraint Index test. On BEA*, ZSM-5, and SSZ-35 the Constraint Index value was similar between the treated and non-treated samples. SSZ-25 did exhibit a difference in Constraint Index behavior but opposite the changes expected if the external surface was influencing the test.

Hydrocarbon adsorption of n-hexane and 3-methylpentane were performed on several structures; ZSM-5, SSZ-23, SSZ-25, SSZ-28, and SSZ-35 that depict the varying differences in uptake of the individual reactants. However, it is not accurate to assume that these results would translate to reaction conditions. A study of the mass build-up in the materials indicates that the caged structures had a higher propensity for build-up than ZSM-5. It is believed that that this is due to the cages providing more room for transition states need to form the deactivating carbon species as opposed to the channels of ZSM-5.

Finally it was noted that by carrying the Constraint Index out over a longer time period it is possible to discern evidence of multiple distinct features in a structure. In structures such as SSZ-25, MOR, or FER there are either two separate pore structures in the case of SSZ-25 or distinct side pockets off of the larger channels in MOR and FER. In these cases, sites located in the different features foul at different rates. When this happens during the Constraint Index test the Constraint Index value can shift. If the test is only run long enough to determine the first point this information would be lost.

The Constraint Index test is derived from an observed relationship between pore size and the reaction rates of n-hexane and 3-methylpentane cracking, and as such it is not surprising that exceptions to the trend exist. This should always be kept in mind when using the Constraint Index test to characterize a material. A one-point Constraint Index measurement may be misleading and should be used in context with other tests and

information. For example, a Constraint Index value similar to ZSM-5 but with much lower activity would suggest a small pore structure with internal cages. Similarly data from adsorption experiments and other reaction-based tests can be used in conjunction to provide a context for characterizing the material. Also further information can be obtained from the behavior of the test over time, which can provide valuable insight.